Dissertations

Theses and Dissertations

8-1-2014

On Motion Mechanisms of Freight Train Suspension Systems

Dennis O'Connor

Southern Illinois University Carbondale, doconno@siue.edu

Follow this and additional works at: http://opensiuc.lib.siu.edu/dissertations

ON MOTION MECHANISMS OF FREIGHT TRAIN SUSPENSION SYSTEMS

by

DENNIS MICHAEL O'CONNOR

B.S., SIUE, Mechanical Engineering, May 2004
M.S., SIUE, Mechanical Engineering, May 2007

A Dissertation
Submitted in Partial Fulfillment of the Requirements for the
PhD in Engineering Science.

Department of Engineering Science
In the Graduate School
Southern Illinois University Carbondale and Edwardsville
August 2014

DISSERTATION APPROVAL

ON MOTION MECHANISMS OF FREIGHT TRAIN SUSPENSION SYSTEMS

by

Dennis Michael O'Connor

A Dissertation Submitted in Partial

Fulfillment of the Requirements

for the Degree of

Doctor of Philosophy

in the field of Mechanical Engineering

Approved by:

Albert C.J. Luo, Chair

Tsuchin Philip Chu

Fengxia Wang

Chunqing Lu

Om Agrawal

Mohammad Sayeh

Graduate School
Southern Illinois University Carbondale
August 2014

ABSTRACT

ON MOTION MECHANISMS OF FREIGHT TRAIN SUSPENSION SYSTEMS

by

Dennis O'Connor

In this dissertation, a freight train suspension system is presented for all possible types of motion. The suspension system experiences impacts and friction between wedges and bolster. The impacts cause the chatter motions between wedges and bolster, and the friction will cause the stick and non-stick motions between wedges and bolster. Due to the wedge effect, the suspension system may become stuck and not move, which cause the suspension lose functions. To discuss such phenomena in the freight train suspension systems, the theory of discontinuous dynamical systems is used, and the motion mechanism of impacting chatter with stick and stuck is discussed. The analytical conditions for the onset and vanishing of stick motions between the wedges and bolster are presented, and the condition for maintaining stick motion was achieved as well. The analytical conditions for stuck motion are developed to determine the onset and vanishing conditions for stuck motion. Analytical prediction of periodic motions relative to impacting chatter with stick and stuck motions in train suspension is performed through the mapping dynamics. The corresponding analyses of local stability and bifurcation are carried out, and the grazing and stick conditions are used to determine periodic motions. Numerical simulations are to illustrate periodic motions of stick and stuck motions. Finally, from field testing data, the effects of wedge angle on the motions of the suspension is presented to find a more desirable suspension response for design.

DEDICATION

This dissertation is dedicated to my two sons Rylan and Nevan O'Connor. The heart of this research is to understand the how and why two systems interact and behave. Indeed, some of my greatest insights into this work have come from raising two boys. How at times they can bring world peace and at other times world destruction, I have often considered through laughing tears and telling headaches. More importantly though, they have sustained my balance and given me an immeasurable richness in life. May they be inspired and tireless in their own pursuits of the stars. Having asked me repeatedly "Daddy, when will you finish?" I owe the completion of this work to their infinite charm and persuasion.

You two are my world.

ACKNOWLEDGMENTS

First and foremost, I would like to thank Dr. Albert Luo. For the depth of knowledge and life philosophy he has bestowed on me, I am forever grateful and indebted. Furthermore, this work was strictly made possible by the teachings and guidance of Dr. Luo. From his breakthrough research on discontinuous dynamical systems, a simplified but incredibly realistic mechanical model was achieved for train suspension. For both helping with the completion of this work and new insights into the rule of mathematics, I owe special thanks to Dr. Chunqing Lu. I would also like to thank my thesis advisory committee members: Dr. Fengxia Wang, Dr. Philip Chu, Dr. Om Agrawal, and Dr. Mohammed Sayeh. And to Amsted Rail for initiating this project and providing useful tips and help to yield a more accurate mechanical model.

For the unyielding support throughout my life and, in particular, during my PhD study, I thank my parents Daniel and Lois O'Connor. Through endless homemade pies and hours of babysitting, they have afforded me the time and peace of mind to complete this work. And to my brothers and many friends, who distracted, encouraged, and helped me along the way, thank you all.

TABLE OF CONTENTS

LIST OF TABLES

LIST OF FIGURES

CHAPTER I

INTRODUCTION

In this chapter, a literature review of research on train suspension systems describes the approaches and progress made in the work of modeling and understanding such systems. While considerable advancements have been made in passenger train suspension systems, far less developments have been realized in freight train suspension systems. Herein, a mechanical model of the freight train suspension system is introduced for investigation. Through this model, the dynamic behaviors of the current suspension system may be better understood and improvements to the overall system realized.

1.1 Bibliography

Train suspension systems are for the comfort and stability of train locomotion, and an effective suspension system is necessary for safety and reliability. With the advancements in control theory and suspension technology, significant improvements have been made for passenger trains. Shieh et al. (2005) developed the optimal control to the passive suspension system of the light rail train using evolution algorithms. A train model with nine degrees of freedom was introduced and a stochastic optimization algorithm was used to optimize the suspension system parameters. Gottzein & Lange (1975) modeled the wheel-less high-speed passenger train to design the magnetic levitation suspension system. For the riding comfort of trains, Wu & Yang (2003) investigated the dynamic responses of trains moving over simply supported bridges through the development of a mechanical model including impact. Sayyaadi & Shokouhi (2009) introduced a system with seventy degrees of freedom for the rail-vehicle

suspension including a nonlinear air-spring damper. Experimental studies showed the effectiveness of the suspension system and the relevance of the mechanical model. Other research has considered the environmental impact of moving trains. Karlstrom (2006) developed an analytical model for the train-induced ground vibrations and simulated the vibration responses at various train speeds. Using a finite element approach, Ju & Lin (2008) investigated the ground vibration from high-speed trains and compared the results with experimental measurements.

On the other hand, less advancement has been attained for the suspension system of freight trains. Indeed, the ubiquitous wedge based friction-damped suspension system for heavy haul freight trains has not been changed too much in the past century while speed and cargo demands have increased greatly. The freight train suspension system uses friction damping in which pairs of wedges perform a force transmission of the track disturbance onto the side frame wall of the train undercarriage. Gardner & Cusumano (1997) discussed the differences between the variable-damping and constant-damping friction wedge model as well as the wedge model used in the dynamic train simulator software NUCARS®. Kaiser et al. (2002) considered a piecewise smooth wedge model with dry friction and gave parameter studies focused on the slip-stick phenomena. In that model, the wedge and bolster remain in contact, and periodic motions were found through numerical and harmonic balance methods. The separation of the wedges and bolster with the directional change of the friction is allowed, and the train suspension system can be investigated with a piecewise linear model including friction and impact.

The impacts between two masses in the train suspension system are similar to the dynamics of gear transmission. Herein, the gear dynamics is reviewed herein to help us work on the dynamics of train suspension systems. For instance, Pfeiffer (1984) presented an impact model to investigate dynamics of gear transmissions, and the regular and chaotic motions in the gear box

were investigated in Karagiannis & Pfeiffer (1991). One also used a piecewise linear model to investigate the dynamics of gear transmission systems (e.g., Comparin & Singh, 1989; Theodossiades & Natsiavas, 2000). To model vibrations in gear transmission systems, Luo & Chen (2005) used an impact model of two oscillators, and the local singularity theory in Luo (2005) was used for grazing and chaotic motions. Luo & O'Connor (2009) discussed the mechanism of impacting chatter with stick, and the analytical prediction of periodic chatter with and without stick was completed. The train suspension system is a dynamical system of three bodies with impact and frictions. One worked on nonlinear dynamics of two systems connected with the friction for many years. For instance, Hundal (1979) examined the response of a base excited system with Coulomb and viscous friction, and Feeny (1992) studied a non-smooth Coulomb friction oscillator. Shaw & Holmes (1983) studied nonlinear dynamics of a piecewise linear oscillator, and Shaw (1986) investigated a piecewise linear oscillator with dry friction. Luo & Gegg (2006) developed the stick and non-stick force criteria for the friction induced oscillator. Combining the friction and impact phenomena, Hinrichs et al. (1997) investigated the dynamics of a system undergoing friction as well as impact. An experimental investigation of stick-slip dynamics in a friction wedge damper was carried out in Chandiramani et al. (2006).

In this paper, a simple model for the train suspension system will be presented. The bolster and two wedges will be considered to be independent, and impacts between the wedge and bolster occur at different locations. When sticking together, the combined wedge and bolster system will experience friction. This train suspension system with friction and impact will be modeled. Following the ideas of Luo & O'Connor (2009), the global nonlinear behaviors of such a suspension system will be discussed and parameter maps will be presented. Numerical illustrations will be given for parameter characteristics of impacting chatter with/without stick for

the train suspension system. The theory for discontinuous dynamical systems can be found from Luo (2009) and (2012).

1.2 Physical Model

To model the freight train suspension system, consider the general configuration of the train suspension system, as shown in Figure 1.1. A major bracket known as the bolster is anchored to the bottom of the train. The bolster rests within the side arm on a set of springs and a pair of wedges. The wedges create friction dampening as they are pressed down and against the wall of the side arm. Since the tracks may not be perfectly level, the track is described by the curve underneath the wheels. Note, each train car has two complete sets of the suspension system described in Figure 1.1. Further, due to symmetry, only one side of the suspension system is shown.

Consider a periodically forced oscillator acted upon by a pair of secondary oscillators, as shown in Figure1.2. The primary mass represents the bolster on the train suspension system, while the pair of secondary masses represents the wedges used for the friction damping. Interaction between the bolster and wedges causes impacting and sticking together. When
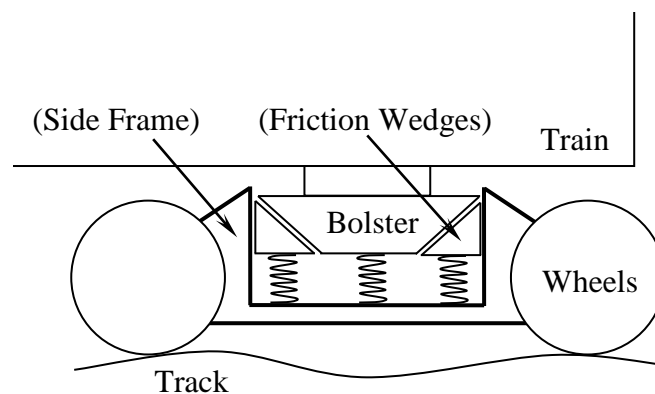
Figure 1.1. A mechanical description of freight train suspension.
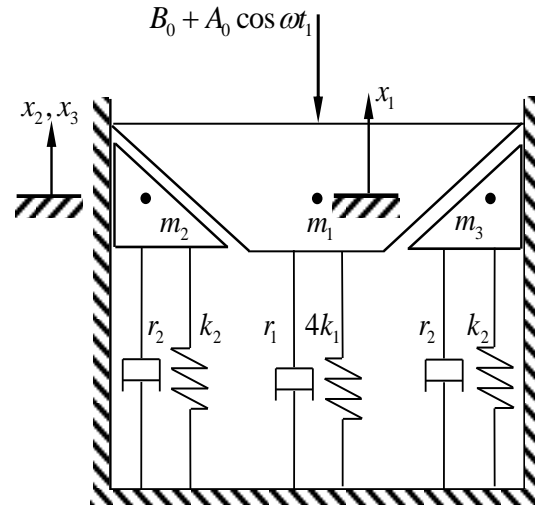
Figure 1.2. A mechanical model for a train suspension system.

sticking occurs, the pressure between the combined systems creates a normal force against the wall surface. This causes a friction force, with coefficient μ_k, that resists the train movement. Each mass m_i $(i = 1, 2)$ connected a spring and a damper. The spring stiffness k_i is from the actual spring, and the damper damping r_i is from internal friction loss in the spring. The external force $B_0 + A_0 \cos \Omega t$ acts on the bolster m_1 where A_0 and Ω are the amplitude and frequency of the truck inertial force input, respectively. B_0 is from the constant load. The displacements of each mass measured from their equilibriums are expressed by $x^{(1)}$, $x^{(2)}$, and $x^{(3)}$. Impacts between oscillators are oblique and described through the impact law with restitution coefficient e.

1.3 Objectives

In this thesis, the freight train suspension system will be modeled by a piecewise linear system with impacts. From the theory of discontinuous dynamical systems, the mechanism of

impacting chatter with stick and stuck will be investigated, and the onset and vanishing conditions of such motions will be developed. The condition for maintaining stick and stuck motion in such a suspension system will be discussed. Motion mappings will be introduced first based on the separation boundaries, and then from the basic mappings, the mapping structures will be developed for periodic motions. Further, the analytical prediction of periodic motions pertaining to impacting chatter with stick and stuck can be completed, and the corresponding local stability and bifurcation of the periodic motion will be analyzed. Analytical conditions will be employed to complete the bifurcation analysis, and numerical simulations will be carried out for illustration of periodic motions and stick criteria.

1.4 Layout

To begin, this thesis conducts a literature survey on related and pertinent works of train suspension systems. Also, a mechanical model for train suspension is developed based on a simplification of the said mechanical system. In Chapter 2, a mathematical description of the train suspension system will be given. Additionally, the equations of motion based on the absolute and relative frames will be developed on the different domains. In Chapter 3, the stick, stuck, and grazing criteria for such a suspension system will be derived from the singularity theory of discontinuous systems on the boundary. In chapter 4, the basic mappings will be introduced for developing the mapping structure of periodic motion. Based on the mapping structure, the periodic motion can be predicted analytically. The corresponding stability and bifurcation analysis will be carried out in Chapter 5. For illustration of the analytical conditions, the displacement response, velocity response, and phase planes of periodic motions in such a suspension system will be presented. In Chapter 6, field data from *Amsted Rail* is implemented

to consider realistic suspension parameters. In addition, an investigation into wedge angle influence of system response through analytical prediction will be conducted. Finally, in Chapter 7 the summary of this thesis project will be given.

1.5 Significance of Research

The simplified train suspension model in Figure 1.2 is investigated in order to better understand the vibration and dynamic phenomena experienced during train locomotion. More specifically, the suspension system discussed herein is investigated so that the underlying behavioral characteristics of train suspension can be identified and controlled to avoid derailment or unsafe vibration. Parametric investigations will provide insights into motion mechanisms for impacting chatter with stick and stuck motion. Moreover, the analytical conditions of such motion phenomena may provide efficient methods to catch the motion switching, and this will give a good physical interpretation of vibration in such a train suspension system. An investigation into the influence of wedge angle can help design future suspension systems to avoid undesirable suspension behavior. Finally, with such a mechanical model, vibration and dynamic behavior of the train can be adjusted through the operating conditions and a better performance may be achieved.

CHAPTER II

MECHANICAL MODEL

In this chapter, the mathematical model of the freight train suspension system described in Chapter 1 will be developed. From Newton's laws, the equations of motion are introduced to describe the different types of motion. Based on the regions for each type of motion, domains and their respective boundaries will be defined. Importantly, the boundaries represent a discontinuity and must be considered carefully to determine how motion may interact in such proximity. To this end, the corresponding state variables for the equations of motion in the absolute and relative reference frames will be defined and boundaries described mathematically.

2.1 Equations of Motion

To obtain equations of motion for the train suspension systems, a free body diagram (FBD) of the wedge and bolster is considered when not in contact. Due to symmetry, the FBD of the bolster and the left wedge is given in Figure 2.1. Positive displacement is measured vertically upward by x_1 and x_2. The spring and damping force are described through the spring stiffness and damping coefficient k_i and r_i for ($i = 1, 2$), respectively. The wedge angle is given by θ. Summation of the forces in Newton's second law yields the following equations of motion for
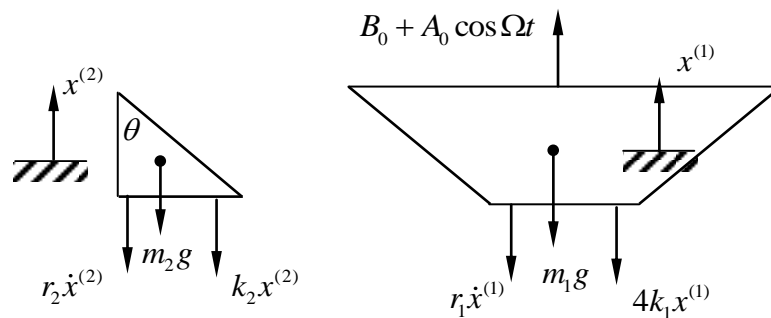
Figure 2.1. Free body diagram of wedge and bolster not in contact.

the wedge and bolster while not in contact, which is called the free flight motion.

$$\ddot{x}_\alpha^{(i)} + 2\zeta_\alpha^{(i)}\dot{x}_\alpha^{(i)} + (\omega_\alpha^{(i)})^2 x_\alpha^{(i)} = b_\alpha^{(i)} + Q_\alpha^{(i)}\cos\Omega t \tag{1}$$

where $\dot{x}_\alpha^{(i)} = dx_\alpha^{(i)}/dt$ and for $\alpha = 1$

$$\left.\begin{array}{l} \zeta_1^{(i)} = \dfrac{r_i}{2m_i}\,(i=1,2,3),\ \omega_1^{(1)} = \sqrt{\dfrac{4k_1}{m_1}}, \\[2mm] b_1^{(1)} = \dfrac{1}{m_1}(-m_1 g + B_0), b_1^{(i)} = -g, \\[2mm] \omega_1^{(i)} = \sqrt{\dfrac{k_i}{m_i}},\ Q_1^{(i)} = 0\,(i=2,3),\ Q_1^{(1)} = \dfrac{A_0}{m_1}, \end{array}\right\} \tag{2}$$

Herein, the position, velocity, and acceleration of the two wedges are assumed identical

(i.e., $x^{(2)} = x^{(3)}$, $\dot{x}^{(2)} = \dot{x}^{(3)}$, $\ddot{x}^{(2)} = \ddot{x}^{(3)}$) for the mechanical model in Figure 2.1. For

$|x_1^{(1)} - x_1^{(2)}| = 0$, an impact between the bolster and two wedges occurs. Since the springs are

unable to support bending moment and the side wall does not allow horizontal movement, the

impact between the wedge and bolster is assumed to take place vertically with direct impact.

From momentum conservation and the simple impact law, velocities of the bolster and wedge

after impacting are

$$\left.\begin{array}{l} \dot{x}_1^{(1)+} = I_1^{(1)}\dot{x}_1^{(1)-} + I_2^{(1)}\dot{x}_1^{(2)-}, \\[1mm] \dot{x}_1^{(2)+} = I_1^{(2)}\dot{x}_1^{(1)-} + I_2^{(2)}\dot{x}_1^{(2)-}, \\[1mm] \dot{x}_1^{(3)\pm} = \dot{x}_1^{(2)\pm}. \end{array}\right\} \tag{3}$$

where the superscripts "-" and "+" represent before and after impact, and the corresponding

coefficients are

$$\left.\begin{array}{l} I_1^{(1)} = \dfrac{m_1 - 2m_2 e}{m_1 + 2m_2},\ I_2^{(1)} = \dfrac{2(1+e)m_2}{m_1 + 2m_2}, \\[2mm] I_1^{(2)} = \dfrac{(1+e)m_1}{m_1 + 2m_2},\ I_2^{(2)} = \dfrac{2m_2 - em_1}{m_1 + 2m_2}. \end{array}\right\} \tag{4}$$
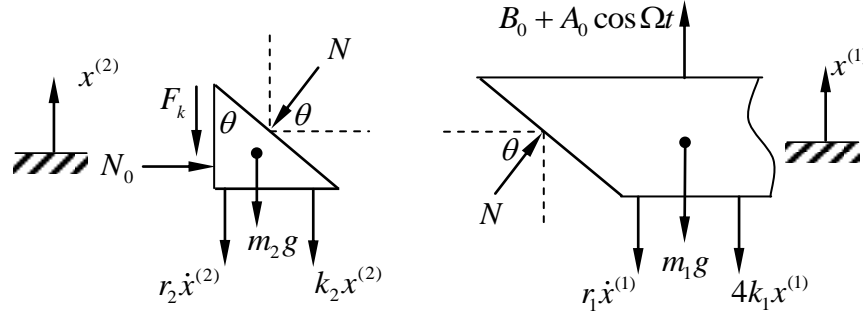
Figure 2.2. Free body diagram of wedge and bolster in contact.

Consider the wedge and bolster to remain in contact, which is called the stick motion. The free body diagram for this scenario is given in Figure 2.2. The normal force N is the contact force between the wedge and bolster. Herein, it is assumed that the wedge and bolster make a point contact and no slipping occurs. Subsequently any friction force acting between the wedge and bolster can be neglected. However, as a result of the wedge angle θ, there is an additional normal force N_0 defining the contact force between the side wall and wedge. This normal force creates a kinetic friction force F_f as defined in Eq.(5).

$$F_f(\dot{x}_2) \begin{cases} = \mu_k N_0 & \dot{x}_2 \in [0, \infty), \\ \in [-\mu_k N_0, \mu_k N_0] & \dot{x}_2 = 0, \\ = -\mu_k N_0 & \dot{x}_2 \in (-\infty, 0]. \end{cases} \tag{5}$$

Further, the normal force N_0 is related to the normal force N, i.e.,

$$N_0 = N \cos\theta. \tag{6}$$

The total forces in Figure 2.2 with Eqs.(5) and (6), the equations of motion for the combined mass system for $i = 1, 2$ and $\alpha = 2, 3$ is given by

$$\ddot{x}_\alpha^{(i)} + 2\zeta_\alpha^{(i)} \dot{x}_\alpha^{(i)} + (\omega_\alpha^{(i)})^2 x_\alpha^{(i)} = b_\alpha^{(i)} + Q_\alpha^{(i)} \cos\Omega t \tag{7}$$

where

$$\zeta_\alpha^{(i)} = \frac{r_1 + \Delta_s r_2}{m_1 + \Delta_s m_2}, \ \omega_\alpha^{(i)} = \sqrt{\frac{4k_1 + \Delta_s k_2}{m_1 + \Delta_s m_2}}, \ Q_\alpha^{(i)} = \frac{A_0}{m_1 + \Delta_s m_2},$$
$$b_\alpha^{(i)} = \frac{-(m_1 + \Delta_s m_2)g + B_0}{m_1 + \Delta_s m_2}, \ \Delta_s = \frac{2\sin\theta}{\sin\theta + \mu_k \cos\theta \, \mathrm{sgn}(\dot{x}_\alpha^{(2)})}.$$

(8)

Region $\alpha = 2$ is used to describe stick motion with positive velocity (i.e., $\dot{x}_\alpha^{(1)} > 0$) while region

$\alpha = 3$ is used to describe the stick motion with negative velocity (i.e., $\dot{x}_\alpha^{(1)} < 0$). From a physics

point of view, the normal force between the wedge and bolster indicates the respective internal

force between the bolster and wedge. Such an internal force requires that the wedge and bolster

remain in contact. From Eqs.(1) and (7), the normal force is given by

$$N_\alpha^{(1)} = \frac{m_1 \ddot{x}_\alpha^{(1)} + r_1 \dot{x}_\alpha^{(1)} + 4k_1 x_\alpha^{(1)} + m_1 g - B_0 - A_0 \cos\Omega t}{2\sin\theta},$$
$$N_\alpha^{(2)} = \frac{-m_2 \ddot{x}_\alpha^{(2)} - r_2 \dot{x}_\alpha^{(2)} - k_2 x_\alpha^{(2)} - m_2 g}{\sin\theta + \mu_k \cos\theta \, \mathrm{sgn}(\dot{x}_\alpha^{(2)})}.$$

(9)

For $\alpha = 2$, we have $\dot{x}_\alpha^{(2)} > 0$. So $\mathrm{sgn}(\dot{x}_\alpha^{(2)}) = 1$. For $\alpha = 3$, we have $\dot{x}_\alpha^{(2)} < 0$. So $\mathrm{sgn}(\dot{x}_\alpha^{(2)}) = -1$.

From the Newton's third law, we have

$$N_\alpha^{(1)} = -N_\alpha^{(2)} \equiv N_\alpha = N$$

(10)

and

$$x_\alpha^{(1)} = x_\alpha^{(2)} \equiv x_\alpha, \ \dot{x}_\alpha^{(1)} = \dot{x}_\alpha^{(2)} \equiv \dot{x}_\alpha, \text{ and } \ddot{x}_\alpha^{(1)} = \ddot{x}_\alpha^{(2)} \equiv \ddot{x}_\alpha$$

(11)

For a better understanding of equation of motion, equation (7) also can be written as

$$\ddot{x}_\alpha^{(i)} + 2\bar{\zeta}_\alpha^{(i)} \dot{x}_\alpha^{(i)} + (\bar{\omega}_\alpha^{(i)})^2 x_\alpha^{(i)} = \bar{b}_\alpha^{(i)} + \bar{Q}_\alpha^{(i)} \cos\Omega t - 2\mu_k \bar{N}_\alpha \cos\theta \, \mathrm{sgn}(\dot{x}_\alpha^{(i)})$$

(12)

where
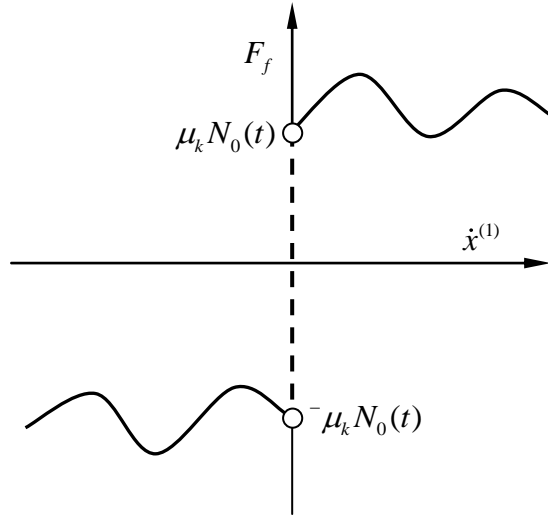
Figure 2.3. Friction model varying with time.

$$\left. \begin{array}{l} \overline{\zeta}_\alpha^{(i)} = \dfrac{r_1 + 2r_2}{m_1 + 2m_2}, \ \overline{\omega}_\alpha^{(i)} = \sqrt{\dfrac{4k_1 + 2k_2}{m_1 + 2m_2}}, \ \overline{N}_\alpha = \dfrac{N_\alpha}{m_1 + 2m_2} \\ \overline{Q}_\alpha^{(i)} = \dfrac{A_0}{m_1 + 2m_2}, \ \overline{b}_\alpha^{(i)} = \dfrac{-(m_1 + 2m_2)g + B_0}{m_1 + 2m_2}. \end{array} \right\} \tag{13}$$

The normal force N_α can be computed from Eqs. (9)–(11). Since the normal force between the

wedge and bolster may vary with time, the force of friction is also a function of time. To

illustrate this, the friction force in Eq.(5) is shown in Figure 2.3. In physics, the normal force is

actually the internal force that keeps the bolster and wedge together, the vanishing of stick

motion vanishing requires for $i = 1, 2$

$$N^{(i)} = N = 0. \tag{14}$$

Consequently, the stick condition for the three oscillators is given for $i = 1, 2$ and $\alpha = 2, 3$

$$N^{(i)} = N > 0. \tag{15}$$

In the region of $\alpha = 1$, the bolster and wedge do not interfere with each other, so $N_\alpha^{(i)} = 0$ holds

always. Finally, if the friction force acting on the combined mass system is greater than or equal

to the resultant dynamic forces, then the bolster and wedges will become "stuck" against the side wall. In other words, the wedge with bolster does not move.

2.2 Absolute Motions

The bolster and pair of wedges represent a discontinuous system because of their possible impacts and the friction force acting on the wedges. Accordingly, the vector fields for each oscillator are discontinuous. Consider the free-flight region described earlier as $\alpha = 1$. For $(i, \bar{i} \in \{1,2\}$ and $i \neq \bar{i}$), domain $\Omega_1^{(i)}$ in phase plane for free-flight motion is defined as

$$\Omega_1^{(i)} = \left\{ (x^{(i)}, \dot{x}^{(i)}) \middle| x^{(i)} \in (x_1^{(\bar{i})}(t_m), \infty), t_m \in (0, \infty) \right\} \tag{16}$$

Since the bolster and wedge displacements are changing with time, $x_1^{(\bar{i})}(t_m)$ describes the lower bound for $x_1^{(i)}$ where t_m is the impact time. The boundary $\partial \Omega_{1\infty}^{(i)}$ of the domain $\Omega_1^{(i)}$ is defined as

$$\partial \Omega_{1\infty}^{(i)} = \left\{ (x^{(i)}, \dot{x}^{(i)}) \middle| \begin{array}{l} \varphi_{1\infty}^{(i)} \equiv x^{(i)} - x_1^{(\bar{i})}(t_m) = 0 \\ \dot{x}^{(i)} \neq \dot{x}_1^{(\bar{i})}(t_m), t_m \in (0, \infty) \end{array} \right\} \tag{17}$$

which is a non-passable boundary or infinite flow barrier. In Figure 2.4, the shaded region is the domains for the free-fright motion. The dash dot curve is the boundary $\partial \Omega_{1\infty}^{(i)}$, which is instantaneous at time t_m with the vertical dotted lines. In Figure 2.4(a), the domain and boundary for the free-flight motion of the bolster is presented. The domain lies on the right side of the boundary relative to the wedges. Since the wedges are below the bolster, the domain and boundary for the free-flight motion of wedges are presented in Figure 2.4(b), and the domain lies on the left side of the boundary relative to the bolster.
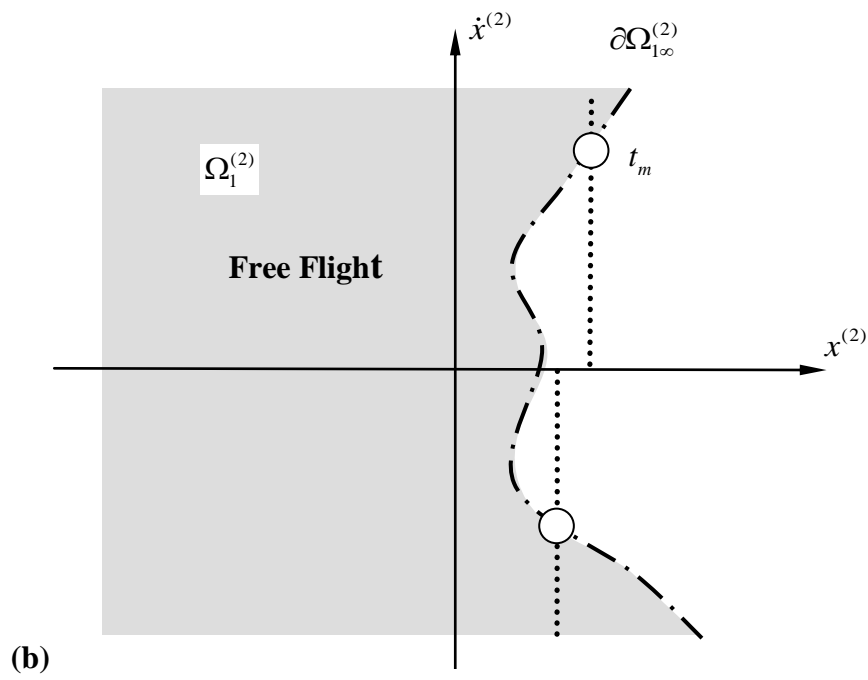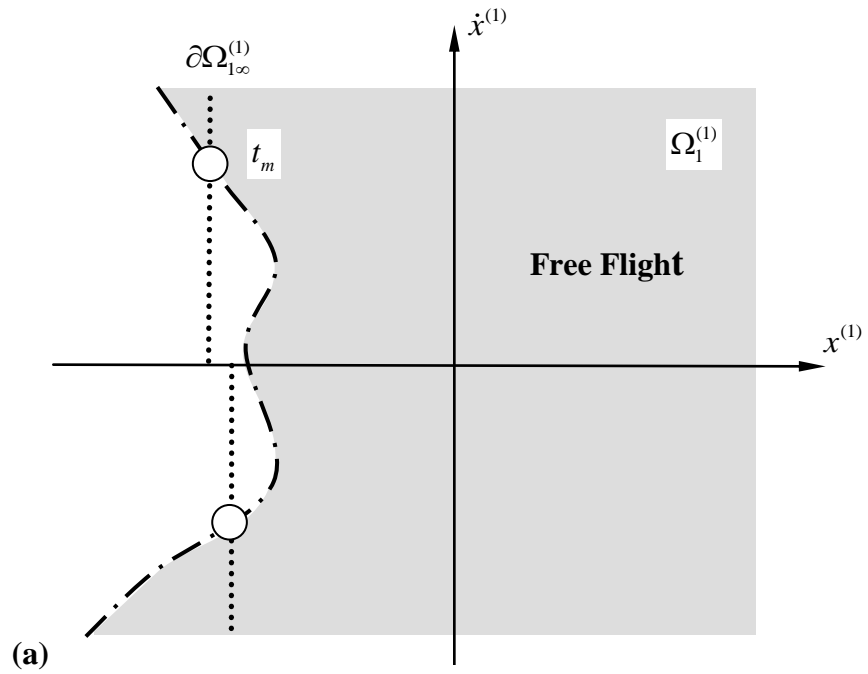
Figure 2.4. Free-flight domain and boundary: (a) bolster and (b) wedges.

Consider the regions ($\alpha = 2, 3$) for stick motion when the bolster and wedges are sticking

together. The domains $\Omega_2^{(i)}$ and $\Omega_3^{(i)}$ in phase plane are for stick motion with frictional force. In

domain $\Omega_2^{(i)}$, the velocity of the combined system is positive, so the frictional force acts in the

negative direction. However, in domain $\Omega_3^{(i)}$, the friction force acts in the positive direction.

$$\Omega_2^{(i)} = \left\{ (x^{(i)}, \dot{x}^{(i)}) \left| \begin{array}{l} x^{(i)} \in (-\infty, \infty),\ \dot{x}_2^{(i)} = \dot{x}_2^{(\bar{i})} \\ \dot{x}^{(i)} \in (0, \infty) \end{array} \right. \right\},$$

$$\Omega_3^{(i)} = \left\{ (x^{(i)}, \dot{x}^{(i)}) \left| \begin{array}{l} x^{(i)} \in (-\infty, \infty),\ \dot{x}_2^{(i)} = \dot{x}_2^{(\bar{i})} \\ \dot{x}^{(i)} \in (-\infty, 0) \end{array} \right. \right\}. \tag{18}$$

Herein $\bar{\Omega}_\alpha^{(i)}$ is defined as the closure of $\Omega_\alpha^{(i)}$ ($i = 1, 2$) and ($\alpha = 2, 3$). The corresponding

separation boundaries $\partial \Omega_{23}^{(i)}$ and $\partial \Omega_{32}^{(i)}$ for the stick motion are defined as for positive and

negative displacement, respectively.

$$\partial \Omega_{23}^{(i)} = \bar{\Omega}_2^{(i)} \cap \bar{\Omega}_3^{(i)} = \left\{ (x^{(i)}, \dot{x}^{(i)}) \left| \begin{array}{l} x^{(i)} - x^{(\bar{i})} = 0,\ x^{(i)} > 0 \\ \varphi_{23}^{(i)} \equiv \dot{x}^{(i)} = 0 \end{array} \right. \right\},$$

$$\partial \Omega_{32}^{(i)} = \bar{\Omega}_2^{(i)} \cap \bar{\Omega}_3^{(i)} = \left\{ (x^{(i)}, \dot{x}^{(i)}) \left| \begin{array}{l} x^{(i)} - x^{(\bar{i})} = 0,\ x^{(i)} < 0 \\ \varphi_{32}^{(i)} \equiv \dot{x}^{(i)} = 0 \end{array} \right. \right\}. \tag{19}$$

In Figure 2.5, the hatched regions are for $\Omega_2^{(i)}$ and $\Omega_3^{(i)}$ ($i = 1, 2$), define the region of stick

motion with positive and negative velocity, respectively. Since the bolster wall is considered as

the fixed inertial reference frame, the velocity boundary separating $\Omega_2^{(i)}$ and $\Omega_3^{(i)}$ is at $\dot{x}^{(i)} = 0$

and is represented by the dotted line. The vertical arrows drawn across the boundary show the

direction of the motion flow. For $i = 1$, the domains for the bolster are presented in Figure 2.5(a).

For $i = 2$, the domain for the wedges are presented in Figure 2.5(b). For the stick motion, the

bolster and wedges are together to form a new oscillator. Thus, the domains and boundary are

same.
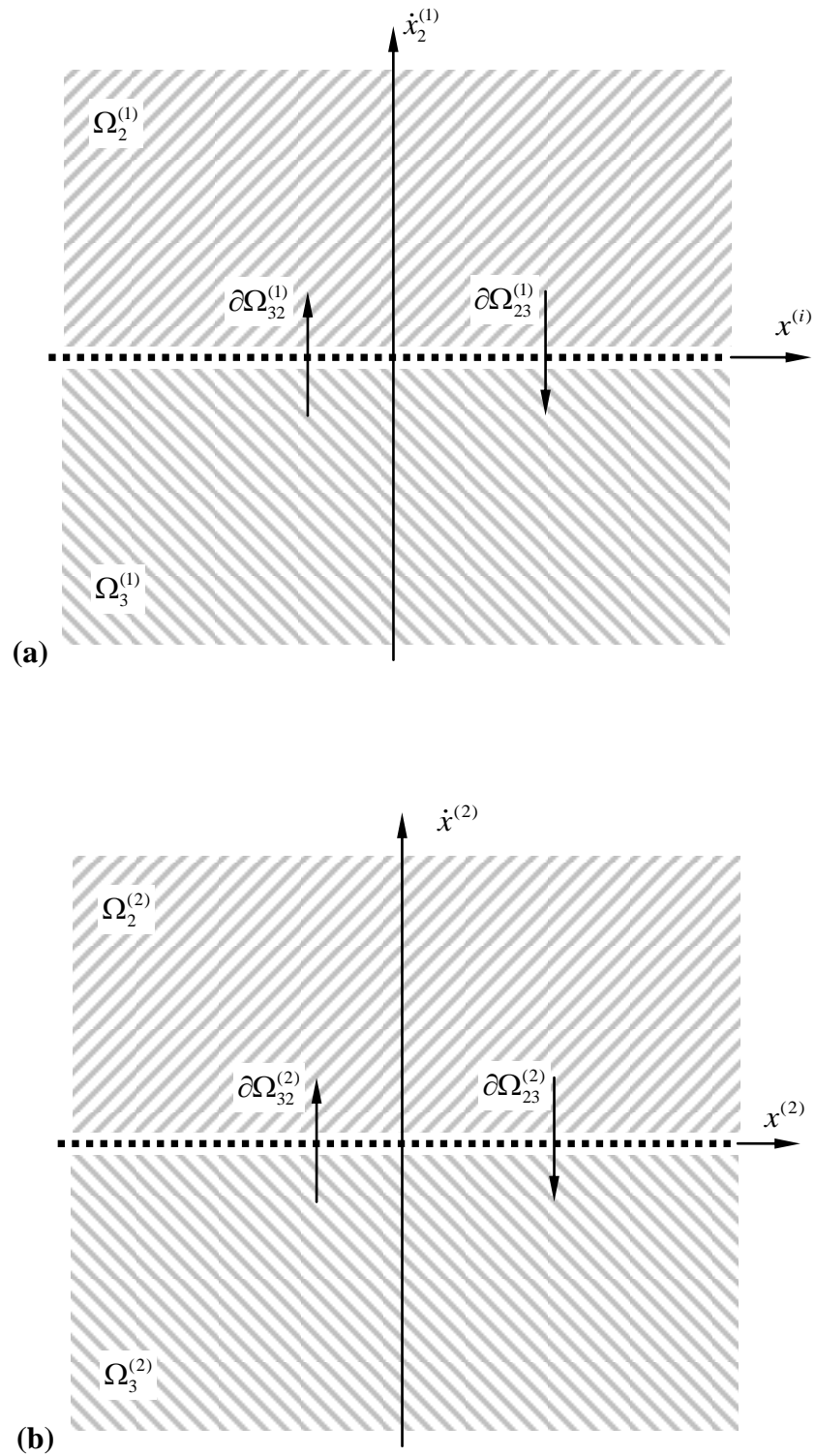
Figure 2.5. Phase plane domains and boundaries for stick motion: (a) bolster and (b). wedges.

The bolster and two wedges may undergo free-flight motion with impacts and stick motion,

From Eq.(18), the displacement for stick domains $\Omega_2^{(i)}$ and $\Omega_3^{(i)}$ was defined for $x^{(i)} \in (-\infty, \infty)$

$(i = 1, 2)$. The free-flight domain has a displacement $x^{(i)} \in (x_2^{(\bar{i})}(t_m), \infty)$ and the two stick

domains require $x^{(i)} \in (-\infty, x_2^{(\bar{i})}(t_m))$. The domain partition of the mixed free flight and stick

motion is related to $x_1^{(\bar{i})}(t_m)$, and the location of the $\bar{i}^{th}$ oscillator is at switching time t_m. The

domains for the mixed free flight and stick motion are defined as

$$
\Omega_1^{(i)} = \left\{ (x^{(i)}, \dot{x}^{(i)}) \middle| \begin{array}{l} x^{(i)} \in (x_1^{(\bar{i})}(t_m), \infty) \\ t_m \in (0, \infty) \end{array} \right\},
$$

$$
\Omega_2^{(i)} = \left\{ (x^{(i)}, \dot{x}^{(i)}) \middle| \begin{array}{l} x^{(i)} \in (-\infty, x_2^{(\bar{i})}(t_m)), \ \dot{x}_2^{(i)} = \dot{x}_2^{(\bar{i})} \\ \dot{x}^{(i)} \in (0, \infty) \end{array} \right\}, \tag{20}
$$

$$
\Omega_3^{(i)} = \left\{ (x^{(i)}, \dot{x}^{(i)}) \middle| \begin{array}{l} x^{(i)} \in (-\infty, x_2^{(\bar{i})}(t_m)), \ \dot{x}_2^{(i)} = \dot{x}_2^{(\bar{i})} \\ \dot{x}^{(i)} \in (-\infty, 0) \end{array} \right\}.
$$

The corresponding boundaries for the mixed motion domains are defined as

$$
\partial \Omega_{21}^{(i)} = \bar{\Omega}_1^{(i)} \cap \bar{\Omega}_2^{(i)} = \left\{ (x^{(i)}, \dot{x}^{(i)}) \middle| \begin{array}{l} x^{(i)} - x_1^{(\bar{i})} = 0 \\ \varphi_{21}^{(i)} \equiv \dot{x}^{(i)} - \dot{x}_1^{(\bar{i})} = 0 \end{array} \right\},
$$

$$
\partial \Omega_{31}^{(i)} = \bar{\Omega}_1^{(i)} \cap \bar{\Omega}_3^{(i)} = \left\{ (x^{(i)}, \dot{x}^{(i)}) \middle| \begin{array}{l} x^{(i)} - x_1^{(\bar{i})} = 0 \\ \varphi_{31}^{(i)} \equiv \dot{x}^{(i)} - \dot{x}_1^{(\bar{i})} = 0 \end{array} \right\},
$$

$$
\partial \Omega_{23}^{(i)} = \bar{\Omega}_2^{(i)} \cap \bar{\Omega}_3^{(i)} = \left\{ (x^{(i)}, \dot{x}^{(i)}) \middle| \begin{array}{l} x^{(i)} - x^{(\bar{i})} = 0 \\ \varphi_{23}^{(i)} \equiv \dot{x}^{(i)} = 0 \end{array} \right\}, \tag{21}
$$

$$
\partial \Omega_{32}^{(i)} = \bar{\Omega}_2^{(i)} \cap \bar{\Omega}_3^{(i)} = \left\{ (x^{(i)}, \dot{x}^{(i)}) \middle| \begin{array}{l} x^{(i)} - x^{(\bar{i})} = 0 \\ \varphi_{32}^{(i)} \equiv \dot{x}^{(i)} = 0 \end{array} \right\}.
$$

For these boundaries, under certain conditions, the motion can pass through the boundary from

one domain to an adjacent domain (i.e., the oscillators can enter the regions of stick motion). No

transport law is needed for motion continuity. The domains of the mixed motion are sketched in
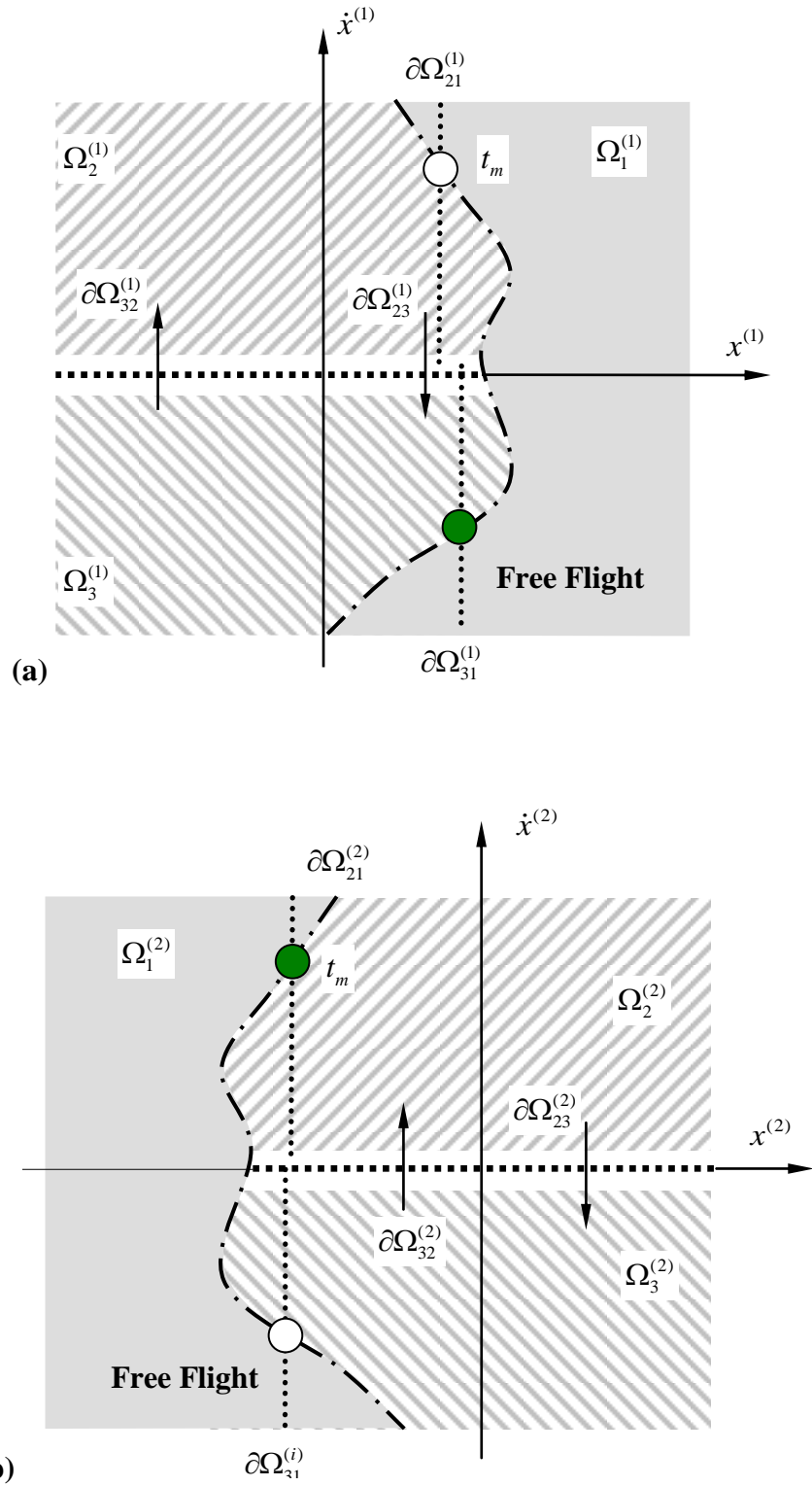
Figure 2.6. Phase plane domains for mixed free-flight and stick motion: (a) bolster and (b) wedge.

Figure 2.6(a) and (b) for the bolster and wedges, respectively. The domain $\Omega_1^{(i)}$ ($i=1,2$) for the flight motion of the bolster is represented by the shaded region, and two domains for stick motions are represented by the two hatched regions, labeled as $\Omega_2^{(i)}$ and $\Omega_3^{(i)}$ ($i=1,2$). Again, the dotted line at $\dot{x}^{(i)}=0$ ($i=1,2$) represents the velocity boundary for wedges' friction with side walls. The boundaries for the onset and vanishing of stick motion are sketched by the dash-dot line, and the switching times t_m mark the locations for the appearance and disappearance of stick motions. The hollow and solid circular symbols represent the starting and ending of stick motion, respectively.

In the absolute reference frame, the following vectors are introduced as

$$
\begin{aligned}
\mathbf{x}_\alpha^{(i)} &= (x_\alpha^{(i)}, \dot{x}_\alpha^{(i)})^T = (x_\alpha^{(i)}, y_\alpha^{(i)})^T, \\
\mathbf{F}_\alpha^{(i)} &= (\dot{x}_\alpha^{(i)}, F_\alpha^{(i)})^T = (y_\alpha^{(i)}, F_\alpha^{(i)})^T.
\end{aligned}
\tag{22}
$$

With Eq.(22), equations of motion for free-fright motion in Eq.(1) and stick motion in Eq.(7) can be represented for as

$$
\dot{\mathbf{x}}_\alpha^{(i)} = \mathbf{F}_\alpha^{(i)}(\mathbf{x}_\alpha^{(i)}, t) \quad \text{for } \alpha = 1,2,3 \text{ and } i=1,2
\tag{23}
$$

where

$$
F_\alpha^{(i)} = -2\zeta_\alpha^{(i)}\dot{x}_\alpha^{(i)} - (\omega_\alpha^{(i)})^2 x_\alpha^{(i)} + b_\alpha^{(i)} + Q_\alpha^{(i)}\cos\Omega t
\tag{24}
$$

and the superscript "i" represents the ith mass and the subscript "α" represents the α-domain. For the boundary $\partial\Omega_{1\infty}$, the flow cannot pass through the boundary, thus the impact chatter will occurs. For the boundary $\partial\Omega_{1\beta}$ ($\beta=2,3$), the flow will pass through the boundary from domain Ω_1 to domain Ω_2 or from domain Ω_3 to domain Ω_1. On the boundary $\partial\Omega_{23}$, there is sliding motion.

$$\dot{\mathbf{x}}_0^{(i)} = \mathbf{F}_0^{(i)}(\mathbf{x}_0^{(i)}, t) \quad \text{for } \alpha, \beta = 2, 3 \text{ and } i = 1, 2 \tag{25}$$

where

$$F_0^{(i)} = 0 \quad \text{for stick}$$
$$F_0^{(i)} \in [-2\mu_k \bar{N}_\alpha \cos\theta, 2\mu_k \bar{N}_\alpha \cos\theta] \quad \text{on boundary } \partial\Omega_{23} \tag{26}$$

2.3 Relative motion

Because the boundaries that separate free-flight and stick motion vary with time, the analytical conditions for the motion mechanisms of bolster and wedge interaction with a moving boundary is be difficult to be obtained. Hence, two relative variables are introduced herein as

$$z_\alpha^{(i)} = x_\alpha^{(i)} - x_{\bar{\alpha}}^{(\bar{i})} \quad \text{and} \quad v_\alpha^{(i)} = \dot{z}_\alpha^{(i)} = \dot{x}_\alpha^{(i)} - \dot{x}_{\bar{\alpha}}^{(\bar{i})}. \tag{27}$$

From the foregoing equation, the equations of motion are for $i, \bar{i} = 1, 2$ ($i \neq \bar{i}$) and $\alpha = 1, 2, 3$

$$\left.\begin{array}{l} \ddot{z}_\alpha^{(i)} + 2\zeta_\alpha^{(i)}\dot{z}_\alpha^{(i)} + (\omega_\alpha^{(i)})^2 z_\alpha^{(i)} = b_\alpha^{(i)} + Q_\alpha^{(i)}\cos\Omega t - \ddot{x}_\alpha^{(\bar{i})} - 2\zeta_\alpha^{(\bar{i})}\dot{x}_\alpha^{(\bar{i})} - (\omega_\alpha^{(\bar{i})})^2 x_\alpha^{(\bar{i})}, \\ \ddot{x}_\alpha^{(\bar{i})} + 2\zeta_\alpha^{(\bar{i})}\dot{x}_\alpha^{(\bar{i})} + (\omega_\alpha^{(\bar{i})})^2 x_\alpha^{(\bar{i})} = b_\alpha^{(\bar{i})} + Q_\alpha^{(\bar{i})}\cos\Omega t. \end{array}\right\} \tag{28}$$

In a similar fashion, two more vectors are introduced as follows.

$$\left.\begin{array}{l} \mathbf{z}_\alpha^{(i)} = (z_\alpha^{(i)}, \dot{z}_\alpha^{(i)})^T = (z_\alpha^{(i)}, v_\alpha^{(i)})^T \\ \mathbf{g}_\alpha^{(i)} = (\dot{z}_\alpha^{(i)}, g_\alpha^{(i)})^T = (v_\alpha^{(i)}, g_\alpha^{(i)})^T \end{array}\right\} \tag{29}$$

From Eqs.(28) and (29), the equations of motion become for $i = 1, 2$ and $\alpha = 1, 2, 3$

$$\left.\begin{array}{l} \dot{\mathbf{z}}_\alpha^{(i)} = \mathbf{g}_\alpha^{(i)}(\mathbf{z}_\alpha^{(i)}, \mathbf{x}_\alpha^{(\bar{i})}, t) \\ \dot{\mathbf{x}}_\alpha^{(\bar{i})} = \mathbf{F}_\alpha^{(\bar{i})}(\mathbf{x}_\alpha^{(\bar{i})}, t) \end{array}\right\} \tag{30}$$

where

$$g_\alpha^{(i)} = -2\zeta_\alpha^{(i)}\dot{z}_\alpha^{(i)} - (\omega_\alpha^{(i)})^2 z_\alpha^{(i)} + b_\alpha^{(i)} + Q_\alpha^{(i)}\cos\Omega t$$
$$-\ddot{x}_\alpha^{(\bar{i})} - 2\zeta_\alpha^{(i)}\dot{x}_\alpha^{(\bar{i})} - (\omega_\alpha^{(i)})^2 x_{\bar{\alpha}}^{(\bar{i})}. \tag{31}$$

Because the stick motion requires the relative motion to vanish between the wedge and bolsters,

the domains $\Omega_2^{(i)}$ and $\Omega_3^{(i)}$ become two points in relative phase space. In the relative frame, the

sub-domains in Eq.(17) can be expressed by

$$
\left.
\begin{aligned}
\Omega_1^{(i)} &= \left\{ (z^{(i)}, \dot{z}^{(i)}) \,\middle|\, z^{(i)} \in (0,\infty),\ \dot{z}^{(i)} \in (-\infty,\infty) \right\}, \\
\Omega_2^{(i)} &= \left\{ (z^{(i)}, \dot{z}^{(i)}) \,\middle\|\, z^{(i)} = 0,\ \dot{z}^{(i)} = 0 \right\}, \\
\Omega_3^{(i)} &= \left\{ (z^{(i)}, \dot{z}^{(i)}) \,\middle|\, z^{(i)} = 0,\ \dot{z}^{(i)} = 0 \right\}.
\end{aligned}
\right\}
\tag{32}
$$

In the relative frame, the impacting chatter boundaries in Eq.(14) become

$$
\partial\Omega_{1\infty}^{(i)} = \left\{ (z^{(i)}, \dot{z}^{(i)}) \,\middle|\, \varphi_{1\infty}^{(i)} \equiv z^{(i)} = 0 \right\}
\tag{33}
$$

Through their subsets, such boundary sets become

$$
\partial\Omega_{1\infty}^{(i)} = {}_+\partial\Omega_{1\infty}^{(i)} \cup {}_-\partial\Omega_{1\infty}^{(i)}
\tag{34}
$$

where

$$
\begin{aligned}
{}_+\partial\Omega_{1\infty}^{(i)} &= \left\{ (z^{(i)}, \dot{z}^{(i)}) \,\middle|\, \varphi_{1\infty}^{(i)} \equiv z^{(i)} = 0,\ \dot{z}^{(i)} \in (0,\infty) \right\}, \\
{}_-\partial\Omega_{1\infty}^{(i)} &= \left\{ (z^{(i)}, \dot{z}^{(i)}) \,\middle|\, \varphi_{1\infty}^{(i)} \equiv z^{(i)} = 0,\ \dot{z}^{(i)} \in (-\infty,0) \right\}.
\end{aligned}
\tag{35}
$$

The stick boundary become one points, which is expressed by

$$
\left.
\begin{aligned}
\partial\Omega_{32}^{(i)} &= \left\{ (z^{(i)}, \dot{z}^{(i)}) \,\middle|\, z^{(i)} = 0,\ \varphi_{23}^{(i)} \equiv \dot{z}^{(i)} = 0_+ \right\}, \\
\partial\Omega_{23}^{(i)} &= \left\{ (z^{(i)}, \dot{z}^{(i)}) \,\middle|\, z^{(i)} = 0,\ \varphi_{23}^{(i)} \equiv \dot{z}^{(i)} = 0_- \right\}.
\end{aligned}
\right\}
\tag{36}
$$

The boundaries in the relative frame are independent of time. The phase partitions in relative

phase space for the bolster and wedges are sketched in Figure 2.7(a) and (b), respectively. The

stick boundaries and domains are presented by the two large dots.
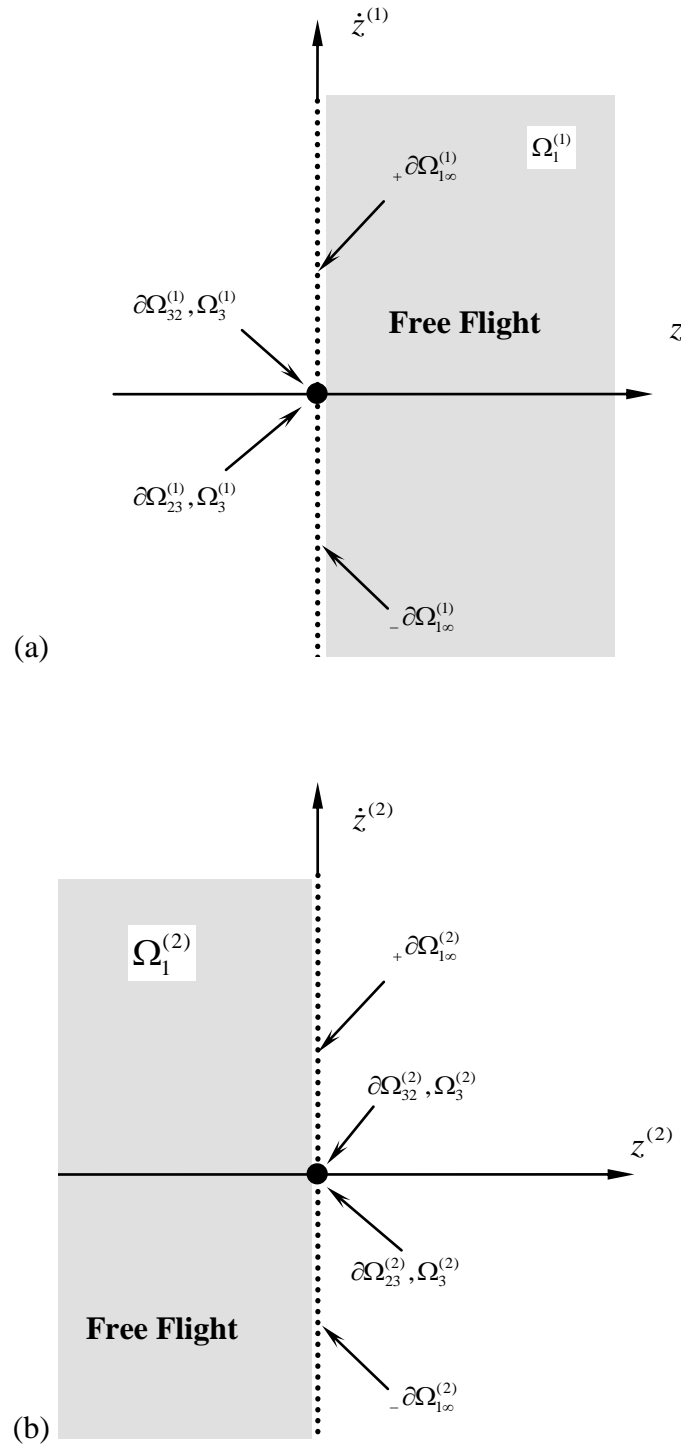
Figure 2.7. Phase plane partition in the relative reference frame: (a) bolster and (b) wedges.

CHAPTER III

MOTION MECHANISMS

The domains and boundaries of the different types of motion were introduced in Chapter 2. This chapter considers how motion may interact with the boundary separating two different domains. In other words, the necessary and sufficient conditions for passable boundaries, grazing, and stick motions will be developed to give analytical conditions for motion mechanisms. Based on discontinuous dynamical system theory, the equations of motion in the relative and absolute reference frame will be utilized to obtain such conditions. To help understand these analytical conditions, physical explanations of such analytical conditions will be presented.

3.1 Stuck and Sliding Conditions

To investigate the motion mechanism of the discontinuous suspension model, both the absolute and relative coordinate systems will be utilized. For the stick motion (i.e., bolster and wedge already joined) and the corresponding velocity boundary, the absolute reference frame will be used. For free flight chatters with possible stick motion, the relative coordinate system will be adopted. To develop analytical conditions for motion switching at the boundary $\partial\Omega_{\alpha\beta}^{(i)}$, from Luo (2009) and (2012), the following G-functions are introduced as

$$G^{(0,\alpha)}(\mathbf{x}_{\alpha}^{(i)}, t_{m\pm}) = \mathbf{n}_{\partial\Omega_{\alpha\beta}^{(i)}}^{\mathrm{T}} \cdot \left[\mathbf{F}_{\alpha}^{(i)}(\mathbf{x}_{\alpha}^{(i)}, t_{m\pm}) - \mathbf{F}_{\alpha\beta}^{(0)}(\mathbf{x}_{\alpha\beta}^{(i)}, t_{m\pm}) \right], \tag{37}$$

$$\begin{aligned} G^{(1,\alpha)}(\mathbf{x}_{\alpha}^{(i)}, t_{m\pm}) = 2D\mathbf{n}_{\partial\Omega_{\alpha\beta}^{(i)}}^{\mathrm{T}} \cdot \left[\mathbf{F}_{\alpha}^{(i)}(\mathbf{x}_{\alpha}^{(i)}, t_{m\pm}) - \mathbf{F}_{\alpha\beta}^{(0)}(\mathbf{x}_{\alpha\beta}^{(i)}, t_{m\pm}) \right] \\ + \mathbf{n}_{\partial\Omega_{\alpha\beta}^{(i)}}^{\mathrm{T}} \cdot \left[D\mathbf{F}_{\alpha}^{(i)}(\mathbf{x}_{\alpha}^{(i)}, t_{m\pm}) - D\mathbf{F}_{\alpha\beta}^{(0)}(\mathbf{x}_{\alpha\beta}^{(i)}, t_{m\pm}) \right], \end{aligned} \tag{38}$$

where $D(\cdot) = \partial(\cdot)/\partial\mathbf{x} \cdot \dot{\mathbf{x}} + \partial(\cdot)/\partial t$. If the normal vector $\mathbf{n}_{\partial\Omega_{\alpha\beta}^{(i)}}$ is a unit vector, the G-function in

Eq.(37) gives the normal component of the difference between the vector field within a domain

and the vector field on a boundary. The time-change rate of the G-function is given in Eq.(38),

which is the first order G-function. The switching time t_m represents the time for motion on the

boundary, and $t_{m\pm} = t_m \pm 0$ reflects the responses in the domains rather than on the boundary.

The vector field $\mathbf{F}_\alpha^{(i)}(\mathbf{x}_\alpha^{(i)}, t_{m\pm})$ is for a flow of the ith oscillator in domain $\Omega_\alpha^{(i)}$, and the vector field

$\mathbf{F}_{\alpha\beta}^{(0)}(\mathbf{x}_{\alpha\beta}^{(i)}, t)$ is for a flow on the boundary $\partial\Omega_{\alpha\beta}^{(i)}$. The normal vector $\mathbf{n}_{\partial\Omega_{\alpha\beta}^{(i)}}$ of the boundary $\partial\Omega_{\alpha\beta}^{(i)}$

is computed by

$$\mathbf{n}_{\partial\Omega_{\alpha\beta}^{(i)}} = \nabla\varphi_{\alpha\beta}^{(i)} = \left(\frac{\partial\varphi_{\alpha\beta}^{(i)}}{\partial x^{(i)}}, \frac{\partial\varphi_{\alpha\beta}^{(i)}}{\partial y^{(i)}}\right)^{\mathrm{T}} \tag{39}$$

where $\nabla = \left(\partial/\partial x, \partial/\partial y\right)^{\mathrm{T}}$ is the Hamilton operator. Because $\mathbf{n}_{\partial\Omega_{\alpha\beta}^{(i)}}^{\mathrm{T}} \cdot \mathbf{F}_{\alpha\beta}^{(0)}(\mathbf{x}_{\alpha\beta}^{(i)}, t_{m\pm}) = 0$, its total

derivative gives

$$D\mathbf{n}_{\partial\Omega_{\alpha\beta}^{(i)}}^{\mathrm{T}} \cdot \mathbf{F}_{\alpha\beta}^{(0)}(\mathbf{x}_{\alpha\beta}^{(i)}, t_{m\pm}) + \mathbf{n}_{\partial\Omega_{\alpha\beta}^{(i)}}^{\mathrm{T}} \cdot D\mathbf{F}_{\alpha\beta}^{(0)}(\mathbf{x}_{\alpha\beta}^{(i)}, t_{m\pm}) = 0. \tag{40}$$

If the boundary $\partial\Omega_{\alpha\beta}^{(i)}$ is a line independent of time t, $D\mathbf{n}_{\partial\Omega_{\alpha\beta}^{(i)}}^{\mathrm{T}} = 0$. Therefore, equation (40)

becomes

$$\mathbf{n}_{\partial\Omega_{\alpha\beta}^{(i)}}^{\mathrm{T}} \bullet D\mathbf{F}_{\alpha\beta}^{(0)}(\mathbf{x}_{\alpha\beta}^{(i)}, t_{m\pm}) = 0. \tag{41}$$

Notice that $\mathbf{F}_{\alpha\beta}^{(0)}(\mathbf{x}, t) = (0,0)^{\mathrm{T}}$ on the boundary $\partial\Omega_{\alpha\beta}^{(i)}$. Taking the time change rate of the

$$D\mathbf{F}_\alpha^{(i)}\left(\mathbf{x}_\alpha^{(i)}, t_{m\pm}\right) = \left(F_\alpha^{(i)}(\mathbf{x}_\alpha^{(i)}, t), \nabla F_\alpha^{(i)}(\mathbf{x}_\alpha^{(i)}, t) \cdot F_\alpha^{(i)}(\mathbf{x}_\alpha^{(i)}, t) + \frac{\partial F_\alpha^{(i)}(\mathbf{x}_\alpha^{(i)}, t)}{\partial t}\right)^{\mathrm{T}}. \tag{42}$$

Further, equations (37) and (38) reduce to

$$
\left.
\begin{aligned}
G^{(0,\alpha)}(\mathbf{x}_\alpha^{(i)}, t_{m\pm}) &= \mathbf{n}_{\partial\Omega_{\alpha\beta}^{(i)}}^{\mathrm{T}} \cdot \mathbf{F}_\alpha^{(i)}(\mathbf{x}_\alpha^{(i)}, t_{m\pm}) = F_\alpha^{(i)}(\mathbf{x}_\alpha^{(i)}, t_{m\pm}),\ \alpha \in \{2,3\} \\
G^{(1,\alpha)}(\mathbf{x}_\alpha^{(i)}, t_{m\pm}) &= \mathbf{n}_{\partial\Omega_{\alpha\beta}^{(i)}}^{\mathrm{T}} \cdot D\mathbf{F}_\alpha^{(i)}(\mathbf{x}_\alpha^{(i)}, t_{m\pm}) = \nabla F_\alpha^{(i)}(\mathbf{x}_\alpha^{(i)}, t) \cdot \mathbf{F}_\alpha^{(i)}(\mathbf{x}_\alpha^{(i)}, t + \frac{\partial F_\alpha^{(i)}(\mathbf{x}_\alpha^{(i)}, t)}{\partial t}.
\end{aligned}
\right\}
\tag{43}
$$

To investigate the stick motions in domains $\Omega_\alpha^{(i)}$ ($\alpha = 2,3$), the condition for a flow to pass

through the velocity boundary of $\varphi_{23}^{(i)} = \dot{x}^{(i)} = 0$ and $\varphi_{32}^{(i)} = \dot{x}^{(i)} = 0$ in Eq.(19) is very important.

From Luo (2009) and (2012), the passable motion to the boundary $\partial\Omega_{\alpha\beta}^{(i)}$ is guaranteed by

$$
\begin{aligned}
L_{\alpha\beta}(t_{m-}) &= G^{(0,\alpha)}(\mathbf{x}_m^{(i)}, t_{m-}) \times G^{(0,\beta)}(\mathbf{x}_m^{(i)}, t_{m+}) \\
&= [\mathbf{n}_{\partial\Omega_{\alpha\beta}^{(i)}}^{\mathrm{T}} \cdot \mathbf{F}_\alpha^{(i)}(\mathbf{x}_m^{(i)}, t_{m-})] \times [\mathbf{n}_{\partial\Omega_{\alpha\beta}^{(i)}}^{\mathrm{T}} \cdot \mathbf{F}_\beta^{(i)}(\mathbf{x}_m^{(i)}, t_{m+})] > 0.
\end{aligned}
\tag{44}
$$

In other words, the conditions for passable motion from domain $\Omega_\alpha^{(i)}$ into $\Omega_\beta^{(i)}$ and vice versa

can be expressed as

$$
\left.
\begin{aligned}
(-1)^\alpha G^{(0,\alpha)}(\mathbf{x}_m^{(i)}, t_{m-}) &= (-1)^\alpha \mathbf{n}_{\partial\Omega_{\alpha\beta}^{(i)}}^{\mathrm{T}} \cdot \mathbf{F}_\alpha^{(i)}(\mathbf{x}_m^{(i)}, t_{m-}) < 0 \\
(-1)^\alpha G^{(0,\beta)}(\mathbf{x}_m^{(i)}, t_{m+}) &= (-1)^\alpha \mathbf{n}_{\partial\Omega_{\alpha\beta}^{(i)}}^{\mathrm{T}} \cdot \mathbf{F}_\beta^{(i)}(\mathbf{x}_m^{(i)}, t_{m+}) < 0
\end{aligned}
\right\} \text{from } \Omega_\alpha^{(i)} \to \Omega_\beta^{(i)} \\
\left.
\begin{aligned}
(-1)^\alpha G^{(0,\beta)}(\mathbf{x}_m^{(i)}, t_{m-}) &= (-1)^\alpha \mathbf{n}_{\partial\Omega_{\alpha\beta}^{(i)}}^{\mathrm{T}} \bullet \mathbf{F}_\alpha^{(i)}(\mathbf{x}_m^{(i)}, t_{m-}) > 0 \\
(-1)^\alpha G^{(0,\alpha)}(\mathbf{x}_m^{(i)}, t_{m+}) &= (-1)^\alpha \mathbf{n}_{\partial\Omega_{\alpha\beta}^{(i)}}^{\mathrm{T}} \bullet \mathbf{F}_\beta^{(i)}(\mathbf{x}_m^{(i)}, t_{m+}) > 0
\end{aligned}
\right\} \text{from } \Omega_\beta^{(i)} \to \Omega_\alpha^{(i)}.
\tag{45}
$$

or more concisely as

$$
\begin{aligned}
L_{\alpha\beta}(t_{m-}) &= G^{(0,\alpha)}(\mathbf{x}_m^{(i)}, t_{m-}) \times G^{(0,\beta)}(\mathbf{x}_m^{(i)}, t_{m+}) \\
&= F_\alpha^{(i)}(\mathbf{x}_m^{(i)}, t_{m-}) \times F_\beta^{(i)}(\mathbf{x}_m^{(i)}, t_{m+}) > 0.
\end{aligned}
\tag{46}
$$

From Eq.(19) and (35), the normal vector $\mathbf{n}_{\partial\Omega_{\alpha\beta}^{(i)}}$ to the boundary $\partial\Omega_{\alpha\beta}^{(i)}$ for $\alpha, \beta \in \{2,3\}, \alpha \neq \beta$ is

given as

$$
\mathbf{n}_{\partial\Omega_{23}^{(i)}} = \mathbf{n}_{\partial\Omega_{32}^{(i)}} = (0,1)^{\mathrm{T}}.
\tag{47}
$$

With Eq.(45) or (47), the passable conditions for $\alpha, \beta \in \{2,3\}, \alpha \neq \beta$ become
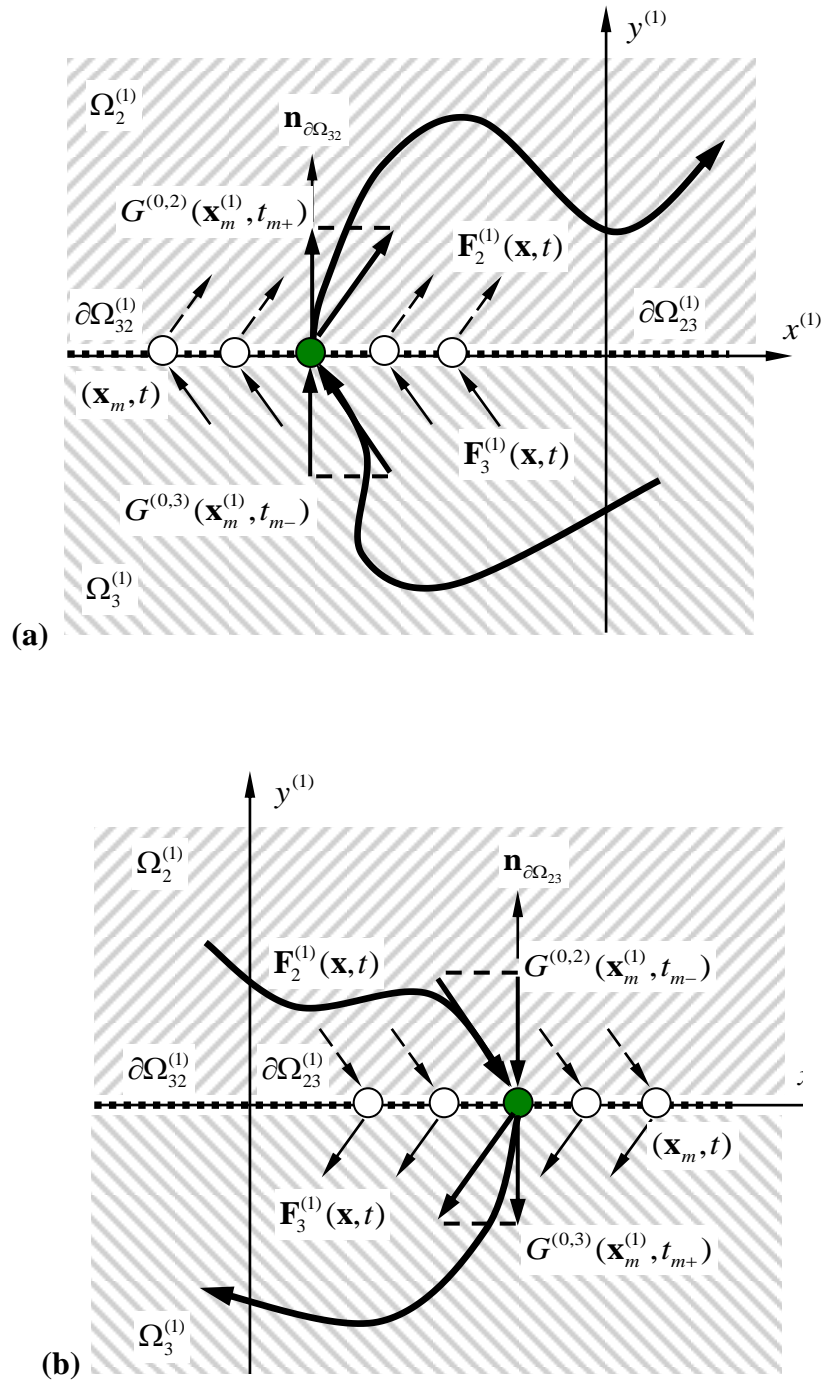
Figure 3.1. Passable flow illustration on (a) $\partial\Omega_{32}^{(1)}$ **and (b)** $\partial\Omega_{23}^{(1)}$ **.**

$$\left.\begin{aligned}
G^{(0,2)}(\mathbf{x}_m^{(i)},t_{m-}) &= F_2^{(i)}(\mathbf{x}_m^{(i)},t_{m-}) < 0 \\
G^{(0,3)}(\mathbf{x}_m^{(i)},t_{m+}) &= F_3^{(i)}(\mathbf{x}_m^{(i)},t_{m+}) < 0
\end{aligned}\right\} \text{from } \Omega_2^{(i)} \to \Omega_3^{(i)},$$

$$\left.\begin{aligned}
G^{(0,3)}(\mathbf{x}_m^{(i)},t_{m-}) &= F_3^{(i)}(\mathbf{x}_m^{(i)},t_{m-}) > 0 \\
G^{(0,2)}(\mathbf{x}_m^{(i)},t_{m+}) &= F_2^{(i)}(\mathbf{x}_m^{(i)},t_{m+}) > 0
\end{aligned}\right\} \text{from } \Omega_3^{(i)} \to \Omega_2^{(i)}.$$

$$(48)$$

The aforementioned conditions are illustrated through the absolute frame as shown in Figure 3.1.

The solid grey curve represents the motion flow as it approaches and then passes through the

boundary at (x_m, t_m). The dashed and solid vectors labeled $\mathbf{F}_2^{(i)}(\mathbf{x},t)$ and $\mathbf{F}_3^{(i)}(\mathbf{x},t)$ illustrate the

vector fields in the domains Ω_2 and Ω_3, respectively. In Figure 3.1(a), the conditions

$G^{(0,2)}(\mathbf{x}_m^{(i)},t_{m+})$ and $G^{(0,3)}(\mathbf{x}_m^{(i)},t_{m-})$ are both drawn in the positive direction along the normal

vector $\mathbf{n}_{\partial\Omega_{\alpha\beta}^{(i)}}$, thus reflecting that the motion passes the boundary $\partial\Omega_{32}^{(i)}$ and enters $\Omega_2^{(i)}$. Further,

for $i = 1$ and 2, the conditions in Eq.(48) are same because oscillators 1 and 2 are combined

together. Thus, the analytical condition is

$$F_2^{(1)}(\mathbf{x}_m^{(1)},t_{m+}) > 0 \text{ and } F_3^{(1)}(\mathbf{x}_m^{(1)},t_{m-}) > 0 \text{ from } \Omega_3^{(1)} \to \Omega_2^{(1)}. \qquad (49)$$

In a similar manner, Figure 3.1(b) can be discussed.

From [Luo, 2009, 2012], the stuck motion on $\partial\Omega_{\alpha\beta}^{(i)}$ is guaranteed by

$$\begin{aligned}
L_{\alpha\beta}(t_{m-}) &= G^{(0,\alpha)}(\mathbf{x}_m^{(i)},t_{m-}) \times G^{(0,\beta)}(\mathbf{x}_m^{(i)},t_{m-}) = \\
&\quad [\mathbf{n}_{\partial\Omega_{\alpha\beta}^{(i)}}^{\mathrm{T}} \cdot \mathbf{F}_\alpha^{(i)}(\mathbf{x}_m^{(i)},t_{m-})] \times [\mathbf{n}_{\partial\Omega_{\alpha\beta}^{(i)}}^{\mathrm{T}} \cdot \mathbf{F}_\beta^{(i)}(\mathbf{x}_m^{(i)},t_{m-})] < 0.
\end{aligned} \qquad (50)$$

Here the stuck condition requires a negative cross product. For the boundary $\partial\Omega_{\alpha\beta}^{(i)}$ with

$\mathbf{n}_{\partial\Omega_{\alpha\beta}^{(i)}}^{\mathrm{T}} \to \Omega_\alpha^{(i)}$ the necessary and sufficient conditions for non-passable motion to the boundary

(i.e., stuck motion) are expressed as

$$(-1)^{\alpha}G^{(0,\alpha)}(\mathbf{x}_m^{(i)},t_{m-}) = (-1)^{\alpha}\mathbf{n}_{\partial\Omega_{\alpha\beta}^{(i)}}^{\mathrm{T}} \cdot \mathbf{F}_{\alpha}^{(i)}(\mathbf{x}_m^{(i)},t_{m-}) < 0,$$

$$(-1)^{\alpha}G^{(0,\beta)}(\mathbf{x}_m^{(i)},t_{m-}) = (-1)^{\alpha}\mathbf{n}_{\partial\Omega_{\alpha\beta}^{(i)}}^{\mathrm{T}} \cdot \mathbf{F}_{\beta}^{(i)}(\mathbf{x}_m^{(i)},t_{m-}) > 0. \tag{51}$$

With Eq.(47), the stuck conditions in Eq.(51) are simplified for $\alpha,\beta \in \{2,3\}$, $\alpha \neq \beta$ as

$$G^{(0,2)}(\mathbf{x}_m^{(i)},t_{m-}) = F_2^{(i)}(\mathbf{x}_m^{(i)},t_{m-}) < 0,$$

$$G^{(0,3)}(\mathbf{x}_m^{(i)},t_{m-}) = F_3^{(i)}(\mathbf{x}_m^{(i)},t_{m-}) > 0, \quad \text{on } \partial\Omega_{23}^{(i)}. \tag{52}$$

The foregoing equation means that for stuck motion to occur for $i=1$, the force per unit mass (or

acceleration) on the boundary $\partial\Omega_{23}^{(1)}$ and $\partial\Omega_{32}^{(1)}$ must be negative just inside $\Omega_2^{(1)}$ and positive just

inside $\Omega_3^{(1)}$. The requirement to keep the stuck motion is given by

$$F_2^{(1)}(\mathbf{x}_m^{(1)},t_{m-}) < 0 \text{ and } F_3^{(1)}(\mathbf{x}_m^{(1)},t_{m-}) > 0. \tag{53}$$

Since the oscillator 1 and oscillator 2 with stick are together. So the oscillator has the same

conditions in Eq,(53). If two coming flows in phase plane reach the velocity boundary $\partial\Omega_{23}^{(1)}$

with conditions in Eq.(53), the stuck motion will exist, as sketched in Figure 3.2. The solid grey

curve represents the motion flow as it approaches and then passes through the boundary at

(x_m,t_m). The dashed and solid vectors depicts the vector fields $\mathbf{F}_2^{(1)}(\mathbf{x},t)$ and $\mathbf{F}_3^{(1)}(\mathbf{x},t)$ in domains

Ω_2 and Ω_3, respectively. In Figure 3.2(a), the G-functions $G^{(0,2)}(\mathbf{x}_m^{(1)},t_{m-})$ and $G^{(0,3)}(\mathbf{x}_m^{(i)},t_{m-})$ are

in the negative and positive direction, respectively. In other words, the coming flow in domain

$\Omega_2^{(1)}$ arrives to the boundary $\partial\Omega_{23}^{(1)}$. However, the vector fields in domain $\Omega_2^{(1)}$ and $\Omega_3^{(1)}$ toward

each other at the boundary on the normal vector $\mathbf{n}_{\partial\Omega_{32}^{(1)}}$, thus the motion will become stuck on the

boundary $\partial\Omega_{23}^{(1)}$. In a similar manner, in Figure 3.2(b), the coming flow in domain $\Omega_3^{(1)}$ arrives to

the boundary $\partial\Omega_{32}^{(1)}$. However, the vector fields in domain $\Omega_2^{(1)}$ and $\Omega_3^{(1)}$ toward each other at the

boundary on the normal vector $\mathbf{n}_{\partial\Omega_{32}^{(1)}}$, thus the motion will become stuck on the boundary $\partial\Omega_{32}^{(1)}$.
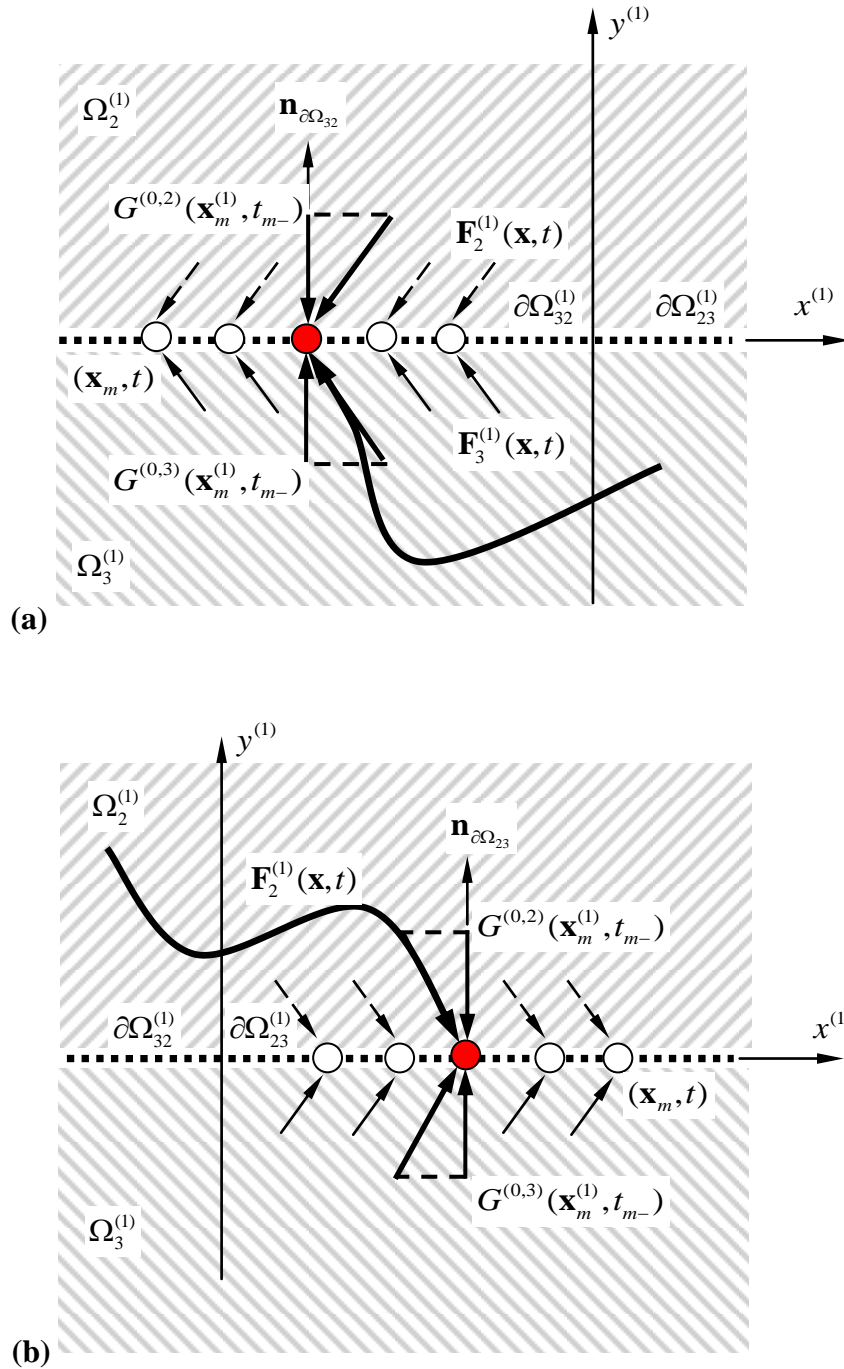
Figure 3.2. Stuck motion on (a) $\partial\Omega_{32}^{(1)}$ **and (b)** $\partial\Omega_{23}^{(1)}$.

For stuck motion vanishing, the wedge combined with the bolster will start to move on the both side walls. The G-function $G^{(0,\alpha)}(\mathbf{x}_m^{(i)}, t_m)$ will equal zero for stuck vanishing and moving to

the domain $\Omega_\alpha^{(i)}$, the time change rate of the G-function (i.e., $G^{(1,2)}(\mathbf{x}_m^{(i)},t_{m\pm})$) must be considered

to guarantee vanishing of the stuck motion. From Luo (2009) and (2012), the analytical

conditions are

$$
\left.
\begin{aligned}
G^{(0,3)}(\mathbf{x}_m^{(i)},t_{m-}) &= \mathbf{n}_{\partial\Omega_{32}^{(i)}}^{\mathrm{T}} \cdot \mathbf{F}_3^{(i)}(\mathbf{x}_m^{(i)},t_{m-}) > 0 \\
G^{(0,2)}(\mathbf{x}_m^{(i)},t_m) &= \mathbf{n}_{\partial\Omega_{32}^{(i)}}^{\mathrm{T}} \cdot \mathbf{F}_2^{(i)}(\mathbf{x}_m^{(i)},t_{m\mp}) = 0 \\
G^{(1,2)}(\mathbf{x}_m^{(i)},t_{m\pm}) &= \mathbf{n}_{\partial\Omega_{32}^{(i)}}^{\mathrm{T}} \cdot D\mathbf{F}_2^{(i)}(\mathbf{x}_m^{(i)},t_{m\mp}) > 0
\end{aligned}
\right\} \text{from } \partial\Omega_{32}^{(i)} \to \Omega_2^{(i)}
\tag{54}
$$

$$
\left.
\begin{aligned}
G^{(0,2)}(\mathbf{x}_m^{(i)},t_{m-}) &= \mathbf{n}_{\partial\Omega_{23}^{(i)}}^{\mathrm{T}} \cdot \mathbf{F}_2^{(i)}(\mathbf{x}_m^{(i)},t_{m-}) < 0 \\
G^{(0,3)}(\mathbf{x}_m^{(i)},t_m) &= \mathbf{n}_{\partial\Omega_{23}^{(i)}}^{\mathrm{T}} \cdot \mathbf{F}_3^{(i)}(\mathbf{x}_m^{(i)},t_{m\mp}) = 0 \\
G^{(1,3)}(\mathbf{x}_m^{(i)},t_{m\pm}) &= \mathbf{n}_{\partial\Omega_{23}^{(i)}}^{\mathrm{T}} \cdot D\mathbf{F}_3^{(i)}(\mathbf{x}_m^{(i)},t_{m\mp}) > 0
\end{aligned}
\right\} \text{from } \partial\Omega_{23}^{(i)} \to \Omega_3^{(i)}.
\tag{55}
$$

From Eq.(39), $G_i^{(1,\alpha)}(\mathbf{x}_\alpha^{(i)},t)$ is given by the following equation

$$
G^{(1,\alpha)}(\mathbf{x}_\alpha^{(i)},t) = -2\zeta_\alpha^{(i)}\ddot{x}_\alpha^{(i)} - (\omega_\alpha^{(i)})^2 \dot{x}_\alpha^{(i)} - Q_\alpha^{(i)}\Omega\sin\Omega t.
\tag{56}
$$

From a physical point of view, equation (56) describes the absolute jerk, namely

$$
J_\alpha^{(i)}(t) = -2\zeta_\alpha^{(i)}\ddot{x}_\alpha^{(i)} - (\omega_\alpha^{(i)})^2 \dot{x}_\alpha^{(i)} - Q_\alpha^{(i)}\Omega\sin\Omega t.
\tag{57}
$$

Consider the stuck motion on $\partial\Omega_{32}^{(1)}$ for $i=1$. If $G^{(0,2)}(\mathbf{x}_2^{(i)},t_m)=0$ and $G^{(1,2)}(\mathbf{x}_m^{(i)},t_{m\pm})>0$,

then for $t > t_m + \varepsilon$, $G^{(0,2)}(\mathbf{x}_2^{(i)},t_{m+})>0$ will be true. The analytical conditions for the vanishing of

stuck motion are further simplified and given below for $\alpha,\beta \in \{2,3\}, \alpha \neq \beta$.

$$
\left.
\begin{aligned}
G^{(0,3)}(\mathbf{x}_m^{(i)},t_{m-}) &= F_3^{(i)}(\mathbf{x}_m^{(i)},t_{m-}) > 0 \\
G^{(0,2)}(\mathbf{x}_m^{(i)},t_m) &= F_2^{(i)}(\mathbf{x}_m^{(i)},t_{m\mp}) = 0 \\
G^{(1,2)}(\mathbf{x}_m^{(i)},t_{m\mp}) &> 0
\end{aligned}
\right\} \text{from } \partial\Omega_{32}^{(i)} \to \Omega_2^{(i)}
\tag{58}
$$

$$
\left.
\begin{aligned}
G^{(0,2)}(\mathbf{x}_m^{(i)},t_{m-}) &= F_2^{(i)}(\mathbf{x}_m^{(i)},t_{m-}) < 0 \\
G^{(0,3)}(\mathbf{x}_m^{(i)},t_m) &= F_3^{(i)}(\mathbf{x}_m^{(i)},t_{m\mp}) = 0 \\
G^{(1,3)}(\mathbf{x}_m^{(i)},t_{m\mp}) &< 0
\end{aligned}
\right\} \text{from } \partial\Omega_{32}^{(i)} \to \Omega_3^{(i)}
\tag{59}
$$

In Figure 3.3, a leaving flow from the boundary to domain is presented when the vanishing of stuck motion occurs. The solid red circle represents the static position where the bolster and wedges are stuck against the wall. The solid grey curve shows the motion leaving the stuck position. The dashed and solid vectors labeled $\mathbf{F}_2^{(i)}(\mathbf{x},t)$ and $\mathbf{F}_3^{(i)}(\mathbf{x},t)$ illustrate the vector fields in the domains Ω_2 and Ω_3, respectively. In Figure 3.3(a), the motion is from the boundary $\partial\Omega_{23}^{(1)}$ to domain $\Omega_2^{(1)}$. Due to $F_2^{(1)}(\mathbf{x}_m^{(1)}, t_{m\mp}) = 0$ with $G^{(1,2)}(\mathbf{x}_m^{(1)}, t_{m\mp}) > 0$, then $F_2^{(1)}(\mathbf{x}_m^{(1)}, t_{m+\varepsilon}) > 0$ for $\varepsilon > 0$. In a similar manner, Figure 3.3(b), a leaving motion is from the boundary $\partial\Omega_{32}^{(1)}$ to domain $\Omega_3^{(1)}$ because $F_3^{(1)}(\mathbf{x}_m^{(1)}, t_{m\mp}) = 0$ with $G^{(1,2)}(\mathbf{x}_m^{(1)}, t_{m\mp}) < 0$, then $F_3^{(1)}(\mathbf{x}_m^{(1)}, t_{m+\varepsilon}) < 0$ for $\varepsilon > 0$.

From Eq.(58) for $i = 1$, when $F_2^{(1)}(\mathbf{x}_m^{(1)}, t_{m\mp}) = 0$, we have $G^{(1,2)}(\mathbf{x}_m^{(1)}, t_{m\mp}) < 0$. As a result, at the next moment $F_2^{(1)}(\mathbf{x}_m^{(1)}, t_{m+\varepsilon}) < 0$ would be negative and the stuck conditions of Eq.(49) would be satisfied. This phenomena is called the grazing of stuck, and the conditions are described as

$$
\left.
\begin{aligned}
&\left.
\begin{aligned}
G^{(0,3)}(\mathbf{x}_m^{(i)}, t_{m-}) &= F_3^{(i)}(\mathbf{x}_m^{(i)}, t_{m-}) > 0 \\
G^{(0,2)}(\mathbf{x}_m^{(i)}, t_m) &= F_2^{(i)}(\mathbf{x}_m^{(i)}, t_{m\mp}) = 0 \\
G^{(1,2)}(\mathbf{x}_m^{(i)}, t_{m\mp}) &< 0
\end{aligned}
\right\} \text{ on } \partial\Omega_{23}^{(i)} \\
&\left.
\begin{aligned}
G^{(0,2)}(\mathbf{x}_m^{(i)}, t_{m-}) &= F_2^{(i)}(\mathbf{x}_m^{(i)}, t_{m-}) < 0 \\
G^{(0,3)}(\mathbf{x}_m^{(i)}, t_m) &= F_3^{(i)}(\mathbf{x}_m^{(i)}, t_{m\mp}) = 0 \\
G^{(1,3)}(\mathbf{x}_m^{(i)}, t_{m\mp}) &> 0
\end{aligned}
\right\} \text{ on } \partial\Omega_{32}^{(i)}
\end{aligned}
\right\}
\tag{60}
$$

Consider the grazing of the stuck motion on the boundary $\partial\Omega_{32}$ for $i = 1$, then $F_3^{(1)}(\mathbf{x}_m^{(1)}, t_{m-}) > 0$ and $F_2^{(1)}(\mathbf{x}_m^{(1)}, t_{m\mp}) = 0$. However, due to $G^{(1,2)}(\mathbf{x}_m^{(1)}, t_{m\mp}) < 0$, at the next instance, we have $F_2^{(1)}(\mathbf{x}_m^{(1)}, t_{m+\varepsilon}) < 0$ and the stuck motion conditions of Eq.(53) will be satisfied.
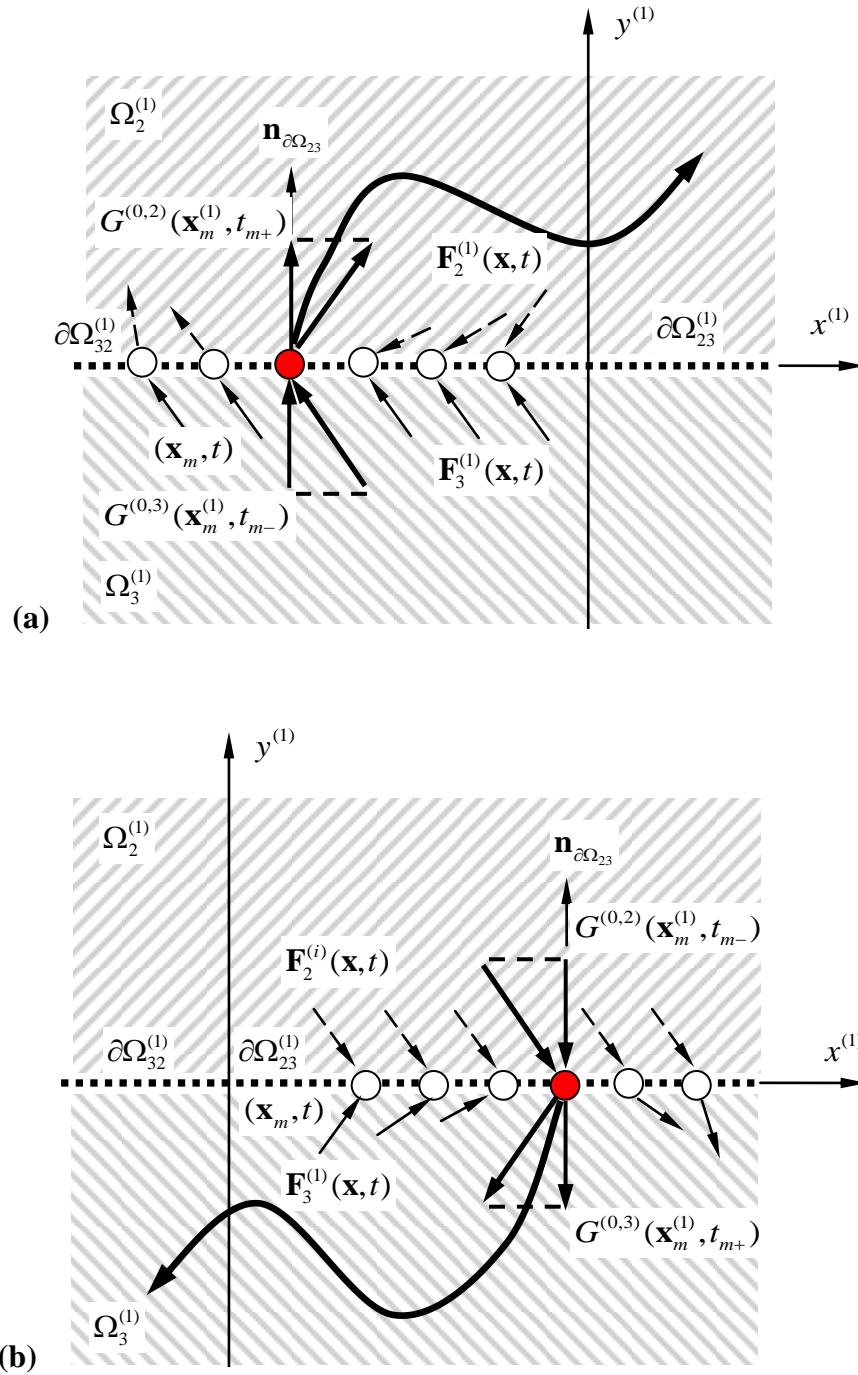
Figure 3.3. Vanishing of stuck motion: (a) from $\partial\Omega_{32}^{(i)}$ **to** $\Omega_2^{(i)}$ **and (b) form** $\partial\Omega_{23}^{(i)}$ **to** $\Omega_3^{(i)}$ **.**

3.2 Free-flight and stick motions

To discuss the free-flight and stick motions, the relative coordinate system is adopted. From

Eq.(30), the relative coordinate systems is utilized to define the following two functions for

$\alpha, \beta \in \{2,3\}, \alpha \neq \beta$.

$$G^{(0,\alpha)}(\mathbf{z}_\alpha^{(i)}, \mathbf{x}_\alpha^{(\bar{i})}, t_{m\pm}) = \mathbf{n}_{\partial\Omega_{\alpha\beta}^{(i)}}^T \cdot \left[\mathbf{g}_\alpha^{(i)}(\mathbf{z}_\alpha^{(i)}, \mathbf{x}_\alpha^{(\bar{i})}, t_{m\pm}) - \mathbf{g}_{\alpha\beta}^{(0)}(\mathbf{z}_{\alpha\beta}^{(i)}, \mathbf{x}_\alpha^{(\bar{i})}, t_{m\pm}) \right], \tag{61}$$

$$\begin{aligned} G^{(1,\alpha)}(\mathbf{z}_\alpha^{(i)}, \mathbf{x}_\alpha^{(\bar{i})}, t_{m\pm}) &= 2D\mathbf{n}_{\partial\Omega_{\alpha\beta}^{(i)}}^T \cdot [\mathbf{g}_\alpha^{(i)}(\mathbf{z}_\alpha^{(i)}, \mathbf{x}_\alpha^{(\bar{i})}, t_{m\pm}) - \mathbf{g}_{\alpha\beta}^{(0)}(\mathbf{z}_{\alpha\beta}^{(i)}, \mathbf{x}_\alpha^{(\bar{i})}, t_{m\pm})] \\ &\quad + \mathbf{n}_{\partial\Omega_{\alpha\beta}^{(i)}}^T \cdot [D\mathbf{g}_\alpha^{(i)}(\mathbf{z}_\alpha^{(i)}, \mathbf{x}_\alpha^{(\bar{i})}, t_{m\pm}) - D\mathbf{g}_{\alpha\beta}^{(0)}(\mathbf{z}_{\alpha\beta}^{(i)}, \mathbf{x}_\alpha^{(\bar{i})}, t_{m\pm})]. \end{aligned} \tag{62}$$

For the free-flight impact chatter, from Eq.(33) the normal vector $\mathbf{n}_{\partial\Omega_{1\infty}^{(i)}}$ to the boundary $\partial\Omega_{1\infty}^{(i)}$ is

$$\mathbf{n}_{\partial\Omega_{1\infty}^{(i)}} = \nabla\varphi_{\alpha\beta}^{(i)} = \left(\frac{\partial\varphi_{\alpha\beta}^{(i)}}{\partial z_\alpha^{(i)}}, \frac{\partial\varphi_{\alpha\beta}^{(i)}}{\partial \dot{z}_\alpha^{(i)}} \right)^T = (1,0)^T. \tag{63}$$

Therefore, equations (61) and (62) give

$$\left. \begin{aligned} G^{(0,1)}(\mathbf{z}_1^{(i)}, \mathbf{x}_1^{(\bar{i})}, t_{m\pm}) &= \mathbf{n}_{\partial\Omega_{1\infty}^{(i)}}^T \cdot \mathbf{g}_1^{(i)}(\mathbf{z}_1^{(i)}, \mathbf{x}_1^{(\bar{i})}, t_{m\pm}) = v_1^{(i)}, \\ G^{(1,1)}(\mathbf{z}_1^{(i)}, \mathbf{x}_1^{(\bar{i})}, t_{m\pm}) &= \mathbf{n}_{\partial\Omega_{1\infty}^{(i)}}^T \cdot D\mathbf{g}_1^{(i)}(\mathbf{z}_1^{(i)}, \mathbf{x}_1^{(\bar{i})}, t_{m\pm}) = g_1^{(i)}(\mathbf{z}_1^{(i)}, \mathbf{x}_1^{(\bar{i})}, t_m). \end{aligned} \right\} \tag{64}$$

From Luo (2009) and (2012), the analytical conditions for grazing motions on the impact

boundary are

$$v_1^{(i)}(t_m) = 0 \text{ and } (-1)^i g_1^{(i)}(\mathbf{z}_1^{(i)}, \mathbf{x}_1^{(\bar{i})}, t_{m\pm}) < 0 \quad \text{on } \partial\Omega_{1\infty}^{(i)} \tag{65}$$

For $i = 1$, the bolster and wedges just contact, the conditions in Eq.(62) give $v_1^{(1)}(t_m) = 0$ and

$g_1^{(1)}(\mathbf{z}_1^{(1)}, \mathbf{x}_2^{(2)}, t_{m\pm}) > 0$. For $t > t_{m+}$, the relative velocity $v_1^{(1)}(t_{m+\varepsilon}) > 0$ because $g_1^{(1)} > 0$. With

negative relative velocity, the relative displacement $z_1^{(1)}(t_{m+}) > 0$ will be satisfied. In other

words, the bolster remains in $\Omega_1^{(1)}$. Such a phenomenon is called grazing motion to the boundary

$\partial\Omega_{1\infty}^{(1)}$, as shown in Figure 3.4. The black curve in $\Omega_1^{(1)}$ approaches the boundary $\partial\Omega_{1\infty}^{(1)}$ but turns

away without interaction to the boundary.

From Luo (2009) and (2012), the passable motion to the boundary $\partial\Omega_{\alpha\beta}^{(i)}$ is guaranteed by

$$
\begin{aligned}
L_{\alpha\beta}(t_{m+}) &= G^{(0,\alpha)}(\mathbf{z}_\alpha^{(i)}, \mathbf{x}_\alpha^{(\bar{i})}, t_{m-}) \times G^{(0,\beta)}(\mathbf{z}_\alpha^{(i)}, \mathbf{x}_\alpha^{(\bar{i})}, t_{m+}) \\
&= [\mathbf{n}_{\partial\Omega_{\alpha\beta}^{(i)}}^{\mathrm{T}} \cdot \mathbf{g}_\alpha^{(i)}(\mathbf{z}_\alpha^{(i)}, \mathbf{x}_\alpha^{(\bar{i})}, t_{m-})] \times [\mathbf{n}_{\partial\Omega_{\alpha\beta}^{(i)}}^{\mathrm{T}} \cdot \mathbf{g}_\beta^{(i)}(\mathbf{z}_\beta^{(i)}, \mathbf{x}_\beta^{(\bar{i})}, t_{m+})] > 0.
\end{aligned}
\tag{66}
$$

Passable motion to the boundary $\partial\Omega_{\alpha\beta}^{(i)}$ means the onset of stick motion (i.e., the bolster and

wedges move as one). From Luo (2009) and (2012), the conditions for stick motion can also be

written as

$$
\left.
\begin{aligned}
(-1)^i G^{(0,\alpha)}(\mathbf{z}_\alpha^{(i)}, \mathbf{x}_\alpha^{(\bar{i})}, t_{m-}) &= (-1)^i \mathbf{n}_{\partial\Omega_{\alpha\beta}^{(i)}}^{\mathrm{T}} \cdot \mathbf{g}_\alpha^{(i)}(\mathbf{z}_\alpha^{(i)}, \mathbf{x}_\alpha^{(\bar{i})}, t_{m-}) > 0, \\
(-1)^i G^{(0,\beta)}(\mathbf{z}_\beta^{(i)}, \mathbf{x}_\beta^{(\bar{i})}, t_{m+}) &= (-1)^i \mathbf{n}_{\partial\Omega_{\alpha\beta}^{(i)}}^{\mathrm{T}} \cdot \mathbf{g}_\beta^{(i)}(\mathbf{z}_\beta^{(i)}, \mathbf{x}_\beta^{(\bar{i})}, t_{m+}) > 0
\end{aligned}
\right\} \text{ for } \mathbf{n}_{\partial\Omega_{\alpha\beta}^{(i)}} \to \Omega_\alpha^{(i)},
$$
$$
\left.
\begin{aligned}
(-1)^i G^{(0,\alpha)}(\mathbf{z}_\alpha^{(i)}, \mathbf{x}_\alpha^{(\bar{i})}, t_{m-}) &= (-1)^i \mathbf{n}_{\partial\Omega_{\alpha\beta}^{(i)}}^{\mathrm{T}} \cdot \mathbf{g}_\alpha^{(i)}(\mathbf{z}_\alpha^{(i)}, \mathbf{x}_\alpha^{(\bar{i})}, t_{m-}) < 0, \\
(-1)^i G^{(0,\beta)}(\mathbf{z}_\beta^{(i)}, \mathbf{x}_\beta^{(\bar{i})}, t_{m+}) &= (-1)^i \mathbf{n}_{\partial\Omega_{\alpha\beta}^{(i)}}^{\mathrm{T}} \cdot \mathbf{g}_\beta^{(i)}(\mathbf{z}_\beta^{(i)}, \mathbf{x}_\beta^{(\bar{i})}, t_{m+}) < 0
\end{aligned}
\right\} \text{ for } \mathbf{n}_{\partial\Omega_{\alpha\beta}^{(i)}} \to \Omega_\beta^{(i)}.
\tag{67}
$$

Figure 3.4. Free-flight motion grazing at $\partial\Omega_{1\infty}^{(1)}$.

With Eq.(36), the normal vector $\mathbf{n}_{\partial\Omega_{\alpha\beta}^{(i)}}$ to the boundary $\partial\Omega_{\alpha\beta}^{(i)}$ for $\alpha,\beta \in \{1,2,3\}, \alpha \neq \beta$ is

$$\mathbf{n}_{\partial\Omega_{21}^{(i)}} = \mathbf{n}_{\partial\Omega_{31}^{(i)}} = (0,1)^{\mathrm{T}}. \tag{68}$$

The G-function in Eq,(67) is

$$\left.\begin{aligned}
G^{(0,\alpha)}(\mathbf{z}_\alpha^{(i)},\mathbf{x}_\alpha^{(\bar{i})},t_{m\pm}) &= \mathbf{n}_{\partial\Omega_{\alpha\beta}^{(i)}}^{\mathrm{T}} \cdot \mathbf{g}_\alpha^{(i)}(\mathbf{z}_\alpha^{(i)},\mathbf{x}_\alpha^{(\bar{i})},t_{m\pm}) = g_\alpha^{(i)}(\mathbf{z}_\alpha^{(i)},\mathbf{x}_\alpha^{(\bar{i})},t_{m\pm}), \alpha \in [2,3] \\
G^{(1,\alpha)}(\mathbf{z}_\alpha^{(i)},\mathbf{x}_\alpha^{(\bar{i})},t_{m\pm}) &= \mathbf{n}_{\partial\Omega_{\alpha\beta}^{(i)}}^{\mathrm{T}} \cdot D\mathbf{g}_\alpha^{(i)}(\mathbf{z}_\alpha^{(i)},\mathbf{x}_\alpha^{(\bar{i})},t_{m\pm}) \\
&= \nabla g_\alpha^{(i)}(\mathbf{z}_\alpha^{(i)},\mathbf{x}_\alpha^{(\bar{i})},t) \cdot \mathbf{g}_\alpha^{(i)}(\mathbf{z}_\alpha^{(i)},\mathbf{x}_\alpha^{(\bar{i})},t) + \frac{\partial g_\alpha^{(i)}(\mathbf{z}_\alpha^{(i)},\mathbf{x}_\alpha^{(\bar{i})},t)}{\partial t}.
\end{aligned}\right\} \tag{70}$$

For motion entering domain Ω_3 from Ω_1, the passable conditions in Eq.(67) is

$$\left.\begin{aligned}
(-1)^i G^{(0,1)}(\mathbf{z}_1^{(i)},\mathbf{x}_1^{(\bar{i})},t_{m-}) &= (-1)^i g_1^{(i)}(\mathbf{z}_1^{(i)},\mathbf{x}_1^{(\bar{i})},t_{m-}) > 0, \\
(-1)^i G^{(0,3)}(\mathbf{z}_3^{(i)},\mathbf{x}_3^{(\bar{i})},t_{m+}) &= (-1)^i g_3^{(i)}(\mathbf{z}_3^{(i)},\mathbf{x}_3^{(\bar{i})},t_{m+}) > 0
\end{aligned}\right\} \text{ for } \Omega_1^{(i)} \to \Omega_3^{(i)}. \tag{71}$$

The conditions for motion from domain $\Omega_1^{(i)}$ to $\Omega_2^{(i)}$ are given by

$$\left.\begin{aligned}
(-1)^i G^{(0,1)}(\mathbf{z}_1^{(i)},\mathbf{x}_1^{(\bar{i})},t_{m-}) &= (-1)^i g_1^{(i)}(\mathbf{z}_1^{(i)},\mathbf{x}_1^{(\bar{i})},t_{m-}) > 0, \\
(-1)^i G^{(0,2)}(\mathbf{z}_2^{(i)},\mathbf{x}_2^{(\bar{i})},t_{m+}) &= (-1)^i g_2^{(i)}(\mathbf{z}_2^{(i)},\mathbf{x}_2^{(\bar{i})},t_{m+}) > 0
\end{aligned}\right\} \text{ for } \Omega_1^{(i)} \to \Omega_2^{(i)}. \tag{72}$$

The foregoing equation gives the analytical conditions for stick motion of the bolster and edges.

The relative force per unit mass (or relative acceleration) in $\Omega_2^{(1)}$ and $\Omega_1^{(1)}$ must be negative on

the boundary $\partial\Omega_{21}^{(1)}$. Also, the relative acceleration in $\Omega_3^{(1)}$ and $\Omega_1^{(1)}$ must be negative on the

boundary $\partial\Omega_{31}^{(1)}$. The stick conditions of Eq.(71) gives

$$g_1^{(1)}(\mathbf{z}_1^{(1)},\mathbf{x}_1^{(2)},t_{m-}) < 0 \text{ and } g_3^{(1)}(\mathbf{z}_1^{(1)},\mathbf{x}_1^{(2)},t_{m+}) < 0. \tag{73}$$

From Eq.(36), the stick motion requires that the relative displacement and velocity equal zero

(i.e., $z_1^{(1)} = 0$ and $\dot{z}_1^{(1)} = 0$). The conditions for stick motion are depicted in the absolute

coordinate system in Figure 3.5.
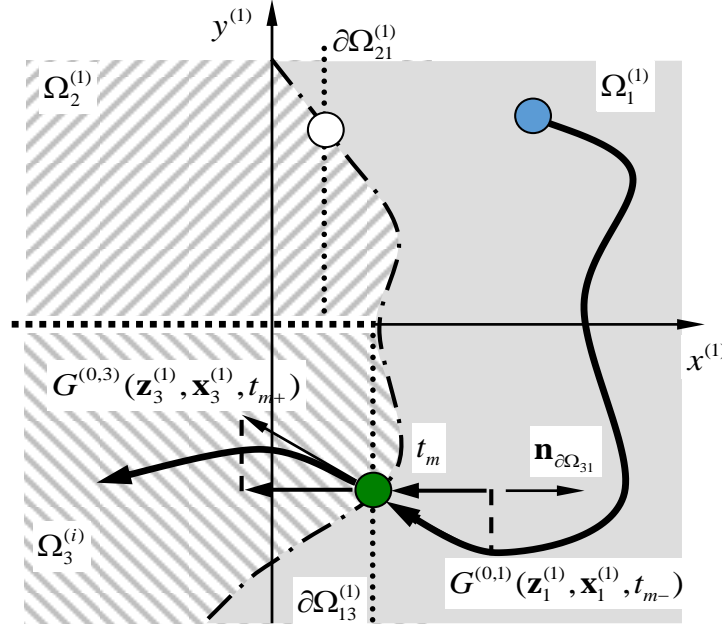
Figure 3.5. Stick motion on $\partial\Omega_{13}^{(1)}$ in the phase plane of bolster.

The vanishing of the stick motion requires that the normal force between the bolster and wedges equal zero, thus the relative force per unit mass must also be zero. From [Luo, 2009, 2012], the analytical conditions for stick vanishing for $\alpha = 2, 3$ and $\beta = 1$ are given by

$$
\left.
\begin{aligned}
(-1)^i\, G^{(0,\alpha)}(\mathbf{z}_\alpha^{(i)}, \mathbf{x}_\alpha^{(\bar{i})}, t_{m-}) &= (-1)^i \mathbf{n}_{\partial\Omega_{\alpha\beta}^{(i)}}^{\mathrm{T}} \cdot \mathbf{g}_\alpha^{(i)}(\mathbf{z}_\alpha^{(i)}, \mathbf{x}_\alpha^{(\bar{i})}, t_{m-}) < 0, \\
G^{(0,\beta)}(\mathbf{z}_\beta^{(i)}, \mathbf{x}_\beta^{(\bar{i})}, t_m) &= \mathbf{n}_{\partial\Omega_{\alpha\beta}^{(i)}}^{\mathrm{T}} \cdot \mathbf{g}_\beta^{(i)}(\mathbf{z}_\beta^{(i)}, \mathbf{x}_\beta^{(\bar{i})}, t_{m\mp}) = 0, \\
(-1)^i\, G^{(1,\beta)}(\mathbf{z}_\beta^{(i)}, \mathbf{x}_\beta^{(\bar{i})}, t_{m\pm}) &= (-1)^i \mathbf{n}_{\partial\Omega_{\alpha\beta}^{(i)}}^{\mathrm{T}} \cdot D\mathbf{g}_\beta^{(i)}(\mathbf{z}_\beta^{(i)}, \mathbf{x}_\beta^{(\bar{i})}, t_{m\mp}) < 0
\end{aligned}
\right\}
\text{ for } \mathbf{n}_{\partial\Omega_{\alpha\beta}^{(i)}} \to \Omega_\beta^{(i)}
\qquad (74)
$$

In Eq.(74), $G^{(1,\beta)}(\mathbf{z}_\beta^{(i)}, \mathbf{x}_\beta^{(\bar{i})}, t_{m\pm})$ can be considered as the relative Jerk and is determined by

$$
\begin{aligned}
G^{(1,\beta)}(\mathbf{z}_\beta^{(i)}, \mathbf{x}_\beta^{(\bar{i})}, t) = &-2\zeta_\beta^{(i)} \ddot{z}_\beta^{(i)} - (\omega_\beta^{(i)})^2 \dot{z}_\beta^{(i)} + Q_\beta^{(i)} \Omega \sin \Omega t \\
&- \dddot{x}_\beta^{(\bar{i})} - 2\zeta_\beta^{(i)} \ddot{x}_\beta^{(\bar{i})} - (\omega_\beta^{(\bar{i})})^2 \dot{x}_\beta^{(\bar{i})}.
\end{aligned}
\qquad (75)
$$

For $\alpha, \beta \in \{1,2,3\}, \alpha \neq \beta$, the analytical conditions for stick vanishing from domain $\Omega_2^{(i)}$ and entering domain $\Omega_1^{(i)}$ become

$$(-1)^i G^{(0,2)}(\mathbf{z}_2^{(i)}, \mathbf{x}_2^{(\bar{i})}, t_{m-}) = (-1)^i g_2^{(i)}(\mathbf{z}_2^{(i)}, \mathbf{x}_2^{(\bar{i})}, t_{m-}) < 0,$$
$$G^{(0,1)}(\mathbf{z}_1^{(i)}, \mathbf{x}_1^{(\bar{i})}, t_m) = g_1^{(i)}(\mathbf{z}_1^{(i)}, \mathbf{x}_1^{(\bar{i})}, t_{m\pm}) = 0, \qquad \text{for } \Omega_2^{(i)} \to \Omega_1^{(i)} \qquad (76)$$
$$(-1)^i G^{(1,1)}(\mathbf{z}_1^{(i)}, \mathbf{x}_1^{(\bar{i})}, t_{m\pm}) < 0.$$

Similarly, the conditions for stick vanishing of domain $\Omega_3^{(i)}$ and entering domain $\Omega_1^{(i)}$ become

$$G^{(0,3)}(\mathbf{z}_3^{(i)}, \mathbf{x}_3^{(\bar{i})}, t_{m-}) = (-1)^i g_3^{(i)}(\mathbf{z}_3^{(i)}, \mathbf{x}_3^{(\bar{i})}, t_{m-}) < 0,$$
$$G^{(0,1)}(\mathbf{z}_1^{(i)}, \mathbf{x}_1^{(\bar{i})}, t_m) = g_1^{(i)}(\mathbf{z}_1^{(i)}, \mathbf{x}_1^{(\bar{i})}, t_{m\pm}) = 0, \qquad \text{for } \Omega_3^{(i)} \to \Omega_1^{(i)} \qquad (77)$$
$$(-1)^i G^{(1,1)}(\mathbf{z}_1^{(i)}, \mathbf{x}_1^{(\bar{i})}, t_{m\pm}) < 0$$

For $i = 1$ in Eq.(76), we have $g_1^{(1)}(\mathbf{z}_1^{(1)}, \mathbf{x}_1^{(2)}, t_m) = 0$. Because $G^{(1,1)}(\mathbf{z}_1^{(1)}, \mathbf{x}_1^{(2)}, t_{m\pm}) > 0$, for $t = t_m + \varepsilon$,

$g_1^{(1)}(\mathbf{z}_1^{(1)}, \mathbf{x}_1^{(2)}, t_{m+}) > 0$. This implies that the relative acceleration of the bolster to the wedge is

positive, and in the next moment the two oscillators must move apart. In Figure 3.6, the

vanishing of stick motion in Eq.(76) is sketched.

Figure 3.6. Stick motion vanishing on $\partial \Omega_{21}^{(1)}$.

From Eq.(23), $g_\alpha^{(i)}(\mathbf{z}_\alpha^{(i)}, \mathbf{x}_\alpha^{(\bar{i})}, t)$ is equivalent to $g_\alpha^{(i)}(\mathbf{z}_\alpha^{(i)}, \mathbf{x}_\alpha^{(\bar{i})}, t)$ because $\mathbf{x}_\alpha^{(\bar{i})}$ is a function of

time and the calculation of $G^{(1,\alpha)}(\mathbf{z}_\alpha^{(i)}, \mathbf{x}_\alpha^{(\bar{i})}, , t)$ from Eq.(75) is given by

$$G^{(1,\alpha)}(\mathbf{z}_\alpha^{(i)}, \mathbf{x}_{\bar{\alpha}}^{(\bar{i})}, t) = -2\zeta_\alpha^{(i)}\ddot{z}_\alpha^{(i)} - (\omega_\alpha^{(i)})^2 \dot{z}_\alpha^{(i)} - Q_\alpha^{(i)}\Omega\sin\Omega t$$
$$-\dddot{x}_\alpha^{(\bar{i})} - 2\zeta_\alpha^{(\bar{i})}\ddot{x}_\alpha^{(\bar{i})} - (\omega_\alpha^{(\bar{i})})^2 \dot{x}_\alpha^{(\bar{i})}. \tag{77}$$

Therefore, the function $G^{(1,\alpha)}(\mathbf{z}_\alpha^{(i)}, \mathbf{x}_\alpha^{(\bar{i})}, t)$ is a relative jerk in domain $\Omega_\alpha^{(i)}$. From Eqs.(29) and

(31), the relative jerk is given by

$$J_\alpha^{(i)}(t) = -2\zeta_\alpha^{(i)}\ddot{z}_\alpha^{(i)} - (\omega_\alpha^{(i)})^2 \dot{z}_\alpha^{(i)} - Q_\alpha^{(i)}\Omega\sin\Omega t$$
$$-\dddot{x}_\alpha^{(\bar{i})} - 2\zeta_\alpha^{(i)}\ddot{x}_\alpha^{(\bar{i})} - (\omega_\alpha^{(\bar{i})})^2 \dot{x}_\alpha^{(\bar{i})}. \tag{78}$$

The function $g_\alpha^{(i)}(\mathbf{z}_\alpha^{(i)}, \mathbf{x}_\alpha^{(\bar{i})}, t)$ is a relative acceleration or a relative force per unit mass. From Luo

(2008) and (2009), the grazing of stick motion requires

$$\left.\begin{array}{l} G^{(0,1)}(\mathbf{z}_1^{(i)}, \mathbf{x}_1^{(\bar{i})}, t_m) = g_1^{(i)}(\mathbf{z}_1^{(i)}, \mathbf{x}_1^{(\bar{i})}, t_{m\pm}) = 0 \\[6pt] G^{(1,1)}(\mathbf{z}_1^{(i)}, \mathbf{x}_1^{(\bar{i})}, t_{m-}) = (-1)^i Dg_1^{(i)}(\mathbf{z}_1^{(i)}, \mathbf{x}_1^{(\bar{i})}, t_{m-}) > 0 \\[6pt] G^{(0,2)}(\mathbf{z}_2^{(i)}, \mathbf{x}_2^{(\bar{i})}, t_m) = g_2^{(i)}(\mathbf{z}_2^{(i)}, \mathbf{x}_2^{(\bar{i})}, t_{m\pm}) = 0 \\[6pt] (-1)^i G^{(1,2)}(\mathbf{z}_2^{(i)}, \mathbf{x}_2^{(\bar{i})}, t_{m\pm}) > 0 \end{array}\right\} \text{for } \mathbf{n}_{\partial\Omega_{21}^{(i)}} \to \Omega_1^{(i)}, \tag{79}$$

$$\left.\begin{array}{l} G^{(0,1)}(\mathbf{z}_1^{(i)}, \mathbf{x}_1^{(\bar{i})}, t_{m\pm}) = g_1^{(i)}(\mathbf{z}_1^{(i)}, \mathbf{x}_1^{(\bar{i})}, t_{m\pm}) = 0 \\[6pt] G^{(1,1)}(\mathbf{z}_1^{(i)}, \mathbf{x}_3^{(\bar{i})}, t_{m-}) = (-1)^i Dg_1^{(i)}(\mathbf{z}_1^{(i)}, \mathbf{x}_3^{(\bar{i})}, t_{m-}) > 0 \\[6pt] G^{(0,3)}(\mathbf{z}_3^{(i)}, \mathbf{x}_3^{(\bar{i})}, t_{m\pm}) = g_3^{(i)}(\mathbf{z}_3^{(i)}, \mathbf{x}_3^{(\bar{i})}, t_{m\pm}) = 0 \\[6pt] (-1)^i G^{(1,3)}(\mathbf{z}_3^{(i)}, \mathbf{x}_1^{(\bar{i})}, t_{m\pm}) > 0 \end{array}\right\} \text{for } \mathbf{n}_{\partial\Omega_{31}^{(i)}} \to \Omega_1^{(i)}. \tag{80}$$

In Figure 3.7, an illustration of grazing motion is presented to help understand the analytical

grazing conditions in Eq.(80). The blue circle designates the starting point within the stick

domain $\Omega_2^{(1)}$. With $G^{(0,2)}(\mathbf{z}_2^{(1)}, \mathbf{x}_2^{(2)}, t) > 0$, the solid black curve approaches the boundary $\partial\Omega_{21}^{(1)}$.

Upon reaching the boundary at time t_m, $G^{(0,2)}(\mathbf{z}_2^{(1)}, \mathbf{x}_2^{(2)}, t_m) = 0$. However $G^{(1,2)}(\mathbf{z}_2^{(1)}, \mathbf{x}_2^{(2)}, t_m) < 0$

so for $t > t_m + \varepsilon$, $G^{(0,2)}(\mathbf{z}_2^{(1)}, \mathbf{x}_2^{(2)}, t_{m+\varepsilon}) < 0$ will be true. With the stick motion conditions of

Eq.(73), the wedge and bolster will remain in Ω_2. Furthermore, with $G^{(0,2)}(\mathbf{z}_m^{(i)}, t_{m+\varepsilon}) < 0$ the

solid black curve in Figure 3.7 will move to back to domain Ω_2 to keep contact without

interaction to the boundary $\partial\Omega_{21}$.
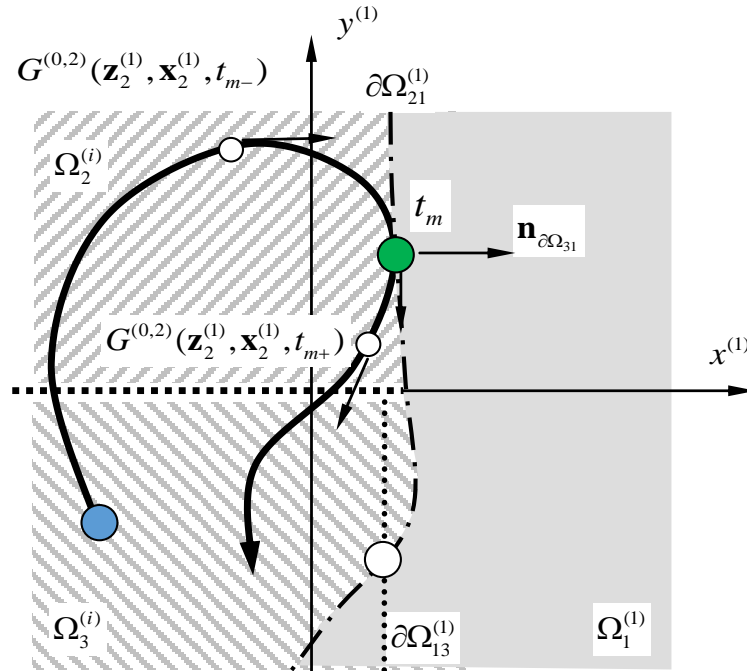
Figure 3.7: Grazing of stick motion at $\partial\Omega_{21}^{(i)}$.

CHAPTER IV

MOTION DESCRIPTION

To discuss periodic impacting chatter with and without stick in the freight train suspension system, the mapping structure will be introduced through the boundaries. Before the mapping structure for a prescribed impacting chatter motion is developed, the switching planes will be defined first, and from the switching planes, the basic mappings will be developed for the mechanical model. Basic mappings will also be defined in the relative frame. A bifurcation scenario will be presented to illustrate complicated motions of the freight train suspension system.

4.1 Switching Sets and Basic Mappings

For a periodic motion with stick motion in the train suspension system, consider the case when the bolster and wedges are sticking together always. Since the discontinuity results from the friction force sign change, the switching planes for stick are defined at zero velocity. However, from Luo & Gegg (2005) and Luo (2009) and (2012), the oscillators may stick to the velocity boundary. From Eq. (19), the corresponding switching planes are defined as

$$
\left.
\begin{aligned}
\Sigma_{23}^{(i)} &= \left\{ (t_k, x_k^{(i)}, \dot{x}_k^{(i)}, \dot{x}_k^{(\bar{i})}) \middle| x_k^{(i)} = x_k^{(\bar{i})} > 0,\ \dot{x}_k^{(i)} = 0 \right\}, \\
\Sigma_{32}^{(i)} &= \left\{ (t_k, x_k^{(i)}, \dot{x}_k^{(i)}, \dot{x}_k^{(\bar{i})}) \middle| x_k^{(i)} = x_k^{(\bar{i})} < 0,\ \dot{x}_k^{(i)} = 0 \right\}, \\
\Sigma_{0}^{(i)} &= \left\{ (t_k, x_k^{(i)}, \dot{x}_k^{(i)}, \dot{x}_k^{(\bar{i})}) \middle| x_k^{(i)} = x_k^{(\bar{i})},\ \dot{x}_k^{(i)} = 0 \right\}.
\end{aligned}
\right\}
\tag{81}
$$

The switching planes $\Sigma_{23}^{(i)}$ and $\Sigma_{32}^{(i)}$ define the switching sets for the zero velocity boundary having a positive or negative displacement, respectively. The switching plane $\Sigma_{0}^{(i)}$ defines the switching set for the zero velocity boundary to stuck with two side walls.
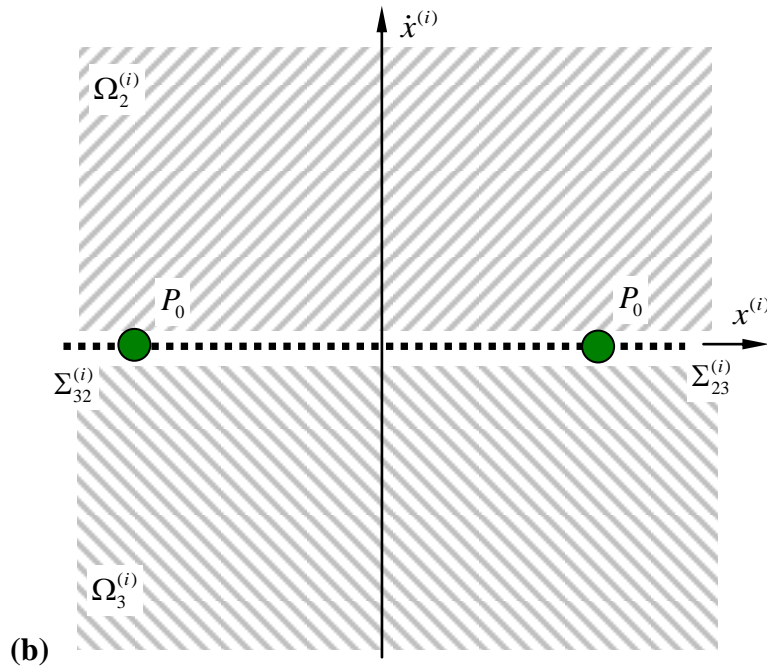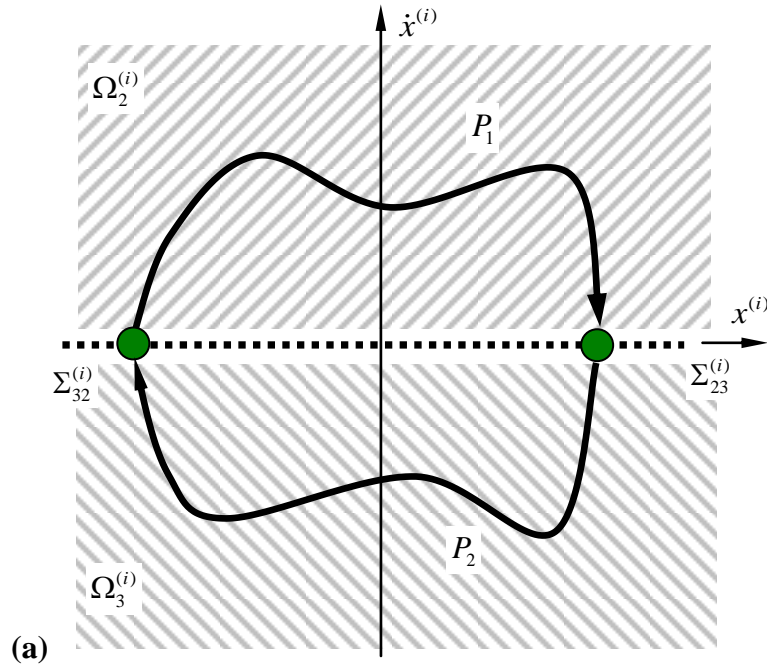
Figure 4.1. Mapping: (a) stick and (b) stuck motion.

From the above switching planes, the mappings are defined as

$$P_0 : \Sigma_0^{(i)} \to \Sigma_0^{(i)}, \; P_1 : \Sigma_{32}^{(i)} \to \Sigma_{23}^{(i)}, \; P_2 : \Sigma_{23}^{(i)} \to \Sigma_{32}^{(i)}. \right\} \tag{82}$$

The P_0 mapping is where the bolster and two wedges are stuck together, but the combined system is also stuck to the wall (i.e., the bolster does not move). The other two mappings (P_1 and P_2) are stick motions with positive and negative velocities, respectively. The switching phase is defined by $\varphi_k = \mathrm{mod}(\Omega t_k, 2\pi)$. To illustrate the stick mappings, P_1 and P_2 are illustrated in Figure 4.1 by the curves with positive and negative velocity, respectively. Since velocity is zero for the stuck mapping P_0, the entire mapping exists as a single point on the phase plane. But, with varying time, the force will be changed, and the stuck motion will start once the force condition is satisfied.

From the discontinuous boundaries, the switching plane based on the impacting chatter boundary is defined as

$$\Sigma_{1\infty}^{(i)} = \left\{ (t_k, x_k^{(i)}, \dot{x}_k^{(i)}, \dot{x}_k^{(\bar{i})}) \middle| x_k^{(\bar{i})} = x_k^{(i)}, \dot{x}_k^{(i)} \neq \dot{x}_k^{(\bar{i})} \right\} \tag{83}$$

for ($i, \bar{i} \in \{1, 2\}$ and $i \neq \bar{i}$). From now on, $x_k^{(i)} \equiv x^{(i)}(t_k)$ and $\dot{x}_k^{(i)} \equiv \dot{x}^{(i)}(t_k)$ are switching displacement and velocity on the separation boundary at time t_k.

Based on the above definition of switching plane, a single mapping for impacting chatter is defined in the absolute frame as

$$P_5 : \Sigma_{1\infty}^{(i)} \to \Sigma_{1\infty}^{(i)}. \tag{84}$$

In Figure 4.2, the P_5 map is illustrated through the curves that connect the switching planes $\Sigma_{1\infty}^{(i)}$. The bolster and two wedges come into contact with repeated impacts but do not stick together (i.e., always free-flight).
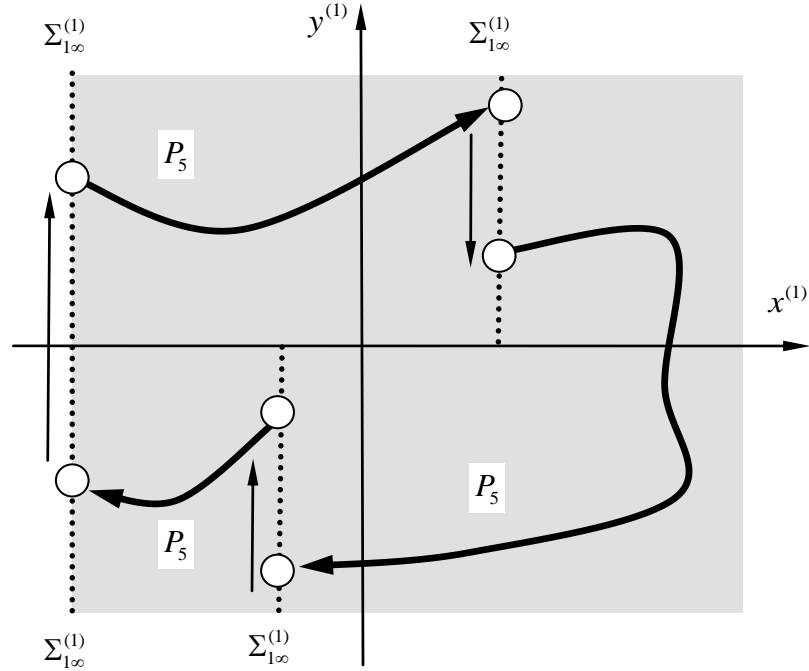
Figure 4.2. The free flight to impacting chatter map P_5.

For the passable stick boundaries $\partial \Omega_{21}^{(i)}$ and $\partial \Omega_{13}^{(i)}$, the corresponding switching sets are

defined as

$$
\left.
\begin{aligned}
\Sigma_{21}^{(i)} &= \left\{ (t_k, x_k^{(i)}, \dot{x}_k^{(i)}, \dot{x}_k^{(\bar{i})}) \,\middle|\, x_k^{(i)} = x_k^{(\bar{i})}, \ \dot{x}_k^{(i)} = \dot{x}_k^{(\bar{i})} > 0 \right\}, \\
\Sigma_{13}^{(i)} &= \left\{ (t_k, x_k^{(i)}, \dot{x}_k^{(i)}, \dot{x}_k^{(\bar{i})}) \,\middle|\, x_k^{(i)} = x_1^{(\bar{i})}, \ \dot{x}_k^{(i)} = \dot{x}_k^{(\bar{i})} < 0 \right\}.
\end{aligned}
\right\}
\tag{85}
$$

Since the stick boundaries separate the free-flight and stick domains, the mappings for other

motions in the mixed domains are defined as

$$
\left.
\begin{aligned}
P_3 &: \Sigma_{32}^{(i)} \to \Sigma_{21}^{(i)}, \ P_4 : \Sigma_{21}^{(i)} \to \Sigma_{1\infty}^{(i)}, \\
P_5 &: \Sigma_{1\infty}^{(i)} \to \Sigma_{1\infty}^{(i)}, P_6 : \Sigma_{13}^{(i)} \to \Sigma_{32}^{(i)}.
\end{aligned}
\right\}
\tag{86}
$$

Upon stick motion separation the motion is described by P_3, and for repeated impacts the motion

is described by P_4. The mappings based on the sticking and impacting switching planes are

presented in Figure 4.3.
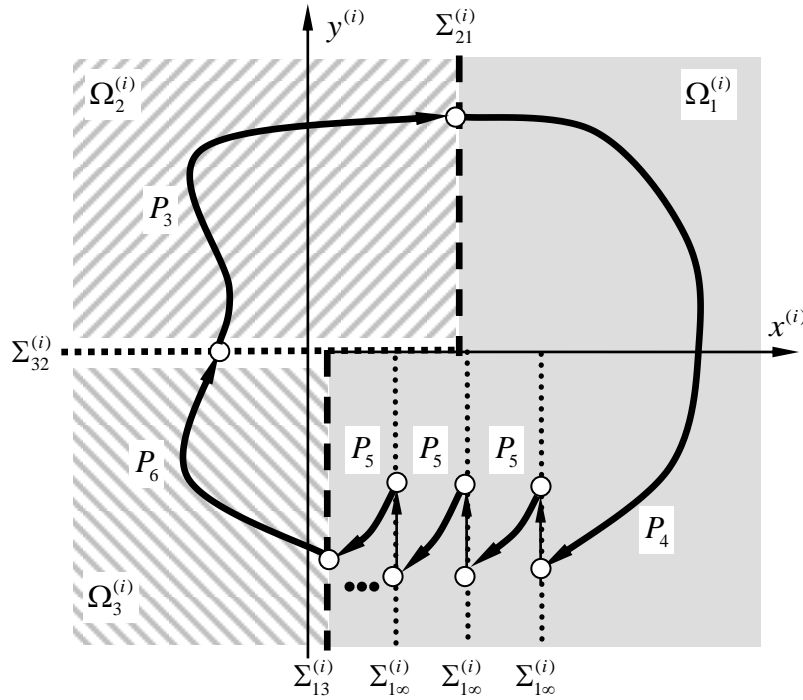
Figure 4.3. Mixed domain mappings with free-flight, chatter, and stick switching.

4.2 Algebraic equations for mappings

For mappings in the absolute and relative frames, set the vectors as

$$\mathbf{y}_k = (t_k, x_k^{(i)}, \dot{x}_k^{(i)}, \dot{x}_k^{(\bar{i})})^{\mathrm{T}}, \text{ and } \mathbf{w}_k = (t_k, z_k^{(i)}, \dot{x}_k^{(i)}, \dot{x}_k^{(\bar{i})})^{\mathrm{T}} \tag{87}$$

For impacting maps P_α ($\alpha = 4, 5$) in the absolute coordinate, $\mathbf{y}_{k+1} = P_\alpha \mathbf{y}_k$ can be expressed by

$$P_\alpha : (t_k, x_k^{(i)}, \dot{x}_k^{(i)}, \dot{x}_k^{(\bar{i})}) \to (t_{k+1}, x_{k+1}^{(i)}, \dot{x}_{k+1}^{(i)}, \dot{x}_{k+1}^{(\bar{i})}) \tag{88}$$

From Appendix A, the absolute displacement and velocity for two gear oscillators can be

obtained with initial conditions $(t_k, x_k^{(i)}, \dot{x}_k^{(i)})$ and $(t_k, x_k^{(\bar{i})}, \dot{x}_k^{(\bar{i})})$. The switching planes require

$x_\gamma^{(i)} = x_\gamma^{(\bar{i})}$ where ($\gamma = k, k+1$), so the final state for time t_{k+1} can be given. The four equations

of displacement and velocity for two oscillators give a set of four algebraic equations, i.e.,

$$\mathbf{f}^{(\alpha)}(\mathbf{y}_k, \mathbf{y}_{k+1}) = 0, \tag{89}$$

where

$$\mathbf{f}^{(\alpha)} = (f_1^{(\alpha)}, f_2^{(\alpha)}, f_3^{(\alpha)}, f_4^{(\alpha)})^\mathrm{T}. \tag{90}$$

For the impact mapping itself, Eq.(86) can be determined from the impact relationships as

$$\left.\begin{aligned}
f_1^{(v)} &= t_{k+1} - t_k, \\
f_2^{(v)} &= x_{k+1}^{(i)} - x_k^{(i)}, \\
f_3^{(v)} &= \dot{x}_{k+1}^{(i)} - I_1^{(i)}\dot{x}_k^{(i)} - I_2^{(i)}\dot{x}_k^{(\bar{i})} \\
f_4^{(v)} &= \dot{x}_{k+1}^{(\bar{i})} - I_1^{(\bar{i})}\dot{x}_k^{(i)} - I_2^{(\bar{i})}\dot{x}_k^{(\bar{i})}
\end{aligned}\right\} \tag{91}$$

For the stick motion, the displacement and velocity of the ith oscillator will be adopted. In

addition, the stick vanishing conditions in Eqs.(75) and (77) will be used.

$$\left.\begin{aligned}
\dot{x}_{k+1}^{(\bar{i})} &= \dot{x}_{k+1}^{(i)}, \\
g_\alpha^{(i)}(t_{k+1}, x_{k+1}^{(\bar{i})}, \dot{x}_{k+1}^{(\bar{i})}, \ddot{x}_{k+1}^{(\bar{i})}) &= 0.
\end{aligned}\right\} \tag{92}$$

With the condition $x_\gamma^{(i)} = x_\gamma^{(\bar{i})}$ for ($\gamma = k, k+1$), the algebraic equations in Eq.(90) can be

obtained. If a mapping starts or ends at the stick boundary, the corresponding displacement plus

the following equation can be employed to obtain Eq.(92).

$$\dot{x}_\gamma^{(i)} = \dot{x}_\gamma^{(\bar{i})} \text{ for } \gamma \in \{k, k+1\} \tag{93}$$

Based on the relative coordinate $(z^{(i)}, \dot{z}^{(i)})$, the relative displacement and velocity can be used

with the initial condition $(t_k, z_k^{(i)}, \dot{z}_k^{(i)})$ on the switching boundary. The displacement and velocity

with an initial condition $(t_k, x_k^{(\bar{i})}, \dot{x}_k^{(\bar{i})})$ can be given. With conditions $z_\gamma^{(i)} = 0$ for ($\gamma = k, k+1$),

the relative and absolute displacements and velocities generate a set of four algebraic equations

as

$$\mathbf{h}^{(\alpha)}(\mathbf{w}_k, \mathbf{w}_{k+1}) = 0 \tag{94}$$

where

$$\mathbf{h}^{(\alpha)} = (h_1^{(\alpha)}, h_2^{(\alpha)}, h_3^{(\alpha)}, h_4^{(\alpha)})^{\mathrm{T}}. \tag{95}$$

In a similar fashion, for stick motion, the stick vanishing condition in Eq.(73) gives

$$\left.\begin{aligned}
\dot{z}_{k+1}^{(i)} &= \dot{z}_k^{(i)} = 0, \\
g_\alpha^{(i)}(t_{k+1}, x_{k+1}^{(\bar{i})}, \dot{x}_{k+1}^{(\bar{i})}, \ddot{x}_{k+1}^{(i)}) &= 0.
\end{aligned}\right\} \tag{96}$$

If a mapping starts or ends at the stick boundary, the relative displacement plus the following

equation can be used to obtain Eq.(94).

$$\dot{z}_\gamma^{(i)} = 0 \text{ for } \gamma \in \{k, k+1\}. \tag{97}$$

For the impact mapping in relative coordinates, the corresponding functions in Eq.(94) are

$$\left.\begin{aligned}
h_1^{(v)} &= t_{k+1} - t_k, \\
h_2^{(v)} &= x_{k+1}^{(\bar{i})} - x_k^{(\bar{i})}, \\
h_3^{(v)} &= \dot{z}_{k+1}^{(i)} - e\dot{z}_k^{(i)} \\
h_4^{(v)} &= \dot{x}_{k+1}^{(\bar{i})} - x_k^{(\bar{i})} - \frac{m_i(1+\delta_i^2)}{m_1+2m_2}(\dot{z}_{k+1}^{(i)} - \dot{z}_k^{(i)})
\end{aligned}\right\} \tag{98}$$

For simplicity of mapping structures of periodic motions, the impact mapping will be dropped

from now on, but the impact relation will be embedded. For stuck motion mapping P_0, the

system of equations to connect the switching points before and after stuck motion are given by

$$\left.\begin{aligned}
\mathbf{f}^{(0)}(\mathbf{y}_k, \mathbf{y}_{k+1}) &= 0, \\
F_2^{(i)}(\mathbf{x}_k^{(i)}, t_k) \times F_3^{(i)}(\mathbf{x}_k^{(i)}, t_k) &< 0
\end{aligned}\right. \tag{99}$$

where

$$\left.\begin{aligned}
f_1^{(0)} &= x_{k+1}^{(i)} - x_k^{(i)}, \\
f_2^{(0)} &= \dot{x}_{k+1}^{(i)}, \\
f_3^{(0)} &= \dot{x}_k^{(i)}, \\
f_4^{(0)} &= F_2^{(i)}(\mathbf{x}_{k+1}^{(i)}, t_{k+1}) \times F_3^{(i)}(\mathbf{x}_{k+1}^{(i)}, t_{k+1}).
\end{aligned}\right\} \tag{100}$$

4.3 Mapping structures

To investigate periodic motions in such a freight train suspension system, the notation for mapping actions of basic mappings is introduced as in Luo (2009) and (2012)

$$P_{n_k \cdots n_1 n_0} \equiv P_{n_k} \circ \cdots \circ P_{n_1} \circ P_{n_0} \tag{101}$$

where the mapping P_{n_j} ($n_j \in \{0,1,\ldots,6\}$, $j = 1,2,\ldots,k$) is defined in the previous section. Consider a generalized mapping structure as

$$P_{\underbrace{(65^{k_{s4}}432^{k_{s3}}1^{k_{s2}}0^{k_{s1}}) \cdots (65^{k_{41}}432^{k_{31}}1^{k_{21}}0^{k_{11}})}_{s-terms}} = P_{(65^{k_{s4}}432^{k_{s3}}1^{k_{s2}}0^{k_{s1}})} \circ \cdots \circ P_{(65^{k_{41}}432^{k_{31}}1^{k_{21}}0^{k_{11}})} \tag{102}$$

where ($k_{\mu\nu} \in \{0,\mathbb{N}\}$, $\mu = 1,2,\cdots,s$, $\nu = 1,2,3,4$). From the generalized mapping structure, consider a simple mapping structure of periodic motions for impacting chatter with stick and stuck motion. For instance, the mapping structure is

$$P_{65^m 430} \equiv P_6 \circ P_{5^m} \circ P_4 \circ P_3 \circ P_0 \tag{103}$$

where $m \in \{0,\mathbb{N}\}$. Such a mapping structure gives $(m+1)$ impacts on the boundary $\partial\Omega_{1\infty}$ which are described by mappings. Consider a periodic motion of $P_{65^m 430}$ with period $T_1 = k_1 T$ ($k_1 \in \mathbb{N}$). If the mapping structure copies itself, the new mapping structure is:

$$P_{(65^m 430)^2} = P_{65^m 430} \circ P_{65^m 430} \tag{104}$$

The periodic motion of $P_{(65^m 430)^2}$ is obtained during a period of $2T_1$. In a similar fashion, such an action of mapping structure continues to copy itself with period-$2^l T_1$.

$$P_{(65^m 430)^{2^l}} = P_{(65^m 430)^{2^{l-1}}} \circ P_{(65^m 430)^{2^{l-1}}} \tag{105}$$

As $l \to \infty$, a chaotic motion relative to mapping structure $P_{65^m 430}$ is formed. The prescribed chaos is generated by period-doubling. However, if grazing bifurcation occurs, such a mapping

structure may not be copied by itself. The new mapping structures are combined by the two different mapping structures. For instance,

$$P_{(65^{m^2}430)(65^{m^1}430)} = P_{65^{m^2}430} \circ P_{65^{m^1}430},$$
$$\vdots \tag{106}$$
$$P_{(65^{ml}430)\cdots(65^{m^1}430)} = \underbrace{P_{65^{ml}430} \circ \cdots \circ P_{65^{m^1}430}}_{l-terms}.$$

Such a grazing bifurcation will cause the discontinuity of periodic motions, and chaotic motions may exist between periodic motions $P_{(65^{ml}430)\cdots(65^{m^1}430)}$ and $P_{(65^{ml-1}430)\cdots(65^{m^1}430)}$. If the wedge and bolster do not have free-flight motion or remain in stick motion always, the mapping structure may take the general form

$$P_{\underbrace{2^{k_3}1^{k_2}0^{k_1}}_{s-terms}} = P_{2^{k_s}31^{k_s}20^{k_s}1} \circ P_{2^{k_3}11^{k_2}10^{k_{11}}} \tag{107}$$

In a similar manner above, the period doubling and grazing bifurcation for stick can be discussed.

4.4 Bifurcation scenario

From the motion mappings, a bifurcation scenario can be presented through the switching displacements, velocities, and phases of the wedge and bolster. All the numerical computations are completed from the closed-form solutions in Appendix A. Herein, a set of system parameters ($m_1 = 3$, $m_2 = 1$, $r_1 = r_2 = 0.1$, $k_1 = k_2 = 20$, $A_0 = 20$, $\mu_k = 0.4$ $\theta = 37.5°$, and $e = 0.6$) are considered to investigate the mechanical model. The impacting chatter with and without stick varying with excitation frequency are presented in the following figures. The switching phase $\varphi_k = \Omega t_k$, displacement $x_k^{(1)}$ are shown Figure 4.4 while the two switching velocities $y_k^{(1)}$ and $y_k^{(2)}$ of the bolster and wedges are shown in Figure 4.5. For the range of frequencies labeled "Chatter w/stick", $\Omega \in (0.001, 1.662)$, the motion consists of multiple chatter impacts which
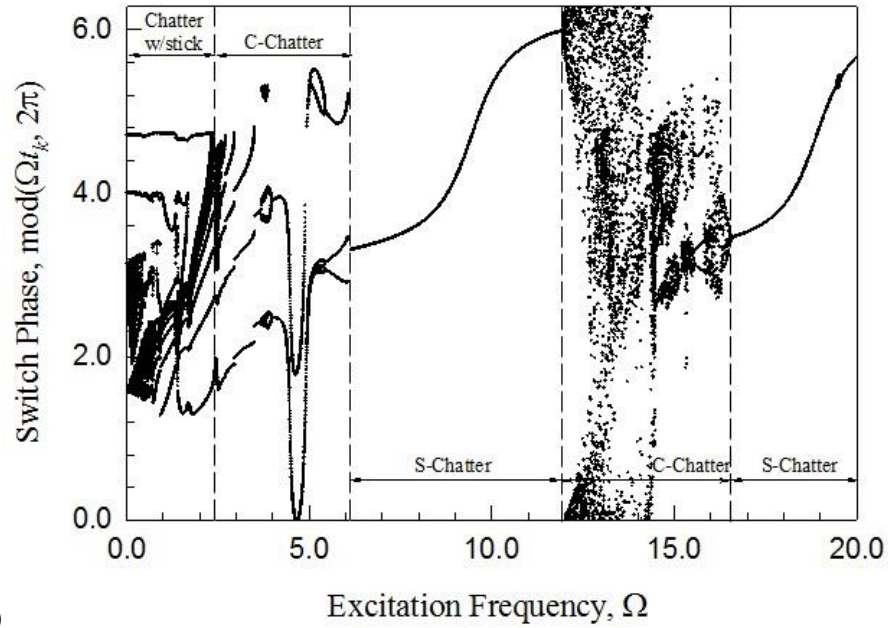
(a)
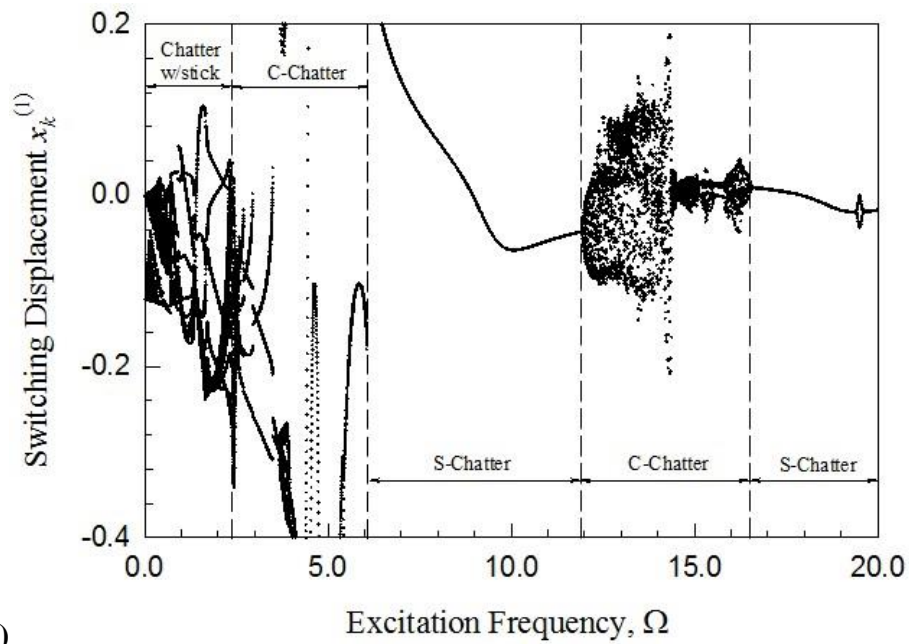
(b)

Figure 4.4. Bifurcation scenario for switching: (a) phase and (b) displacement,
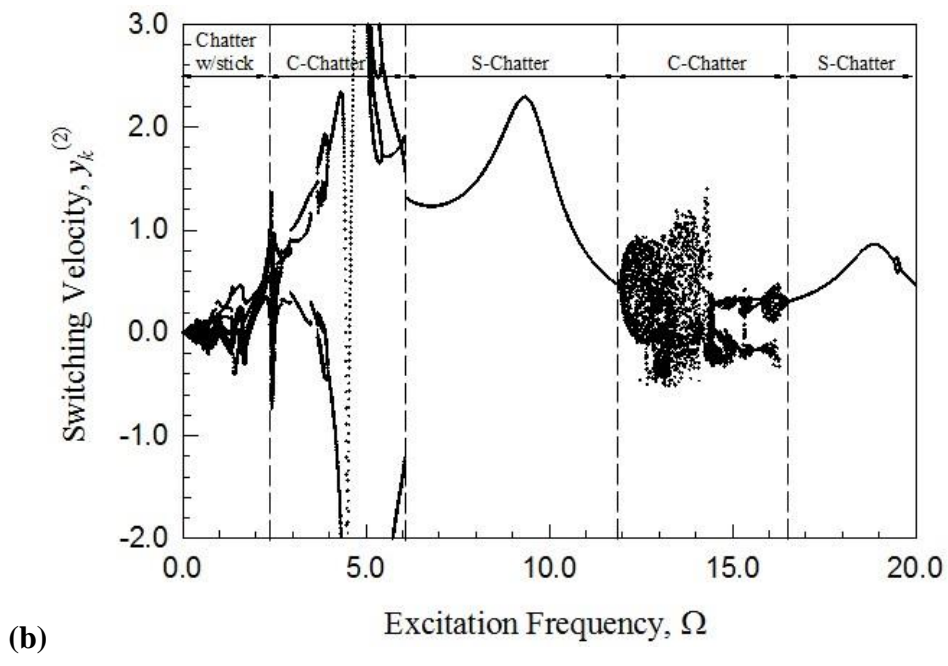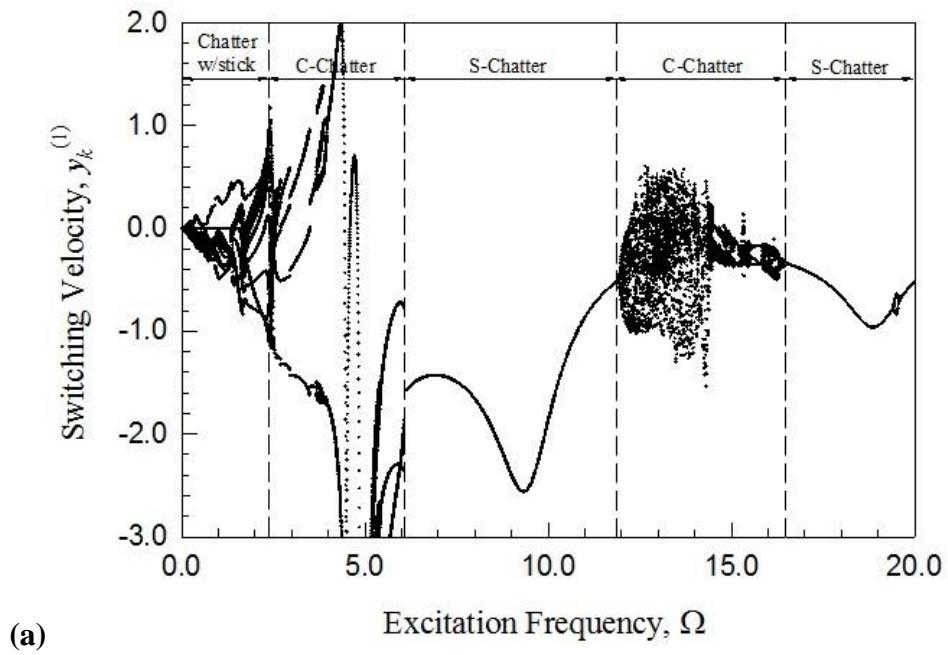
Figure 4.5. Bifurcation scenario for switching: (a) bolster velocity and (b) wedge velocity.

lead to stick motion as well as the possibility of stuck motion. For $\Omega > 1.662$, the stick motion no longer occurs. The "C-chatter" and "S-chatter" describe the ranges for complicated and simple impacting chatters without stick, respectively. For higher frequencies $\Omega \in (5.791, 11.940)$ and $\Omega \in (16.520, 21.500)$, the impacting chatter motion possesses a simple mapping structure, namely P_5. However, for the range $\Omega \in (11.940, 16.519)$ the motion consists of chaotic impacting chatters.

Table 4.1. Summary of excitation frequency for impacting chatter with stick.

Mapping Structure		*Excitation Frequency*, Ω
P_5	P(2T)	(16.520,21.500)
	chaos	(11.940,16.519)
P_{55}	P(2T)	(5.748,5.791)
P_{555}	P(2T)	(4.926,6.059)
$P_{(555)^2}$	P(4T)	(5.026,5.426)
P_5	P(T)	(2.71,5.779), (5.791,11.940)
P_{55}	P(T)	(3.959,4.889)
$P_{(55)^2}$	P(2T)	(3.675,3.9543)
P_{5^3}	P(T)	(2.866,3.495)
P_{5^4}	P(T)	(2.648,2.9465)
P_{5^5}	P(T)	(2.585,2.69424)
P_{5^6}	P(T)	(2.382,2.4351)
$P_{435^{22}}$	P(T)	(1.748,2.316)
$P_{4365^{22}}$	P(T)	(1.667,1.747)

Table 4.2. Summary of excitation frequency for impacting chatter with stuck.

Mapping Structure		Excitation Frequency, Ω
$P_{435^{23}}$	P(T)	(1.748,2.316)
$P_{4365^{22}}$	P(T)	(1.667,1.747)
$P_{43015^{22}}$	P(T)	(1.408,1.662)
$P_{4302015^{19}}$	P(T)	(1.3916,1.4066)
$P_{43020165^{19}}$	P(T)	(1.3830,1.3914)
$P_{4302015^{20}}$	P(T)	(1.3754,1.3828)
$P_{4302065^{20}}$	P(T)	(1.3692,1.3752)
$P_{(43065^{20})(4302065^{20})}$	P(2T)	(13618,1.3690)
$P_{(43065^{20})(4302065^{21})}$	P(2T)	(1.3566, 1.3616)
$P_{(43065^{21})^2}$	P(2T)	(1.352,1.3564)
$P_{43065^{22}}$	P(T)	(0.910,1.330)
$P_{43065^{21}}$	P(T)	(0.7254,0.816), (1.3310,1.3515)
$P_{4302065^{22}}$	P(T)	(0.710,0.7252), (0.8169,0.909)
$P_{(43065^m)^N}$	P(NT), $(m=1,2,3,...k)$	(0.001,0.709)

This pattern of a range of simple impacting chatter switching to a range of chaotic impacting chatter is repeated each time for the excitation frequency near the system's natural frequency. Details of the mapping structures for impacting chatter with and without stick are tabulated in Table 1 and Table 2, respectively.

CHAPTER V

GENERAL PREDICTION RESULTS

In this Chapter, the analytical prediction of periodic motion will be completed through the mapping structure, and the corresponding local stability and bifurcation analysis will be carried out through the eigenvalue analysis. The generalized methodology for analytical prediction and stability analysis of periodic motions will be presented first. The two periodic motions with and without stick will be discussed. The switching displacement, velocity, and phase varying with excitation frequency will be given. Finally, the stability and bifurcation analysis will be presented through the eigenvalues of the prescribed periodic motions.

5.1 Periodic Motions

From mapping structures of periodic motions, the switching sets for any specific periodic motion can be determined through solving a set of nonlinear algebraic equations. Consider a periodic motion of mapping structure $P_{(65^{k_{s4}}432^{k_{s3}}1^{k_{s2}}0^{k_{s1}})\cdots(65^{k_{41}}432^{k_{31}}1^{k_{21}}0^{k_{11}})}$ and the following relation holds.

$$P_{(65^{k_{s4}}432^{k_{s3}}1^{k_{s2}}0^{k_{s1}})\cdots(65^{k_{41}}432^{k_{31}}1^{k_{21}}0^{k_{11}})}\mathbf{y}_k = \mathbf{y}_{k+2s+\sum_{m=1}^{s}\sum_{j=1}^{4}k_{mj}} \tag{108}$$

where $\mathbf{y}_k = (t_k, x_k^{(i)}, \dot{x}_k^{(i)}, \ddot{x}_k^{(\bar{i})})^{\mathrm{T}}$. A set of vector equations is as

$$
\left.
\begin{aligned}
&\mathbf{f}^{(2)}\left(\mathbf{y}_{k+1},\mathbf{y}_{k}\right)=0,\\
&\mathbf{f}^{(2)}\left(\mathbf{y}_{k+2},\mathbf{y}_{k+1}\right)=0,\\
&\vdots\\
&\mathbf{f}^{(6)}\left(\mathbf{y}_{k+2s+\sum_{m=1}^{s}\sum_{j=1}^{4}k_{mj}},\mathbf{y}_{k+2s+\sum_{m=1}^{s}\sum_{j=1}^{4}k_{mj}-1}\right)=0;
\end{aligned}
\right\}
\tag{109}
$$

where $\mathbf{f}^{(\sigma)}=(f_1^{(\sigma)},f_2^{(\sigma)},f_3^{(\sigma)},f_4^{(\sigma)})^{\mathrm{T}}$ is relative to governing equations of mapping P_σ

($\sigma\in\{1,2,\cdots,6\}$). The periodicity of the period-1 motion per N-periods requires

$$
\mathbf{y}_{k+2s+\sum_{m=1}^{s}\sum_{j=1}^{4}k_{mj}}=\mathbf{y}_k
\tag{110}
$$

or

$$
\left.
\begin{aligned}
&x^{(i)}_{k+2s+\sum_{m=1}^{s}\sum_{j=1}^{4}k_{mj}}=x_k^{(i)},\quad \dot{x}^{(i)}_{k+2s+\sum_{m=1}^{s}\sum_{j=1}^{4}k_{mj}}=\dot{x}_k^{(i)},\quad \dot{x}^{(\bar{i})}_{k+2s+\sum_{m=1}^{s}\sum_{j=1}^{4}k_{mj}}=\dot{x}_k^{(\bar{i})},\\
&\Omega t_{k+2s+\sum_{m=1}^{s}\sum_{j=1}^{4}k_{mj}}\equiv\Omega t_k+2N\pi.
\end{aligned}
\right\}
\tag{111}
$$

Solving Eqs.(109) and (110) generates the switching sets for periodic motions. Once the

analytical prediction of any periodic motion is obtained, the corresponding stability and

bifurcation analysis can be completed.

5.2 Stability

The local stability and bifurcation for such a period-1 motion is determined through the

corresponding Jacobian matrix of the Poincaré mapping. From Eq.(109), the Jacobian matrix is

computed by the chain rule,

$$DP = DP_{(65^{k_{s4}}432^{k_{s3}}1^{k_{s2}}0^{k_{s1}})\cdots(65^{k_{41}}432^{k_{31}}1^{k_{21}}0^{k_{11}})}$$

$$= \prod_{m=1}^{n}\left(DP_6 \cdot DP_5^{k_{m4}} \cdot DP_4 \cdot DP_3 \cdot DP_2^{k_{m3}} \cdot DP_1^{k_{m2}} \cdot DP_0^{k_{m1}}\right) \quad (112)$$

where

$$DP_\lambda = \left[\frac{\partial(t_{\nu+1}, x_{\nu+1}^{(i)}, y_{\nu+1}^{(i)}, \partial y_{\nu+1}^{(\bar{i})})}{\partial(t_\nu, x_\nu^{(i)}, y_\nu^{(i)}, \partial y_\nu^{(\bar{i})})}\right] \quad (113)$$

for $\nu = k, k+1, \cdots, k+2s + \sum_{m=1}^{s}\sum_{j=1}^{4} k_{mj} - 1$, and all the Jacobian matrix components can be

computed through Eq.(96). The variational equation for a set of switching points

$\{\mathbf{y}_k^*, \cdots, \mathbf{y}_{k+2s+\sum_{m=1}^{s}\sum_{j=1}^{4}k_{mj}-1}^*\}$ is

$$\Delta\mathbf{y}_{k+2s+\sum_{m=1}^{s}\sum_{j=1}^{4}k_{mj}} = DP(\mathbf{y}_k^*)\Delta\mathbf{y}_k. \quad (114)$$

A derivation of Eq.(109) is shown in Appendix C. The eigenvalues are computed by

$$|DP - \lambda\mathbf{I}| = 0. \quad (115)$$

The Jacobian matrix DP is 4x4, and the eigenvalues can be determined by the QR factorization.

A C++ version of the QR factorization is shown in Appendix D. Because DP is a 4x4 matrix,

there are four eigenvalues. If the four eigenvalues lie inside the unit circle, then the period-1

motion is stable. If one of them lies outside the unit circle, the periodic motion is unstable.

i. If the eigenvalues to be

$$|\lambda_j| < 1, \quad (j = 1, 2, 3, 4). \quad (116)$$

the periodic motion is table.

ii. If the magnitude of any eigenvalue is greater than one,

$$|\lambda_j| > 1, \quad (j \in \{1, 2, 3, 4\}) \quad (117)$$

the periodic motion is unstable. The corresponding bifurcation conditions are summarized as follows.

i. For $|\lambda_j|<1$ $(j=3,4)$ and real λ_j $(j=1,2)$, if

$$\max\{\lambda_j,\, j=1,2\}=1,\quad \min\{\lambda_j,\, j=1,2\}\in(-1,1),\tag{118}$$

then the saddle-node (SN) bifurcation occurs; if

$$\min\{\lambda_j,\, j=1,2\}=-1,\quad \max\{\lambda_j,\, j=1,2\}\in(-1,1),\tag{119}$$

then the period-doubling bifurcation occurs.

ii. For $|\lambda_j|<1$ $(j=3,4)$ and complex λ_j $(j=1,2)$, if

$$|\lambda_j|=1\ (j=1,2),\tag{120}$$

then the Neimark bifurcation occurs.

5.3 Impacting Chatter Prediction

Using the mapping structure in Eq.(102), all the periodic motions for the entire range of excitation frequency can be determined analytically. The mapping structure gives the nonlinear algebraic equations similar to Eqs.(99) and (100), which can be solved by the Newton-Raphson method. Once the first solution is obtained, the rest of the solutions with varying parameters can be determined through the corresponding mapping structure. The generic parameters ($m_1=3$, $m_2=1$, $r_1=r_2=0.1$, $k_1=k_2=20$, $A_0=20$, $\mu_k=0.4$ $\theta=37.5°$, and $e=0.6$) are also used for the analytical prediction of periodic motions. Firstly, the analytical prediction of the simplest periodic motion P_5 is shown in Figures 5.1 and 5.2. The switching phase and displacement of

the bolster (i.e., $y_k^{(1)}$) is plotted in Figure 5.1(a) and (b), respectively. The solid black curve

represents the stable periodic switching phase and displacement while the red dashed curve

represents the unstable periodic switching solutions. Also, the solid blue curve describes the

switching sets for P_{55} after period doubling motion occurs at $\Omega = 5.80$. Note, at switching

points, the switching phase and displacement of the bolster and wedge are identical since they

make contact at $x_k^{(1)} = x_k^{(2)}$ and the wedges have no forcing function. The switching velocities for

each oscillator is presented in Figure 5.2. Due to the impact relationships defined in Chapter 1,

the switching velocity sets are only recorded just before impact.

The corresponding eigenvalues to the analytical prediction of P_5 periodic motion are

presented in Figure 5.3. From local stability analysis gives the excitation frequency range for

stable and unstable periodic motion. The stable range for periodic motion P_5 is found for the

three sets $\Omega \in (16.520, 21.500)$, $\Omega \in (2.71, 5.779)$, and $\Omega \in (5.791, 11.940)$. Again, the solid

black curves and dashed red curves correspond to stable and unstable switching sets,

respectively. Note, the vertical dashed lines show the bifurcation points. Also, "GB" stands for

grazing bifurcation, "NB" stands for Neimark bifurcation, and "PD" stands for period doubling.

From Figure 5.3(a), period doubling occurs when the real part of one eigenvalue equals -1.0 at

$\Omega = 5.791$. The range for stable P_{55} is $\Omega \in (5.748, 5.791)$ with the motion disappearing from a

grazing bifurcation at $\Omega = 5.748$. In Figure 5.4, the eigenvalue magnitudes are plotted to help

show the Neimark bifurcation points. To verify the stability of the period doubling solution P_{55},

the corresponding eigenvalues are plotted in Figure 5.4(b).
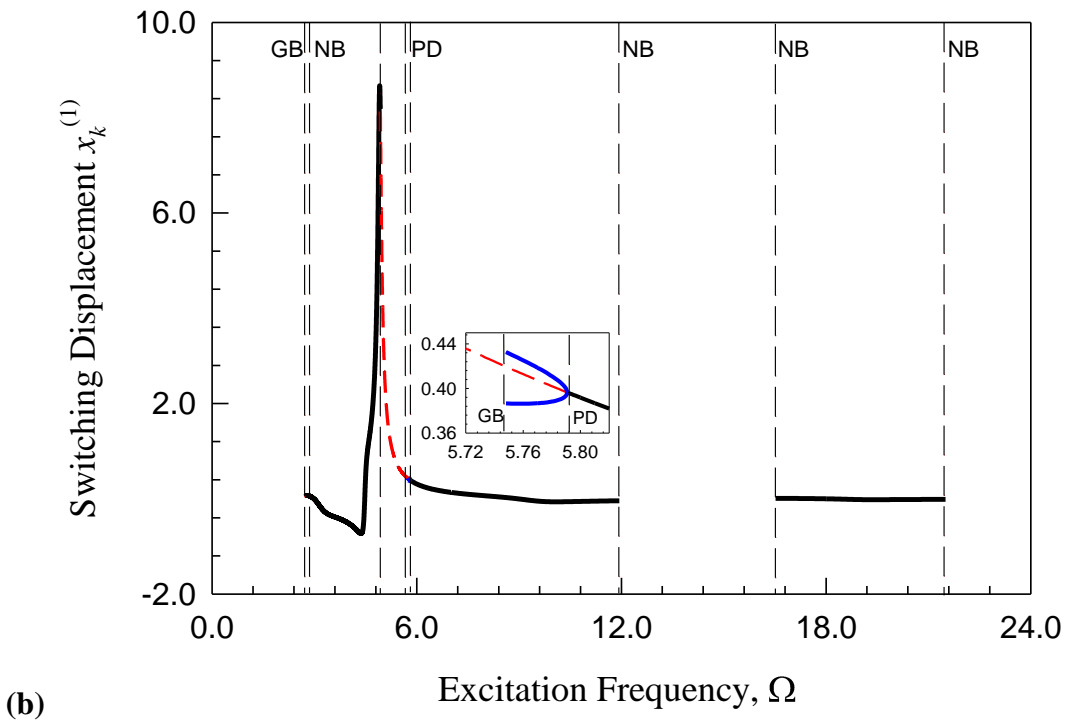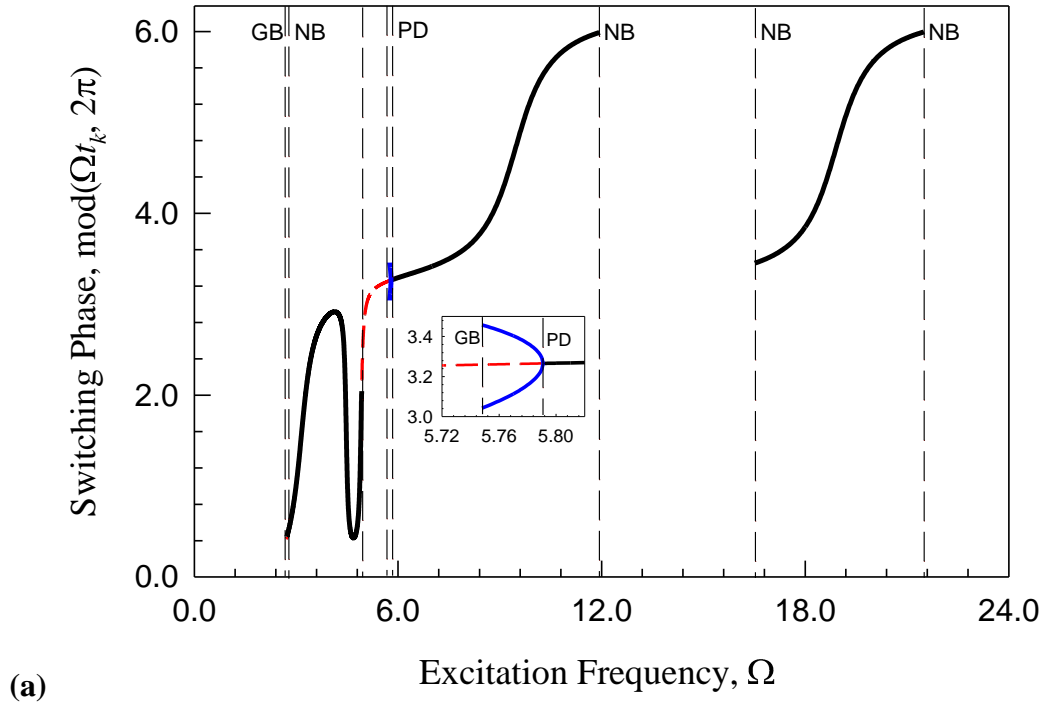
Figure 5.1. Analytical prediction of (a) switching phase and (b) displacement for P_5.
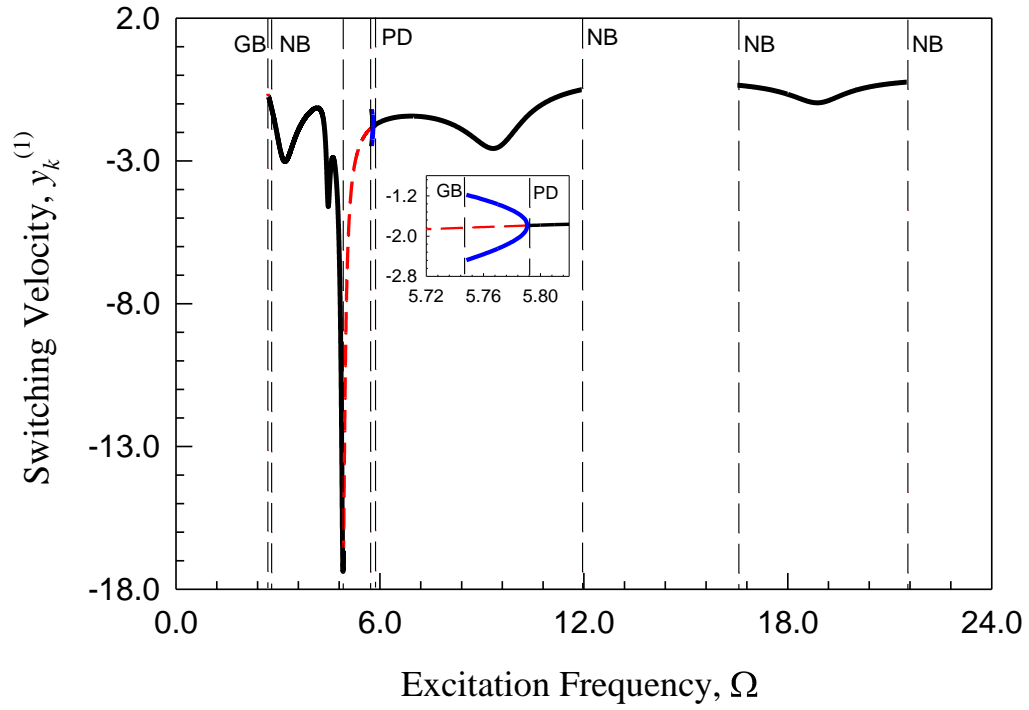
(a)
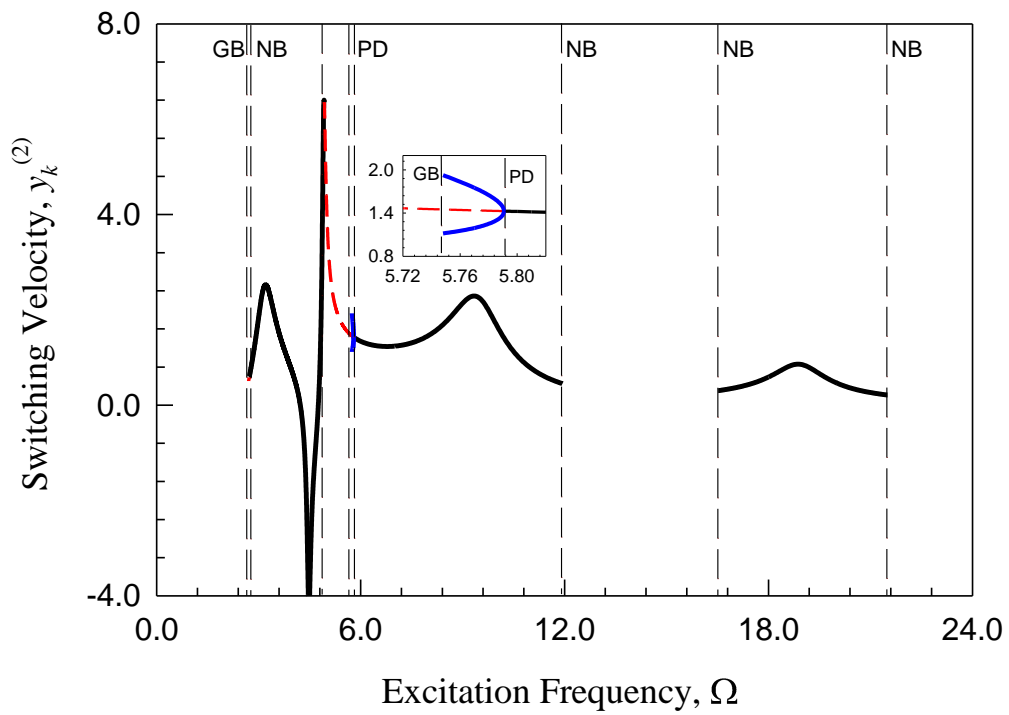
(b)

Figure 5.2. Analytical prediction of switching velocities for P_5.

(a)

(b)
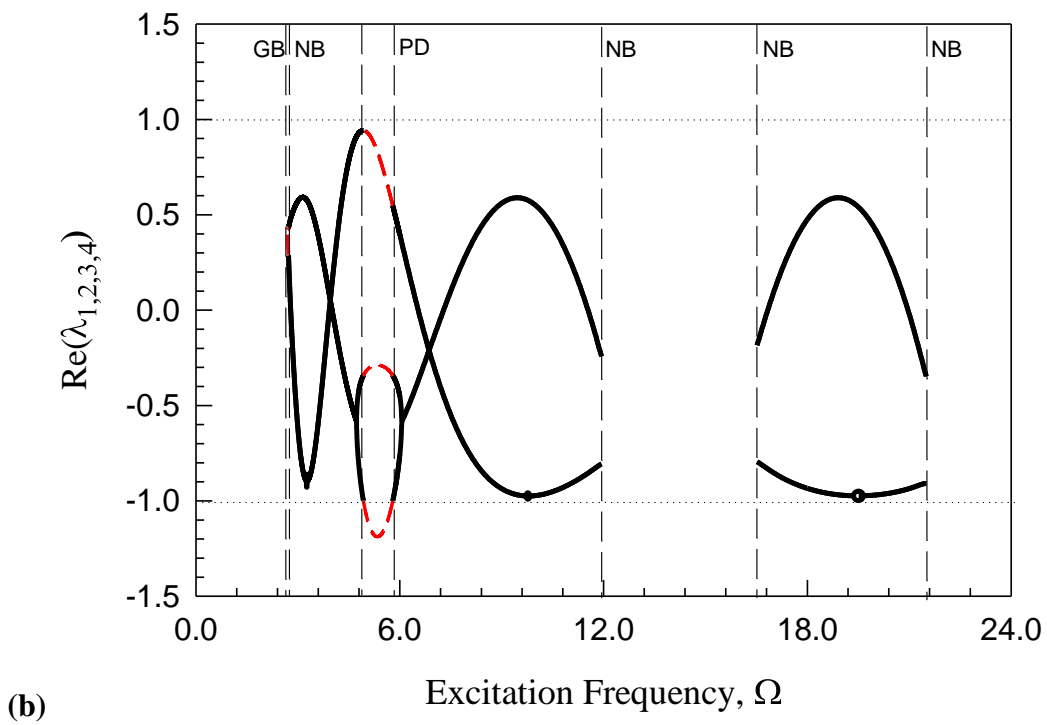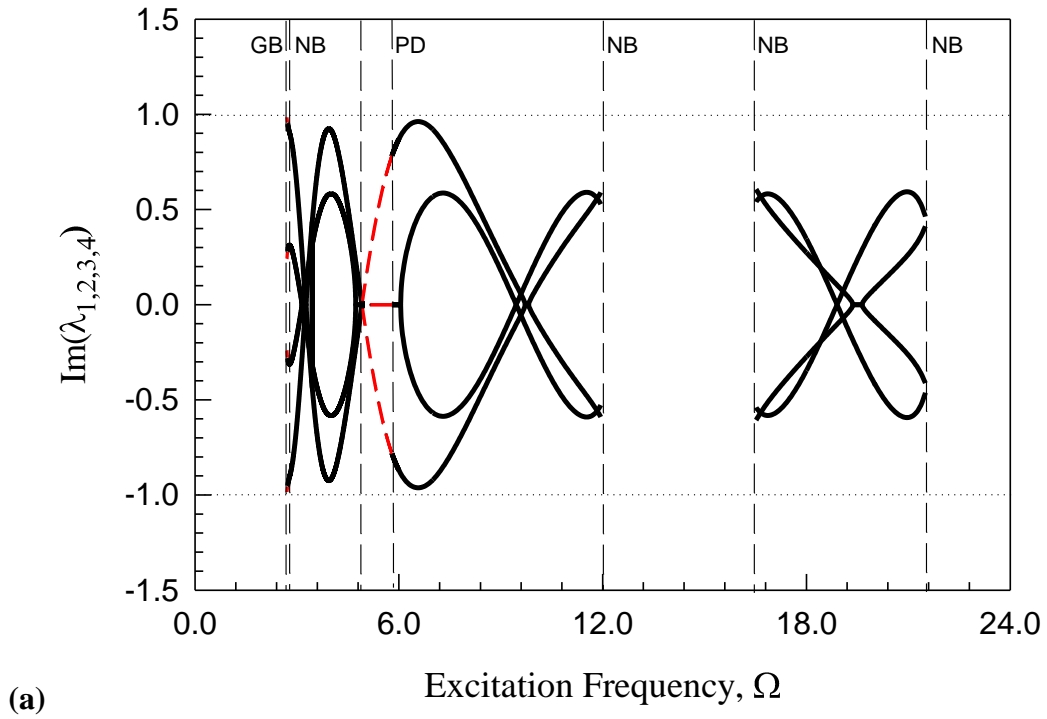
Figure 5.3. Analytical eigenvalues (a) $\text{Re}(\lambda_{1,2,3,4})$ **and (b)** $\text{Im}(\lambda_{1,2,3,4})$ **for** P_5**.**

(a)

(b)
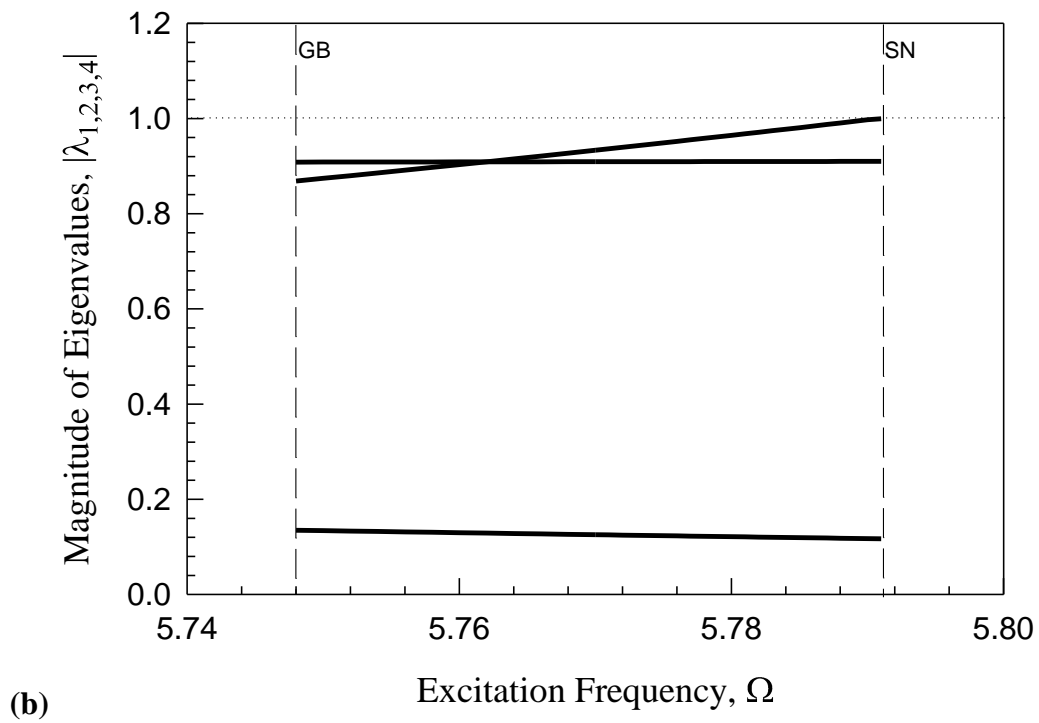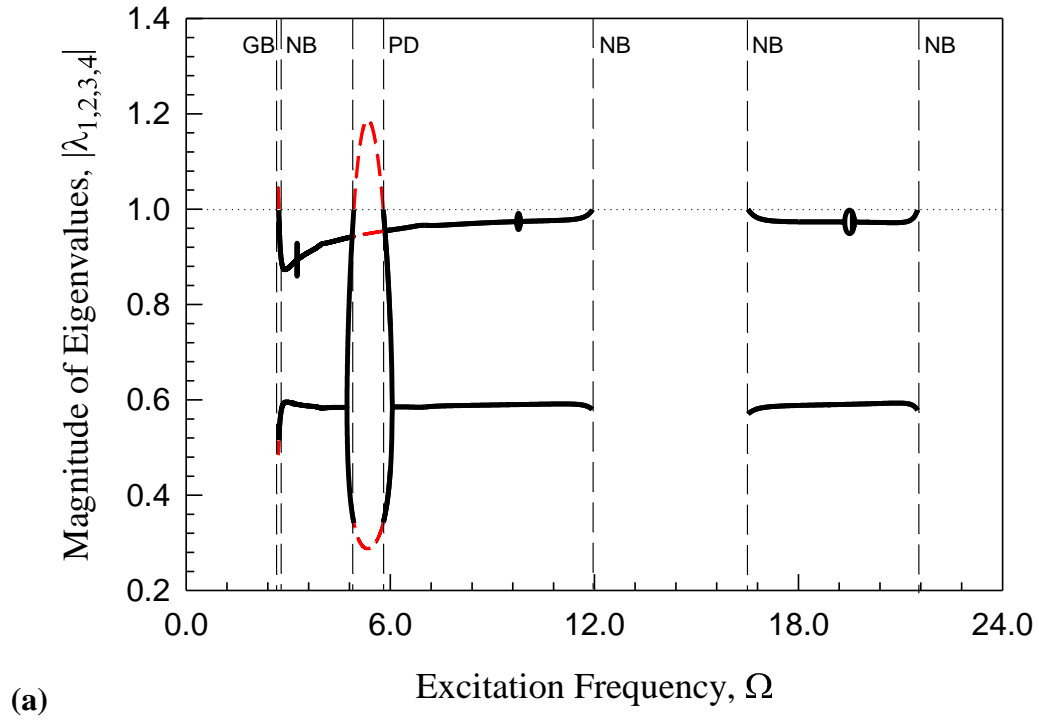
Figure 5.4. Magnitude of eigenvalues for (a) P_5 **and (b)** P_{55}**.**

5.4 Impacting Chatter with Stick and Stuck Prediction

The analytical prediction of periodic motions with stick and stuck motion is also given herein. Using the generic parameters ($m_1 = 3,\ m_2 = 1,\ r_1 = r_2 = 0.1,\ k_1 = k_2 = 20,\ A_0 = 20,\ \mu_k = 0.4\ \theta = 37.5°,$ and $e = 0.6$), the corresponding switching sets varying with excitation frequency are presented in Figures 5.5 through 5.9. Because the computational time is very consuming, the impacting chatters with stick and stuck are predicted only in the range of excitation frequency $\Omega \in (0.710, 2.316)$. In Figure 5.5(a), the switching phase is plotted for the complete set of impacting chatter with stick and stuck. For the range, $\Omega \in (1.667, 2.316)$ there is impacting chatter and stick motion. On the other hand, for the range $\Omega \in (0.710, 1.662)$ there is both impacting chatter with stick as well as stuck motion. Recall, stuck motion is defined by the P_0 map. Due to the complicated motion switching, Figure 5.5(b) describes in more detail the switching phase solutions and mapping structures for the excitation frequency $\Omega \in (1.35, 1.40)$.

The eigenvalues of impacting chatter with stick and stuck motion are presented in Figure 5.9. Note that eigenvalues $\lambda_{3,4}$ are necessarily zero for the entire range of stick motion. Moreover, for stuck motion, the eigenvalues $\lambda_{2,3,4}$ are necessarily zero. In Figure 5.9(a), the vertical dashed lines labeled "SB" represents the stick bifurcations. On the far right, the impacting chatter with stick disappears after $\Omega \approx 2.316$. Consider the range $\Omega \in (1.408, 1.662)$ with mapping structure $P_{43015^{22}}$, the end of stuck motion occurs with a saddle node bifurcation at $\Omega \approx 1.662$. Finally, in impacting chatter to stick motion computation, the computational criterion $|\dot{x}_k^{(1)} - \dot{x}_k^{(2)}| < 10^{-6}$ was embedded as a tolerance to minimize the number of impacts before considering the stick conditions.
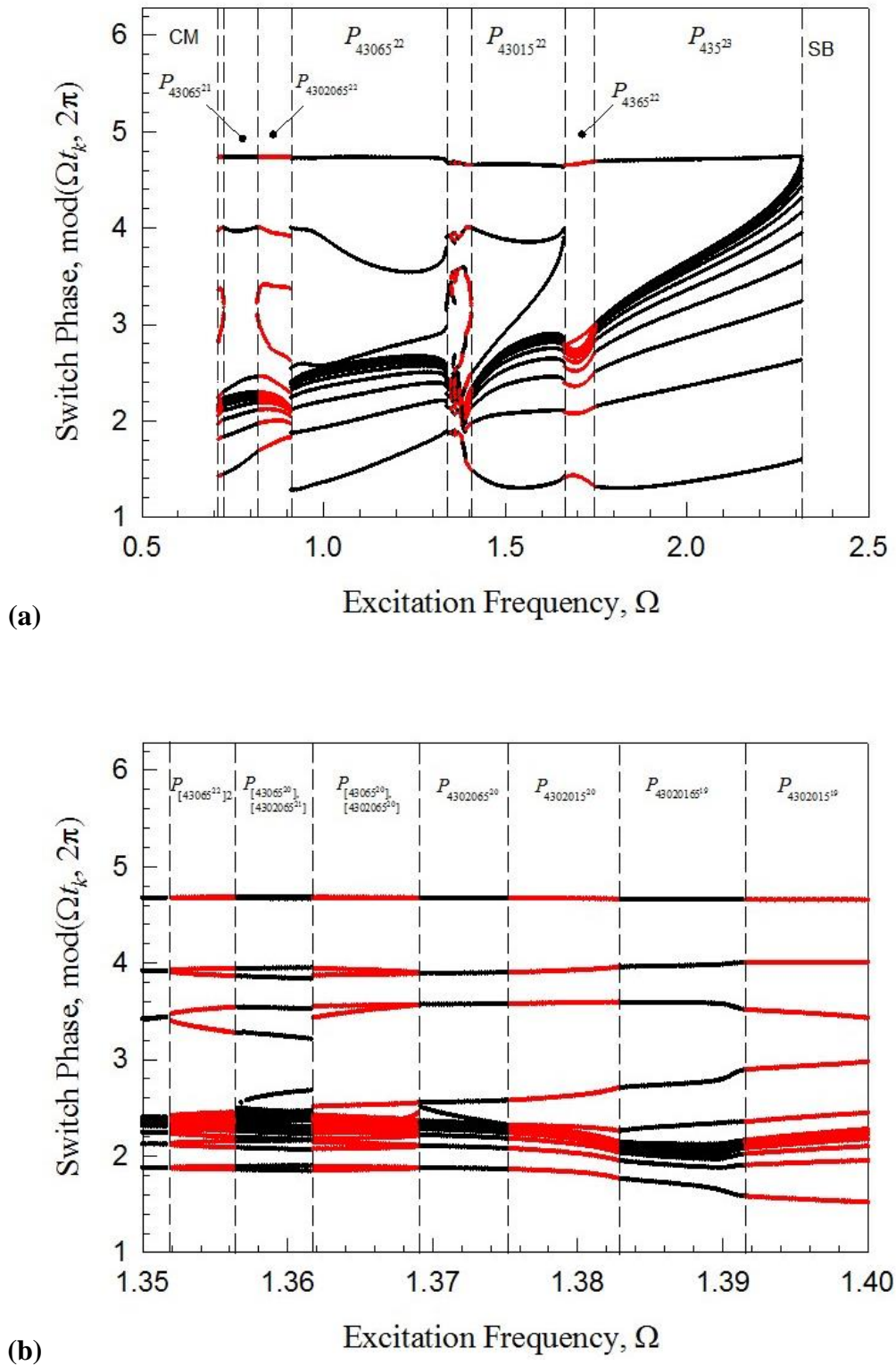
Figure 5.5. Analytical prediction of (a) switching phase (b) zoomed $\Omega \in (1.35, 1.40)$ portion

for chatter with stick and stuck.

(a)

(b)
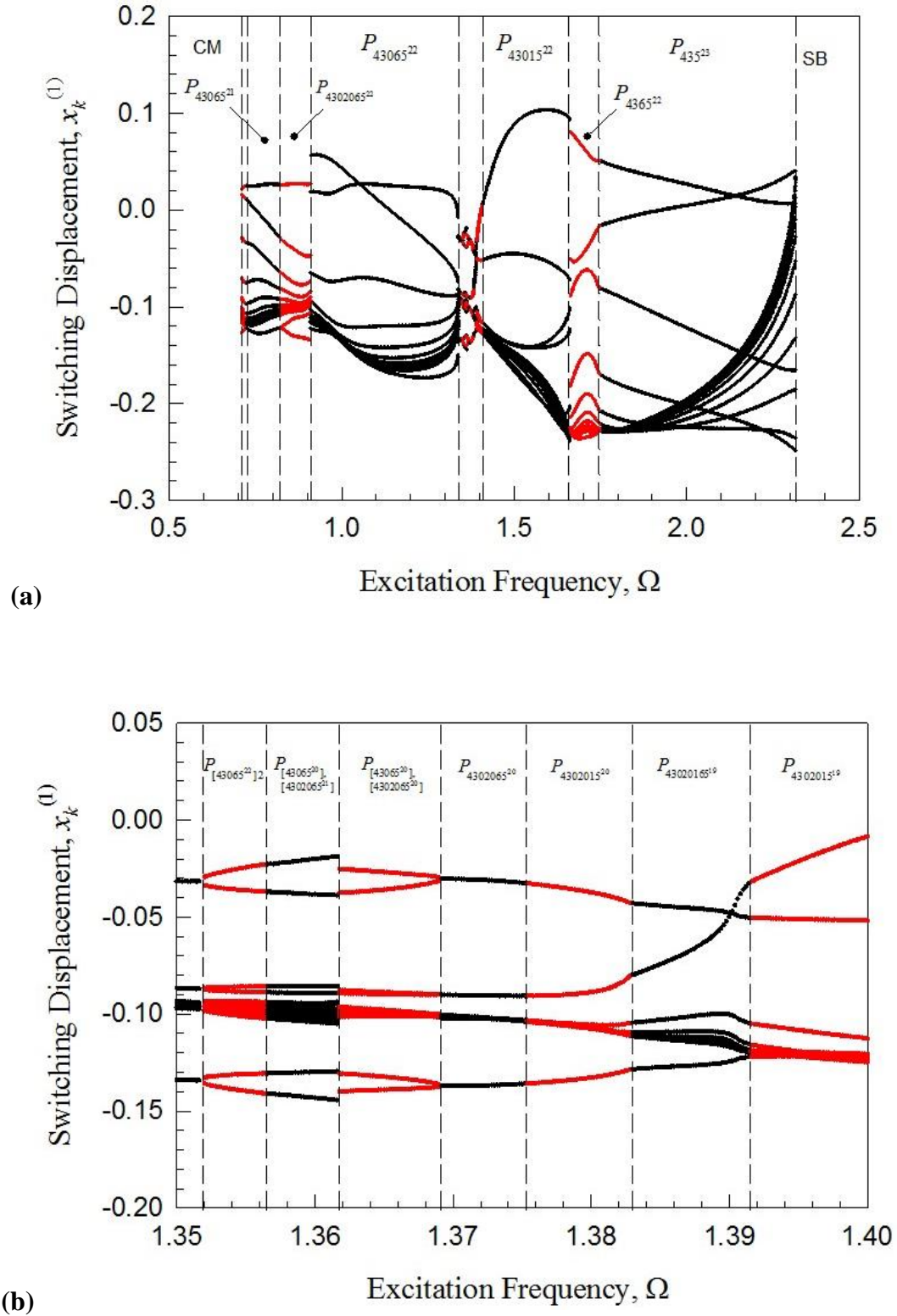
Figure 5.6. Analytical prediction of (a) switching displacement and (b) zoomed

$\Omega \in (1.35, 1.40)$ **portion for chatter with stick and stuck.**

(a)

(b)
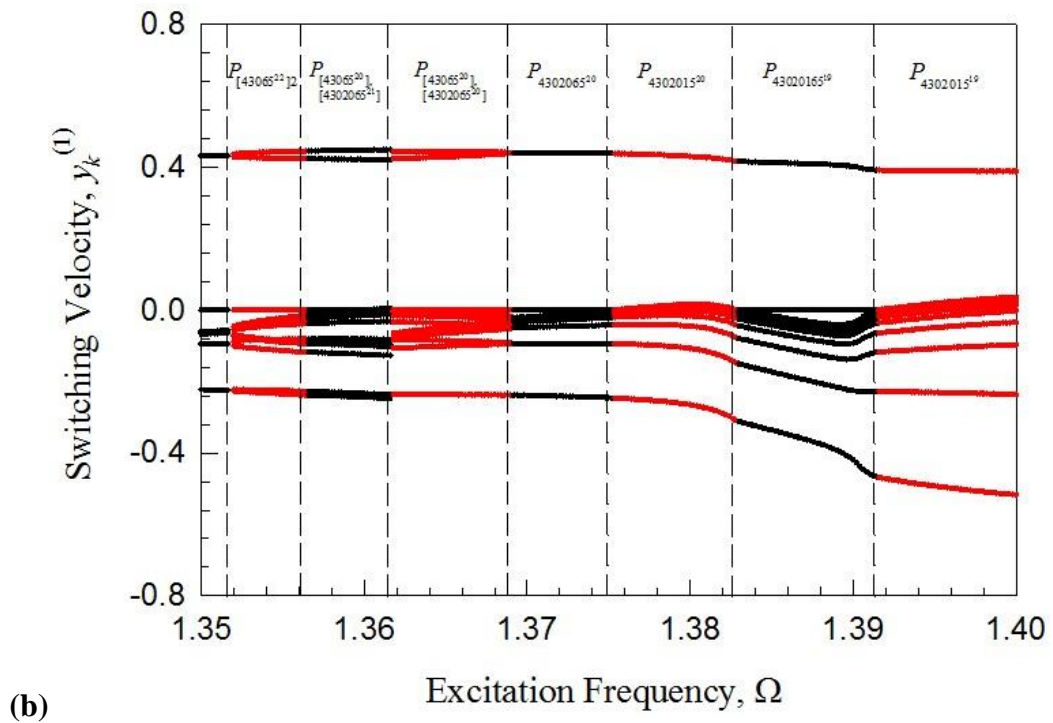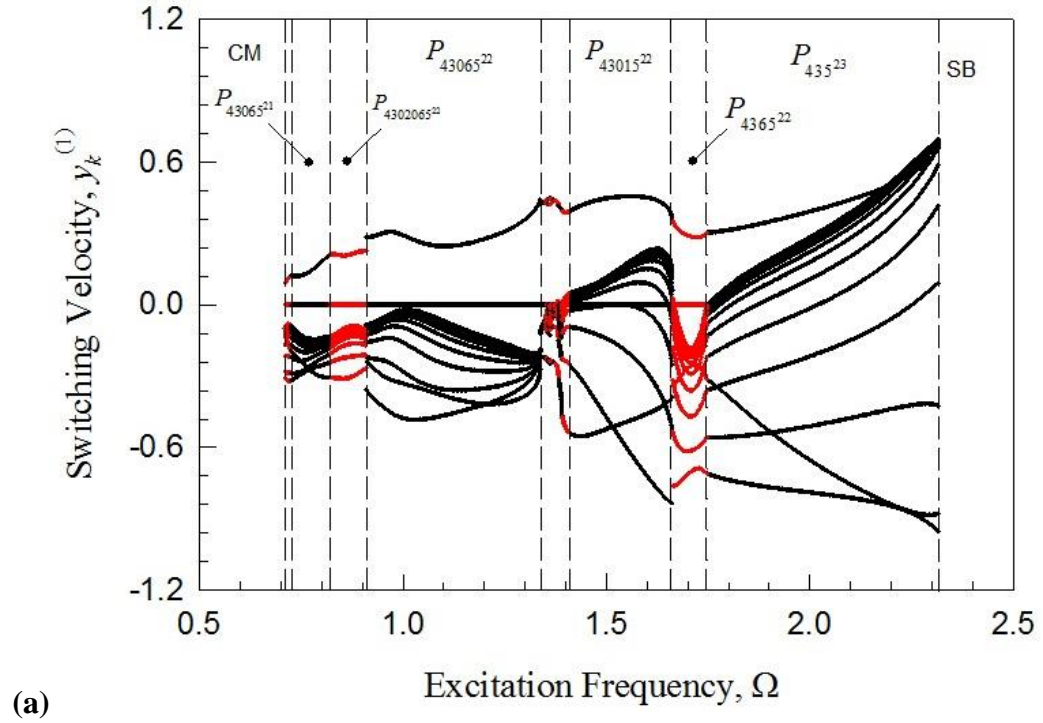
Figure 5.7. Analytical prediction of (a) switching velocity $y^{(1)}$ and (b) zoomed

$\Omega \in (1.35, 1.40)$ **portion for chatter with stick and stuck.**

(a)

(b)
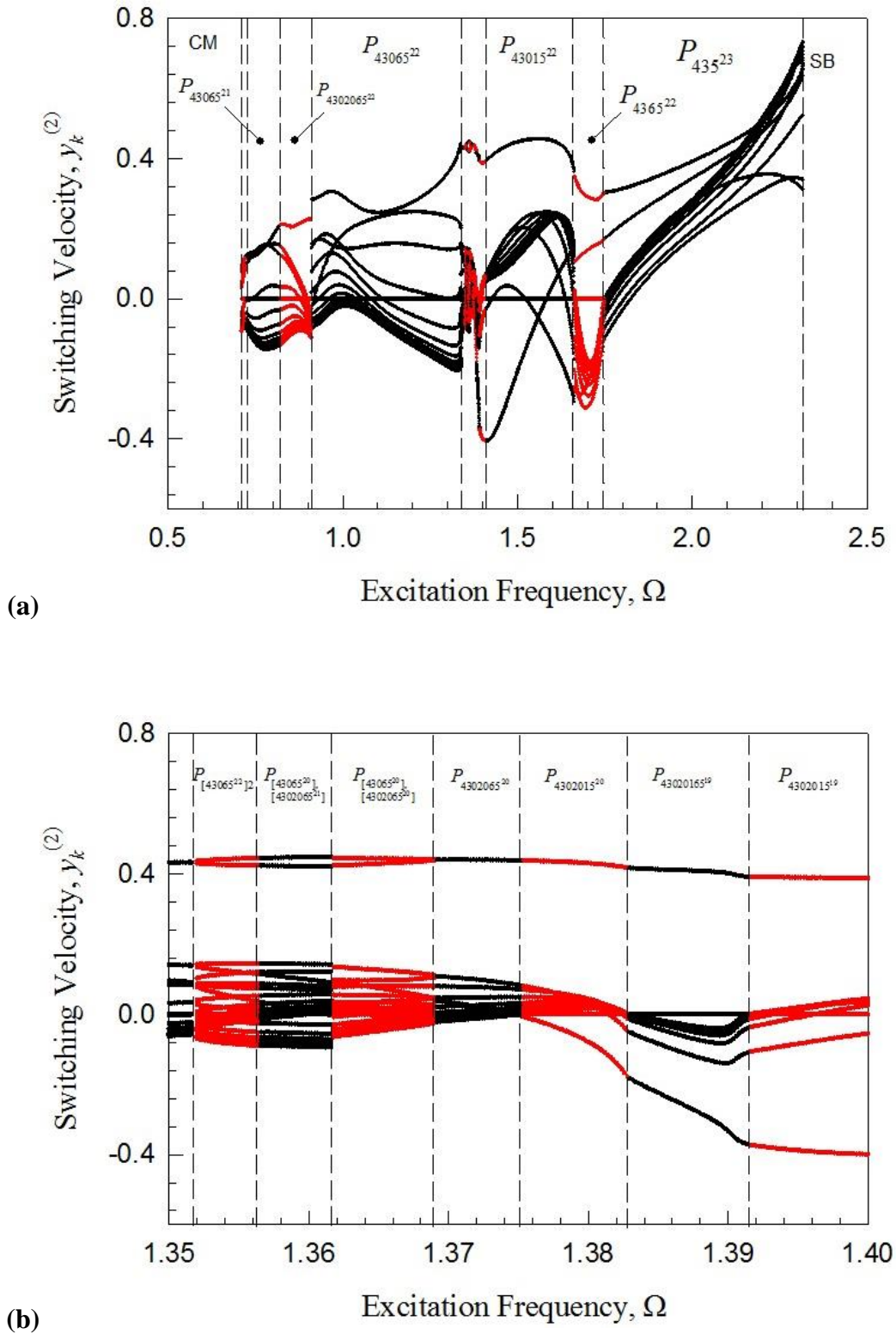
Figure 5.8. Analytical prediction of (a) switching velocity $y^{(2)}$ and (b) zoomed

$\Omega \in (1.35, 1.40)$ **portion for chatter with stick and stuck.**
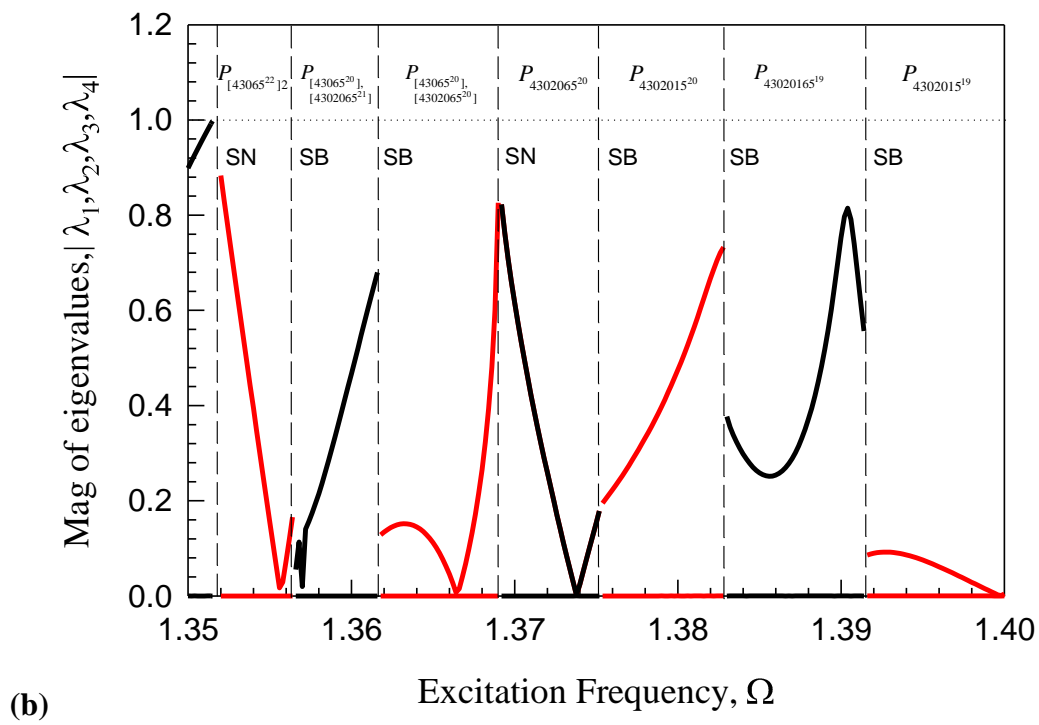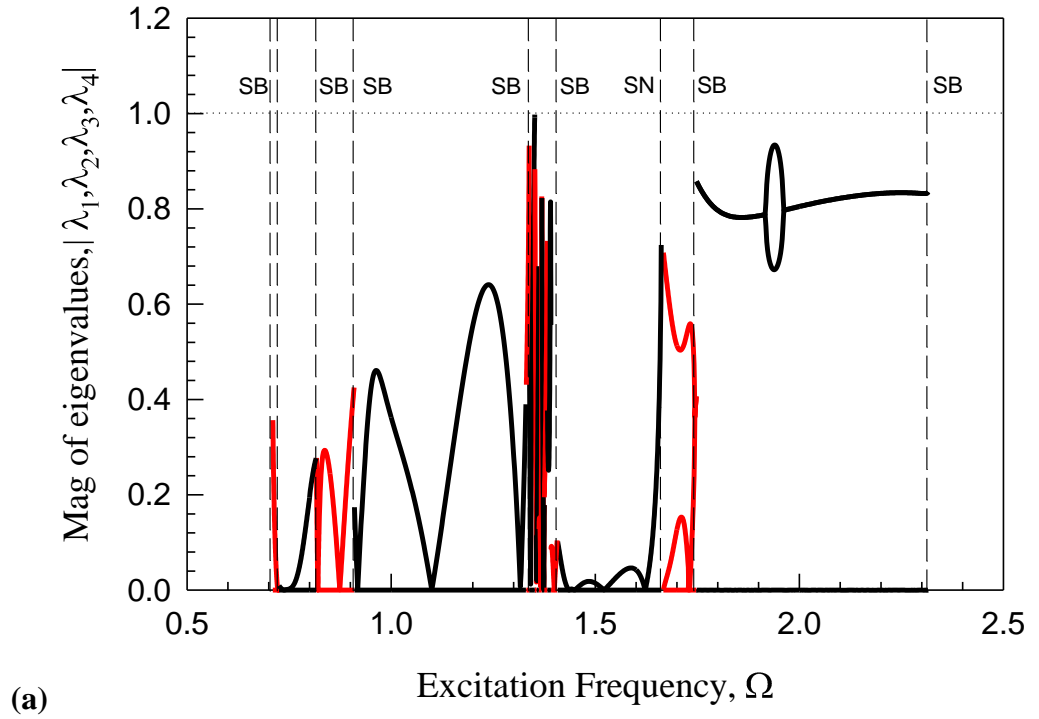
Figure 5.9. Magnitude of eigenvalues for chatter with stick and stuck.

5.5 Numerical Simulation of Periodic Chatter

Numerical illustrations of periodic motions will help one better understand the motion mechanisms of such a mechanical model for a train suspension system. From the analytical prediction of simple impact chatter, the periodic motions will be plotted to illustrate the basic impact phenomena. In addition, the analytical condition for stick motion will be shown to not be satisfied during simple impacting chatter. For the parameters ($m_1 = 3$, $m_2 = 1$, $r_1 = r_2 = 0.1$, $k_1 = k_2 = 20$, $A_0 = 20$, $\mu_k = 0.4$ $\theta = 37.5°$, and $e = 0.6$), consider the excitation frequency $\Omega = 6.0$. The analytical prediction gives the initial condition (i.e., $t_0 = 0.54879846$

$x_0^{(1)} \approx 0.3097066$, $x_0^{(2)} \approx 0.3097066$, $y_0^{(1)} \approx 0.26900707$, $y_0^{(2)} \approx -1.51636088$) for the stable simple periodic impact P_5.

With displacement and velocity time-histories, trajectories of the wedge and bolster are presented in Figures 5.10 and 5.11. All the responses of the bolster and wedge are represented by the thick and thin curves, respectively. The switching points before and after impacts are represented by the small circles. The large circle designates the initial condition for starting simulation while the vertical dashed line describes one period. From Figure 5.10(a), the bolster and wedge impact when their displacements are equal causing a velocity jump as seen in Figure 5.10(b). To verify the periodicity of this simple impact chatter, Figure 5.11 shows the bolster and wedge phase plane trajectories for P_5. The single loop and velocity jump is observed for both the wedge and bolster. In Figure 5.12, the relative force and jerk are plotted to show why the wedge and bolster do not stick together. After impact, $g^{(1)} > 0$ and $g^{(2)} < 0$. This means that the acceleration of the bolster is greater than that of the wedge indicating that the bolster will tend to move apart from the wedge (i.e., $\ddot{x}^{(1)} > \ddot{x}^{(2)}$ which yields a positive relative velocity).

(a)

(b)
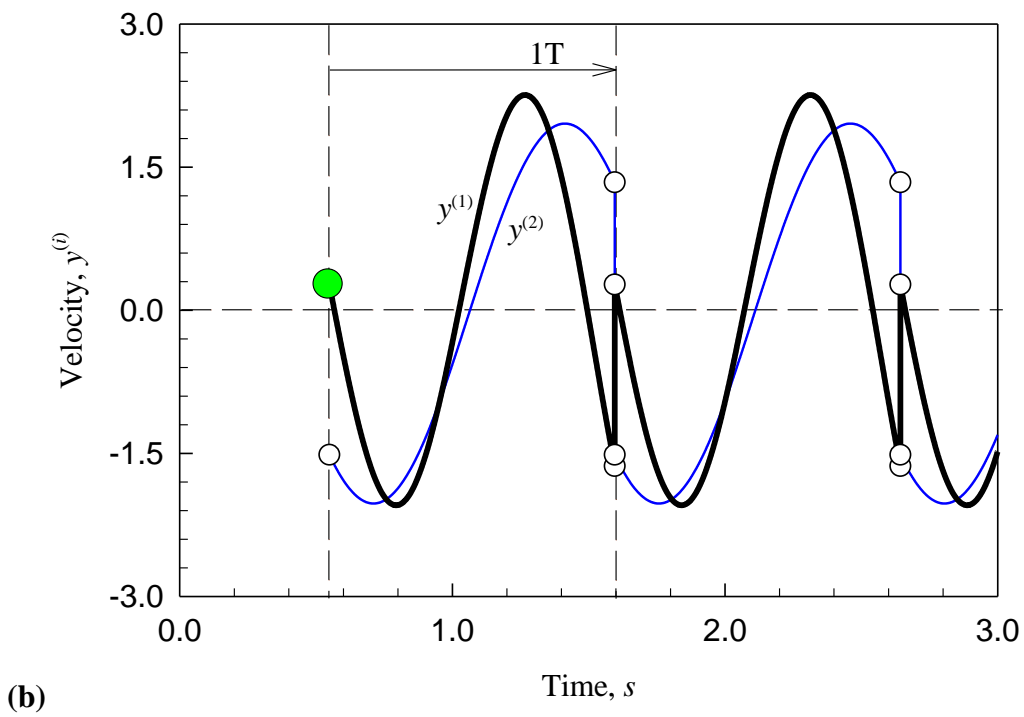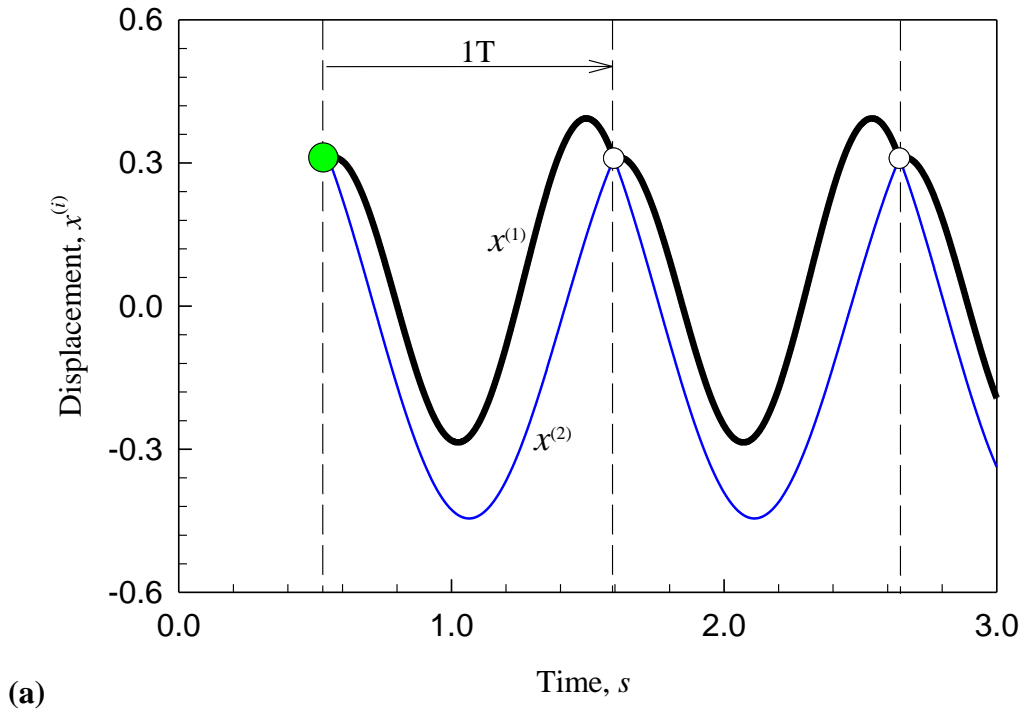
Figure 5.10. Displacement and velocity response for simple impacting chatter P_5 **.**

(a)

(b)
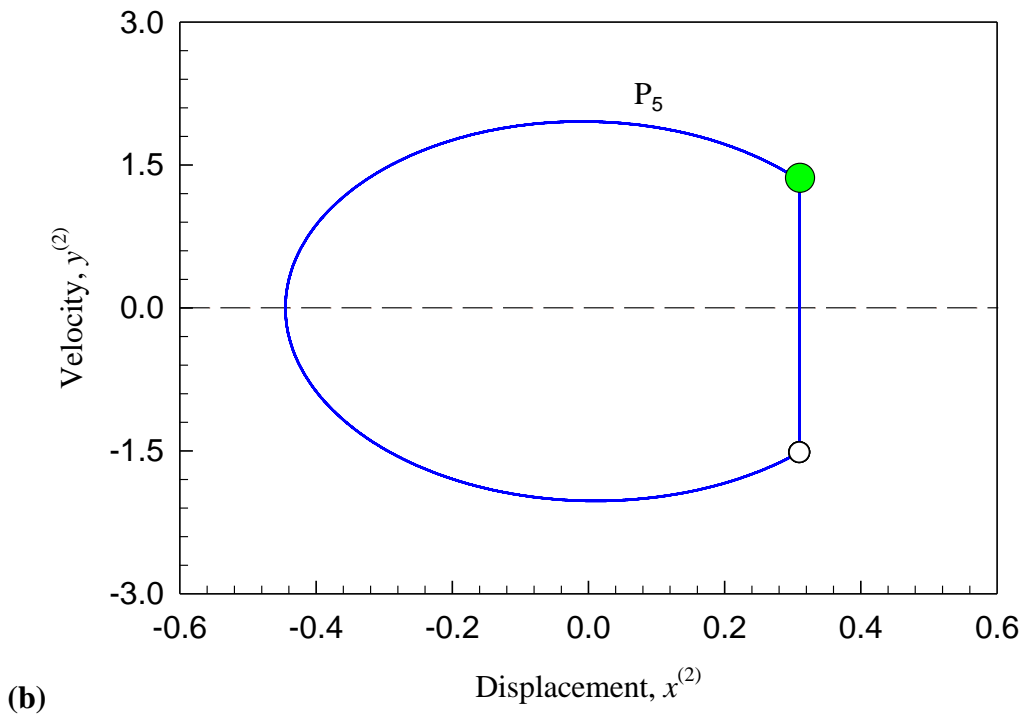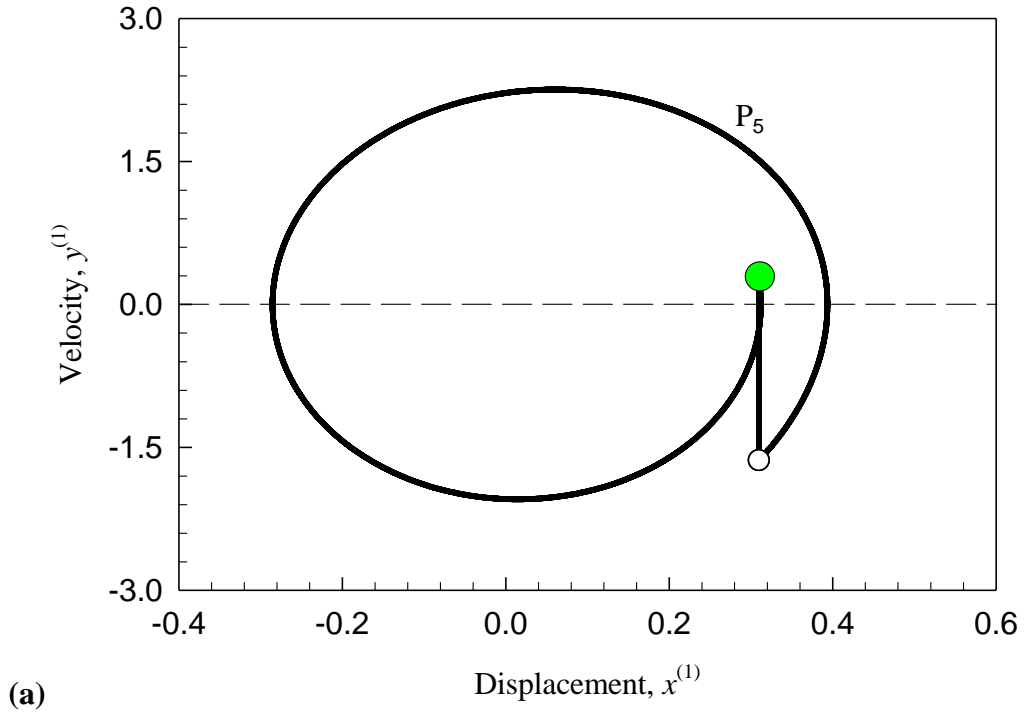
Figure 5.11: Phase plane trajectories for simple impacting chatter P_5.
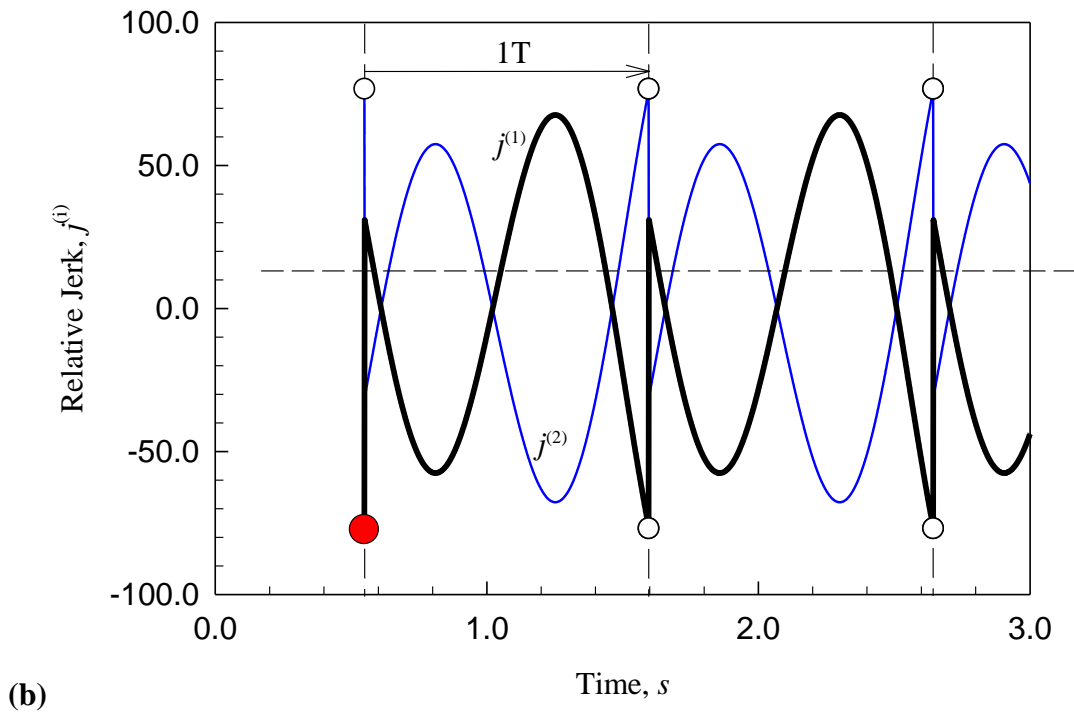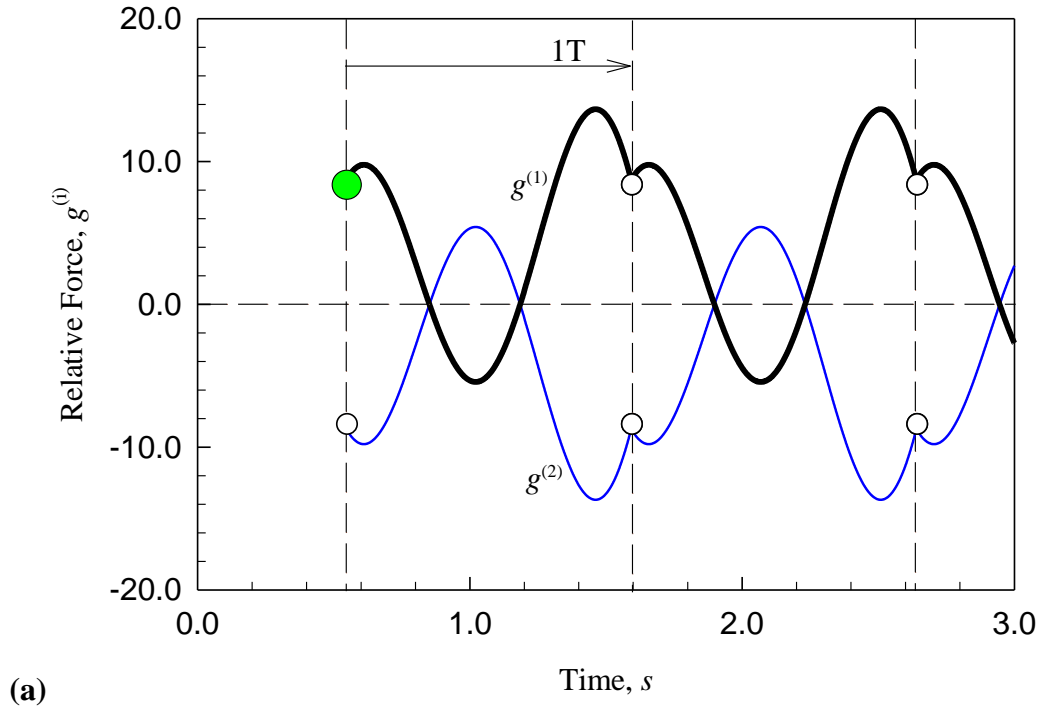
Figure 5.12: Relative force and jerk response for simple for simple impacting chatter P_5.

5.6 Numerical Simulation of Chatter with Stick and Stuck Motion

The impacting chatter with stick and stuck motion for the train suspension model will be discussed through the mapping structure of $P_{5^{21}4306}$. For $\Omega = 1.35$, the same parameters as before ($m_1 = 3$, $m_2 = 1$, $r_1 = r_2 = 0.1$, $k_1 = k_2 = 20$, $A_0 = 20$, $\mu_k = 0.4$ $\theta = 37.5°$, and $e = 0.6$) will be adopted for this illustration. From the analytical prediction, the initial condition is selected from the switching point $t_0 \approx 1.78307254$, $x_0^{(1)} = x_0^{(2)} \approx -0.09712064$, and $y_0^{(1)} = y_0^{(2)} \approx -0.062413071$. From such an initial condition, the bolster and wedge begin with stick motion. During the stick motion, the two become stuck having zero velocity and acceleration. After a brief moment, they continue with stick motion until the analytical conditions allow for the wedge and bolster to separate. After the stick vanishes, the two oscillators endure free-flying motion. Eventually they make contact with repeated impacts until finally $y_k^{(1)} = y_k^{(2)}$ and stick motion is observed.

In Figure 5.13 the displacement and velocity trajectories are presented. The shaded area is used for stick motion, and the letters "SSP" and "SEP" represent the stick motion starting and ending point, respectively. The vertical dashed lines define the boundaries for stick and stuck motion. Accordingly, the letters "WS" describe the section of wall stuck motion. In Figure 5.13(a), the displacement responses of the bolster and wedge are presented. After stick motion, the thick black curve and the thin blue curve describe the separate free-flight motions of the bolster and wedge, respectively. Before stick motion is observed again, 21 impacts occur. To further confirm the impacts, velocity responses for each oscillator are presented in Figure 5.13(b). Notice, during the wall stuck motion, the velocity is zero and the displacement remains constant. Also, as seen in the acceleration time-history, Figure 5.14(a) shows the acceleration to be zero during wall stuck motion. Near the end of the free-flight motion, the acceleration $a^{(1)} < 0$

and $a^{(2)} > 0$ is observed. This explains why the bolster and wedge are headed for collision, (i.e., the bolster's velocity is decreasing while the wedge's velocity is speeding up). After enough collisions to satisfy the condition $y^{(1)} = y^{(2)}$, Figure 5.14(b) shows the normal Force between the wedge and bolster. At the onset and during stick motion, the normal force is positive. However, at stick motion vanishing, the normal force reduces to zero. Finally, the mapping structure can be realized through the phase plane trajectories of the bolster and wedge as shown in Figure 5.15.

For a further understanding of the motion phenomena associated with the train suspension model, the analytical conditions introduced in Chapter 3 must be examined. In Figure 5.16(a), the g-function for wall stuck is plotted within the shaded region of stick motion. Observe that $F_2^{(1)} < 0$ and $F_3^{(1)} > 0$ for the duration of wall stuck. For vanishing stuck $F_2^{(1)} = 0$ and $F_3^{(1)} > 0$; however in Figure 5.16(b), $G_1^{(2,1)} > 0$ which means in the next moment $F_2^{(1)} > 0$ thus satisfying the analytical vanishing stuck conditions. Next consider the motion mechanisms of stick motion. On the switching boundary with $y_k^{(1)} = y_k^{(2)}$, the stick motion requires $g_\alpha^{(1)}(t_k) < 0$. In Figure 5.17(a), the relative force $g^{(1)} < 0$ is satisfied. In other words, the bolster tends to push down relative to the wedge. With $g^{(2)} > 0$, the wedge is pushing up relative to the bolster. For the vanishing of stick motion, it can be observed that the relative force $g^{(1)} = 0$ at the switching boundary. In Figure 5.17(b), the corresponding relative jerk $J^{(1)} > 0$ which means that for $t > t_k + \varepsilon$, $g^{(1)} > 0$. Note, during stick motion, the relative displacement and velocity are zero. At the next moment with a positive relative force, $\dot{z}^{(1)} = y^{(1)} - y^{(2)} > 0$ which means $z^{(1)} = x^{(1)} - x^{(2)} > 0$, (i.e., $x^{(1)} > x^{(2)}$). In other words, the bolster and wedge lie in the state of free-flying motion, and the stick disappears.

(a)

(b)
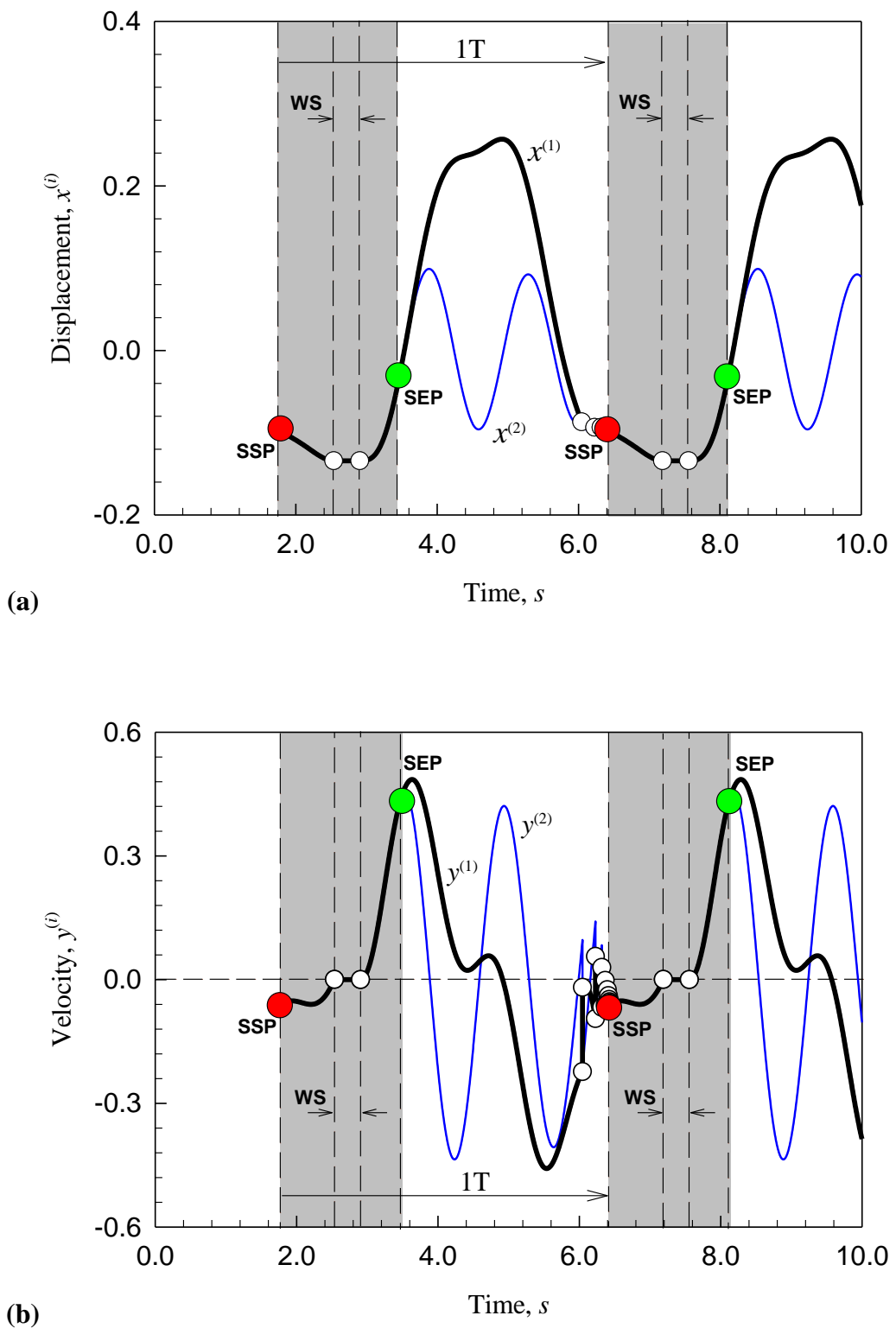
Figure 5.13. Displacement and velocity response for impacting chatter with stick and stuck motion $P_{5^{2!}4306}$ **.**
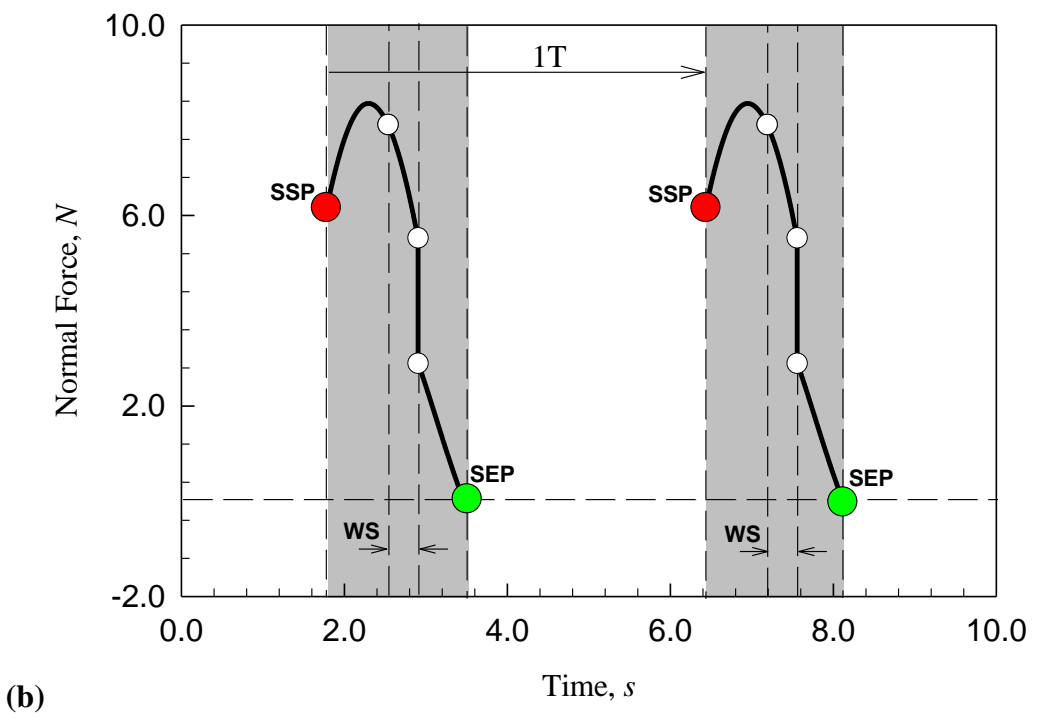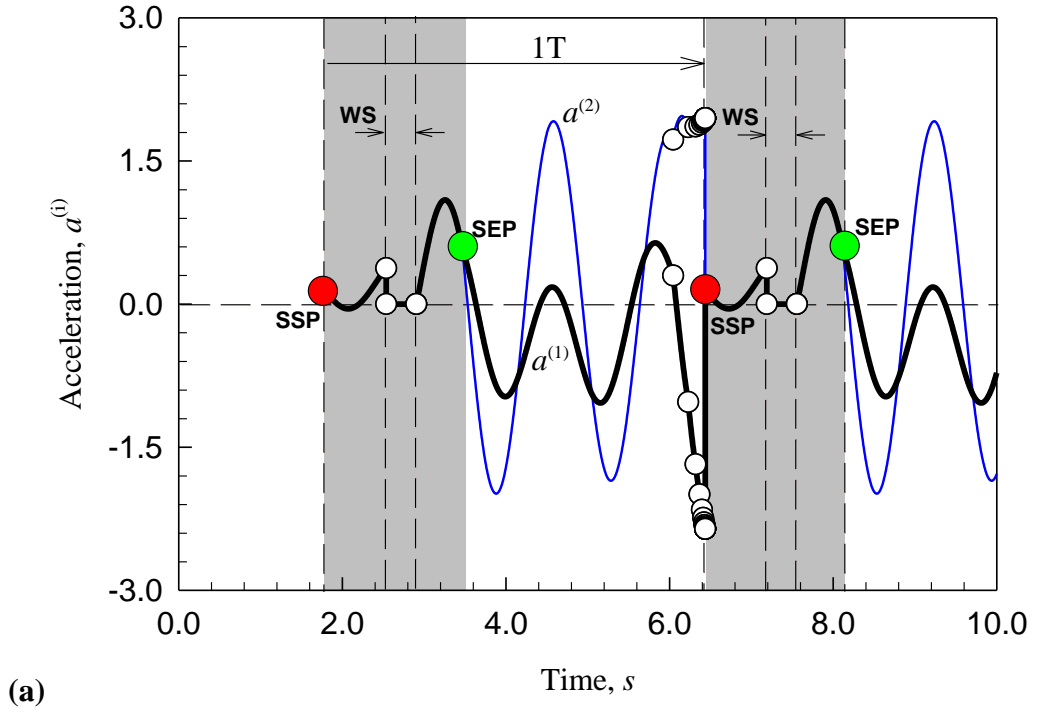
Figure 5.14. Acceleration and Normal Force response for impacting chatter with stick and stuck motion $P_{5^{2!}4306}$.

(a)

(b)
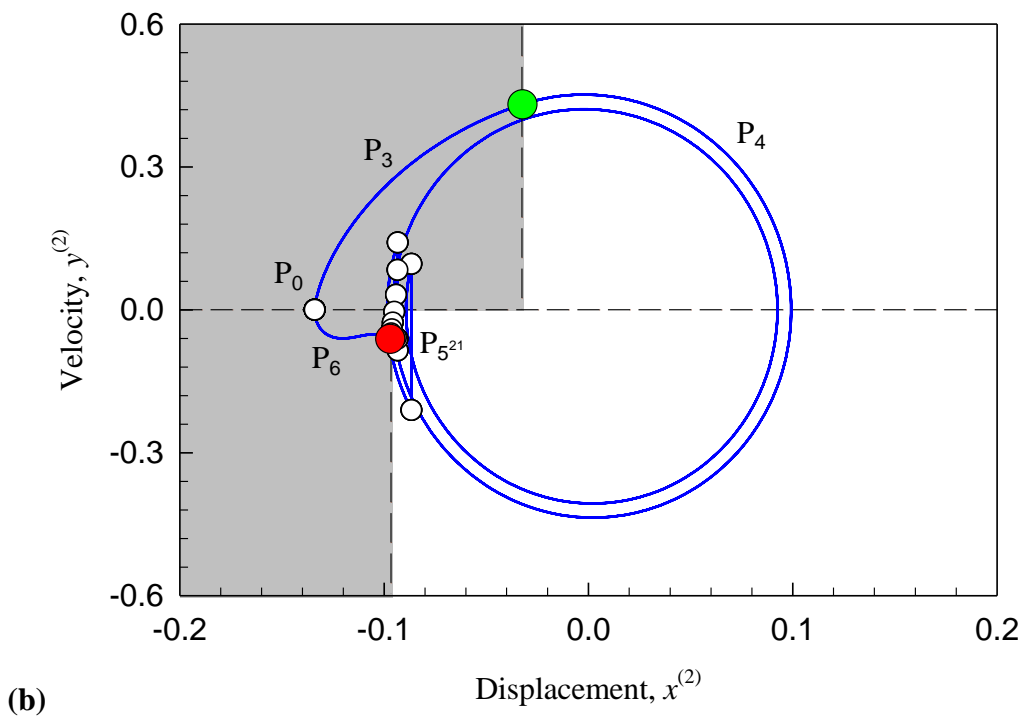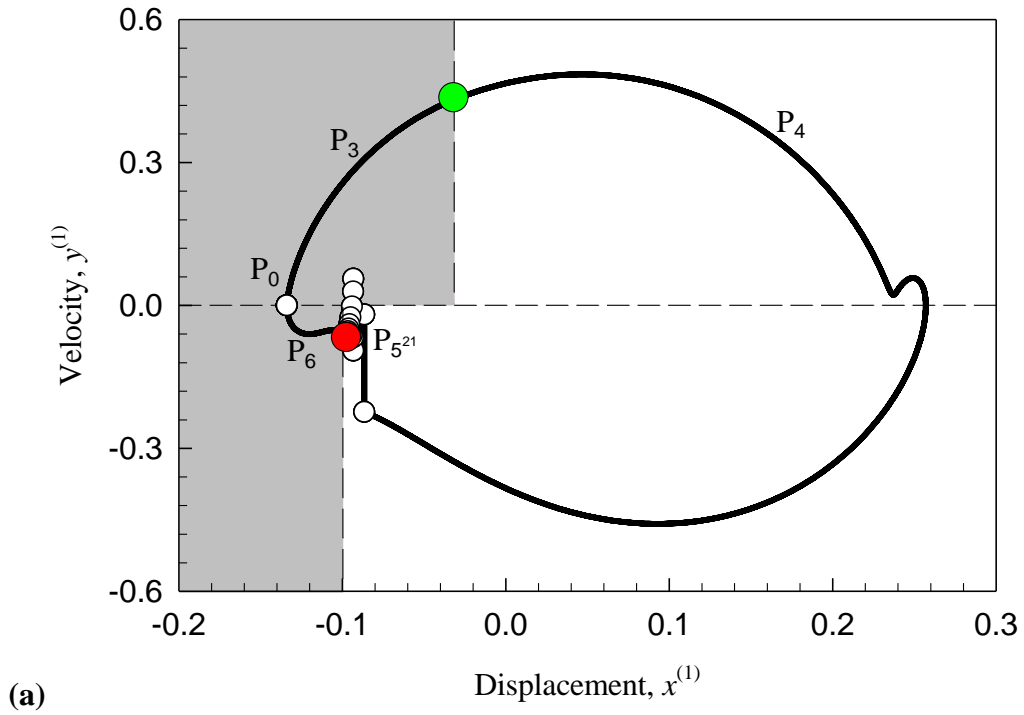
Figure 5.15. Phase plane trajectories of bolster and wedge for impacting chatter with stick and stuck motion $P_{5^{21}4306}$.
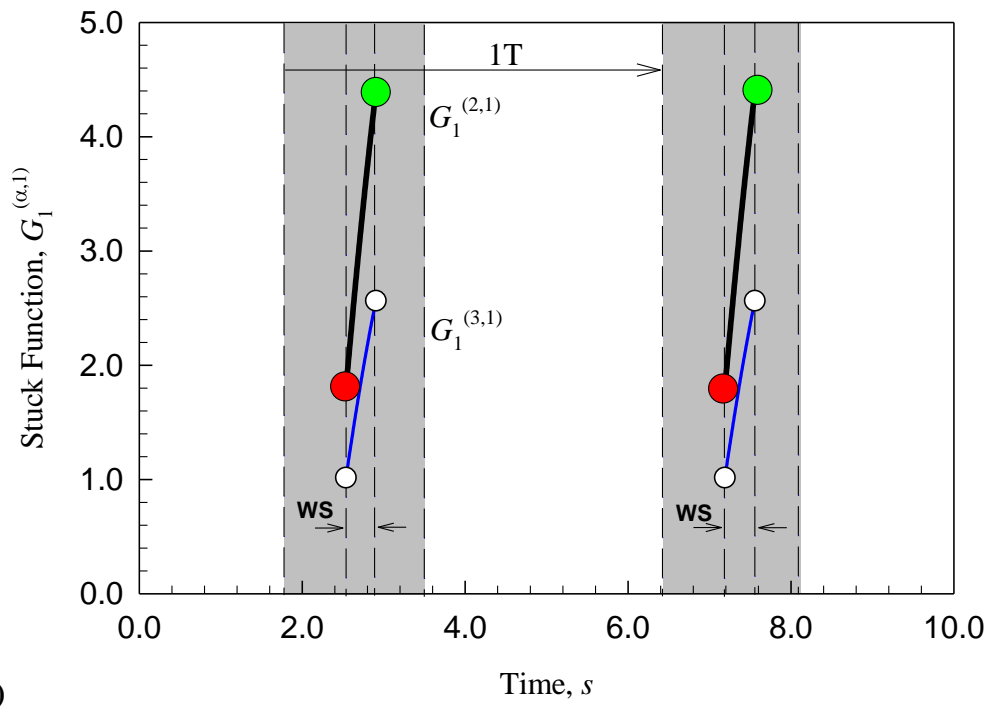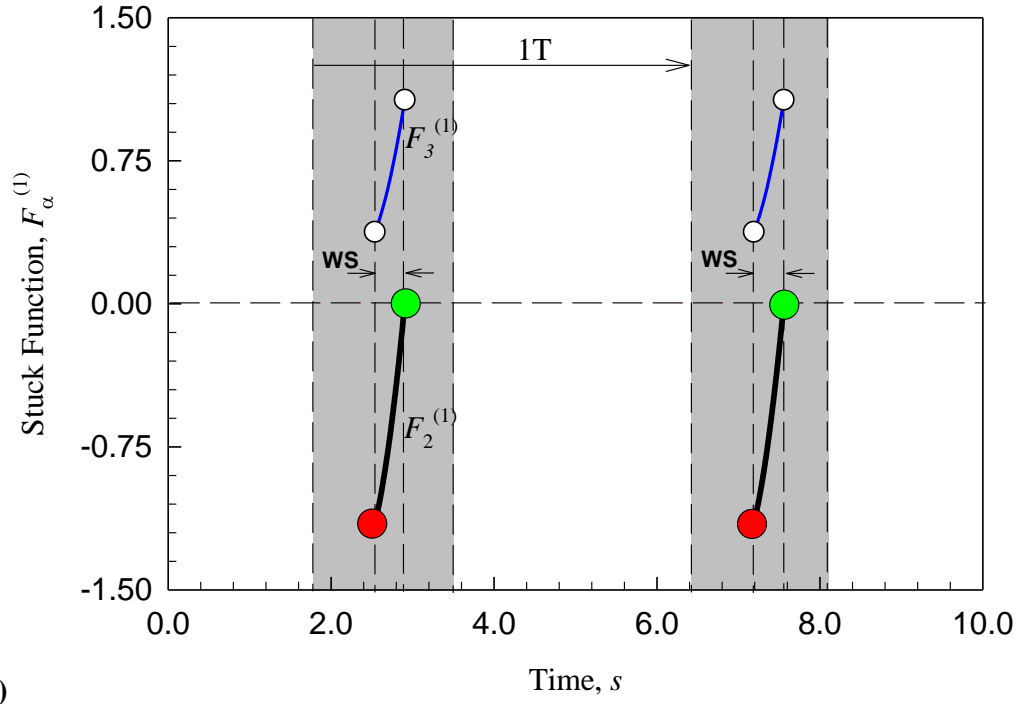
Figure 5.16. First and second order stuck condition function for motion $P_{5^{21}4306}$.
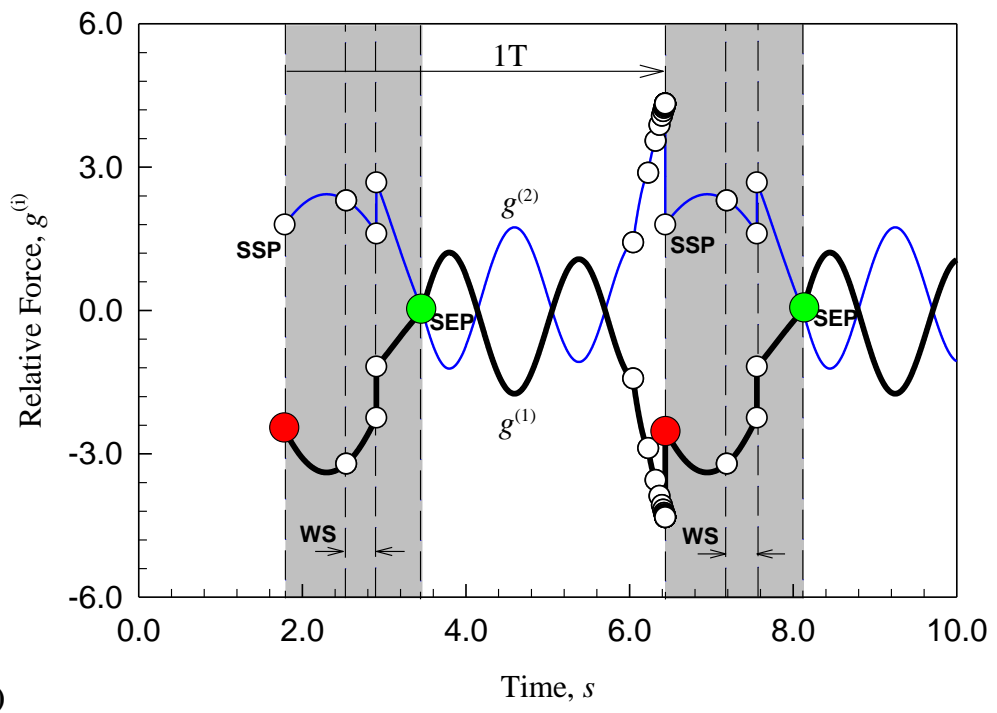
(a)
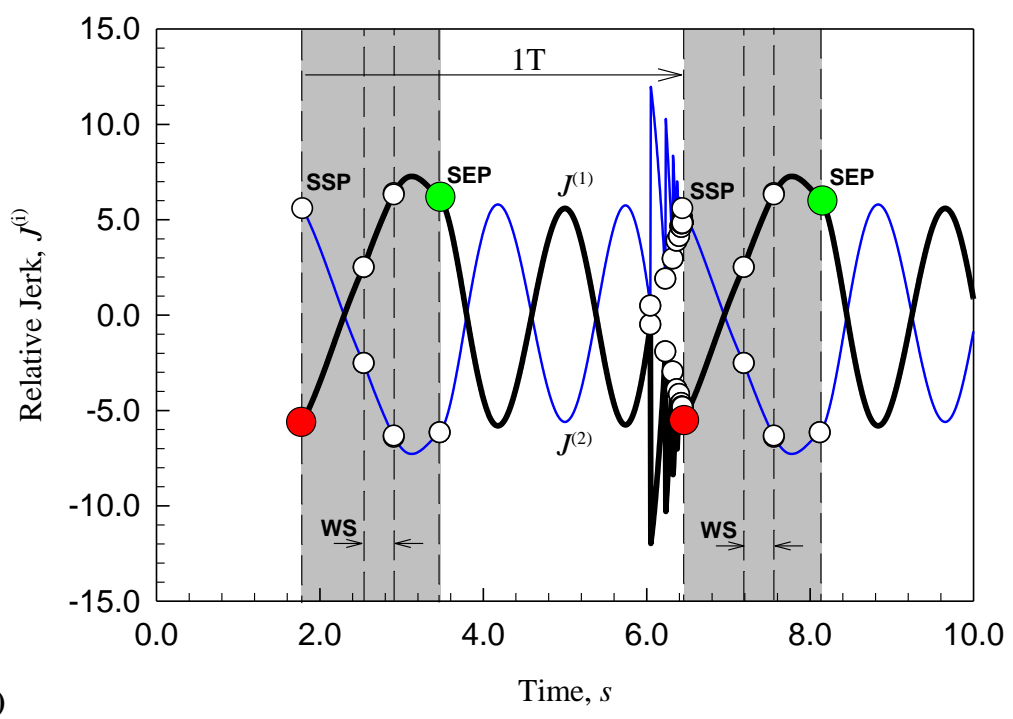
(b)

Figure 5.17. Relative force and jerk time-history for $P_{5^{21}4306}$.

CHAPTER VI

WEDGE ANGLE EFFECTS

Wedge angle plays an important role in freight train suspension systems. Herein, wedge angle effects on the motions of the freight train suspension systems. Before discussion, the field testing data will be presented and discussed. The possibility of a better performing freight train suspension system will be investigated. The analytical prediction of periodic motion will be completed for a range of wedge angles and the corresponding local stability and bifurcation analysis will be carried out through the eigenvalue analysis. From the predicted solutions, the switching displacement, velocity, and forces will be analyzed to investigate the dynamic effects of the wedge angle. Based on the mapping structure and work done by friction, the wedge angle can be shown to provide more desirable performance.

6.1 Field Data Results

Based on the goal to model the freight train suspension system, Amsted Rail provided field testing data to help validate the suspension model herein and to help us investigate the suspension problems encountered during train locomotion. In Figure 6.1(a), the wedge displacement response is given for a typical load scenario. The solid black curve moves in a smooth sinusoidal fashion. In Figure 6.1(b), the relative movement between the wedge and bolster is shown to validate the assumption herein that the bolster and wedge are assumed to move strictly in the vertical direction. Also, with negligible relative movement, the mechanical model can also safely ignore any internal friction and sliding between the wedge and bolster. Based on field measurements, the normal force acting on the wedge is plotted in Figure 6.2(a).

(a)

(b)
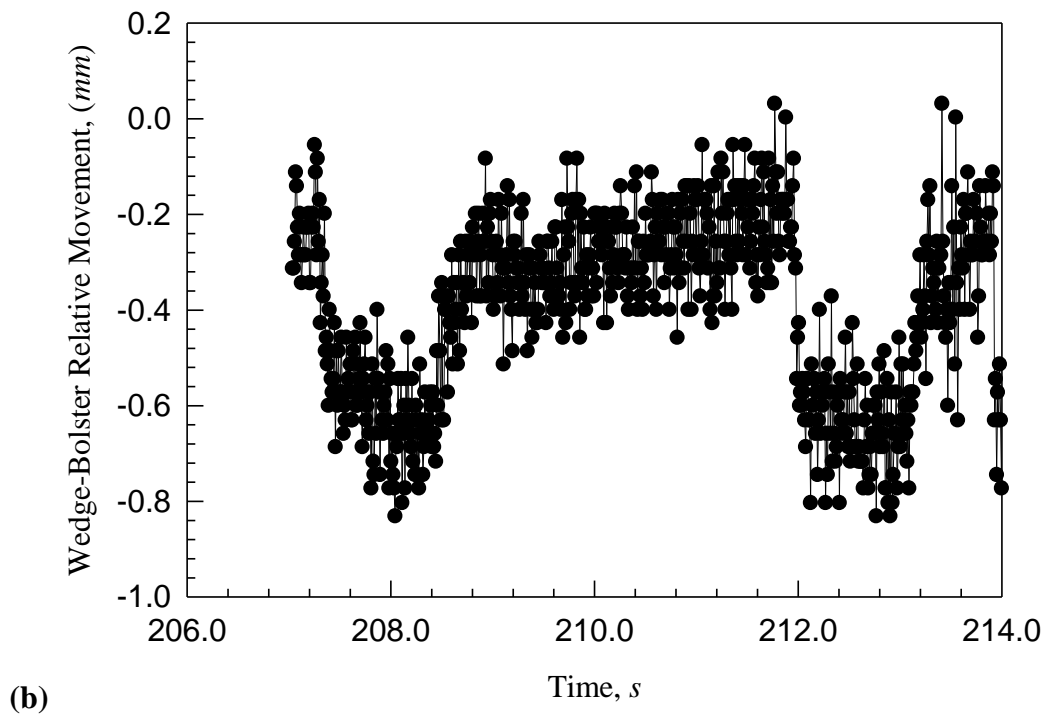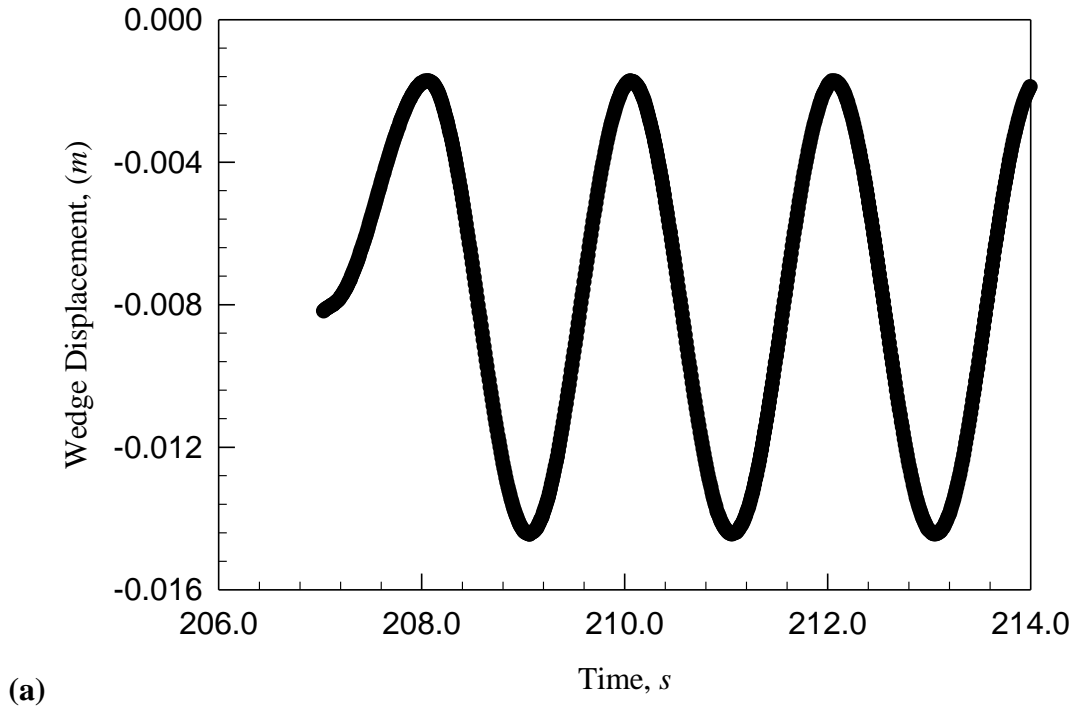
Figure 6.1. Field data of wedge vertical displacement and wedge-bolster relative movement,

Amsted Rail Inc.

(a)

(b)
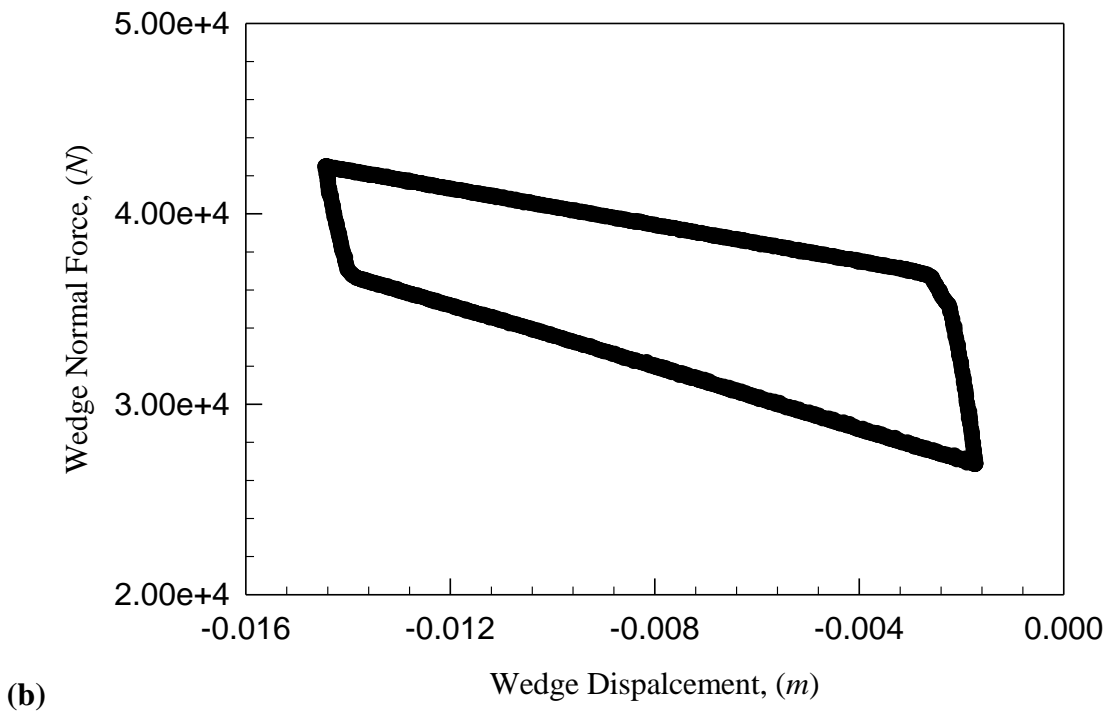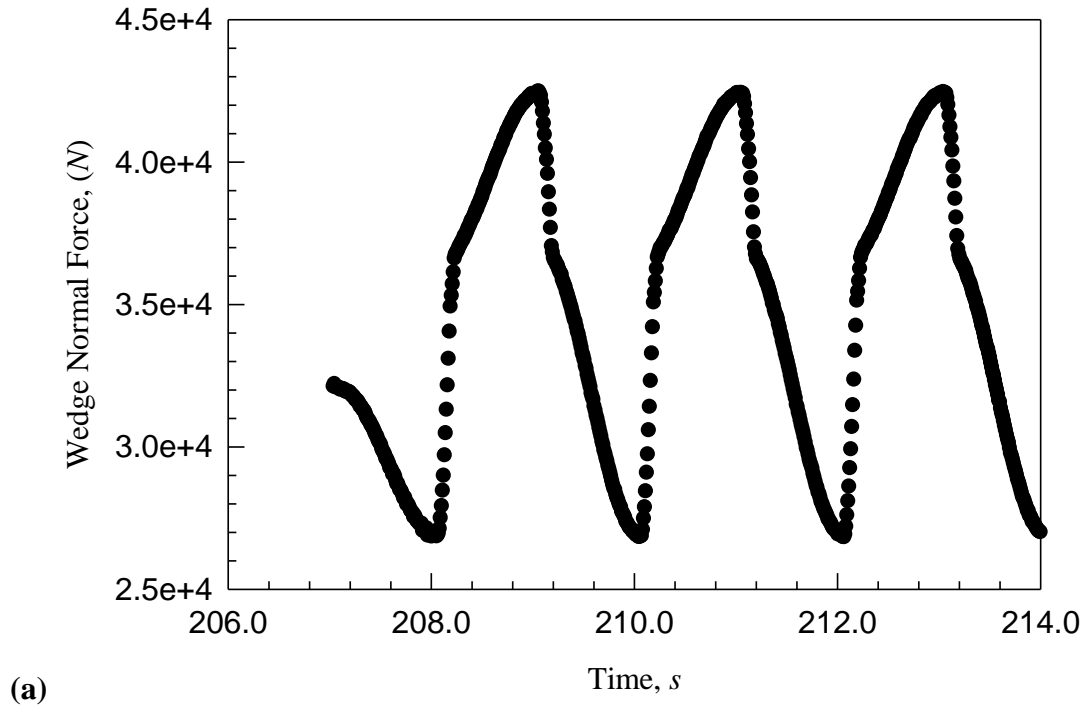
Figure 6.2. Field data of wedge normal force time-history and wedge normal force versus displacement, *Amsted Rail Inc.*

Clearly, there is a significant periodic jump in the normal force which is caused by a change in direction. When the velocity of the bolster and wedge system switches from positive to negative the side-wall friction must also switch direction from negative to positive, and vice versa. With friction acting in a reverse direction, the normal force experienced between the wedge and bolster will respond accordingly. In Figure 6.2(b), the normal force versus displacement is plotted to show the hysteresis completed in one cycle of movement. Notice that the normal force jumps when at the displacement extremes. This is exactly when the wedge and bolster are switching directions.

6.2 Analytical Prediction

From experimental measurements of spring stiffness and approximated cargo loads, the parameter set ($m_1 = 50000$, $m_1 = 100$, $r_1 = r_2 = 0.1$, $k_1 = k_2 = 367747.3$, $A_0 = 50000$, $B_0 = -100000$, $\Omega = 3.14$, $\mu_k = 0.2$, and $e = 0.6$) is utilized to investigate the effects of the wedge angle to the dynamic response of the suspension model. Using the mapping structure in Eq.(90), all the periodic motions for the entire range of wedge angle can be determined analytically. As discussed in Chapter 5, the mapping structure gives the nonlinear algebraic equations, which can be solved to obtain the periodic switching set solutions. The wedge angle is constrained between zero and 90 degrees, (i.e., $\theta \in (0, \pi/2)$). For the entire possible range of wedge angle, the switching phase and displacement is plotted in Figure 6.3(a) and (b), respectively. The solid black and red curves represents the stable periodic switching phase and displacement. The purpose of the alternating colors is to help differentiate between the different mapping structure solutions. Note, the switching phase and displacement of the bolster and

(a)

(b)
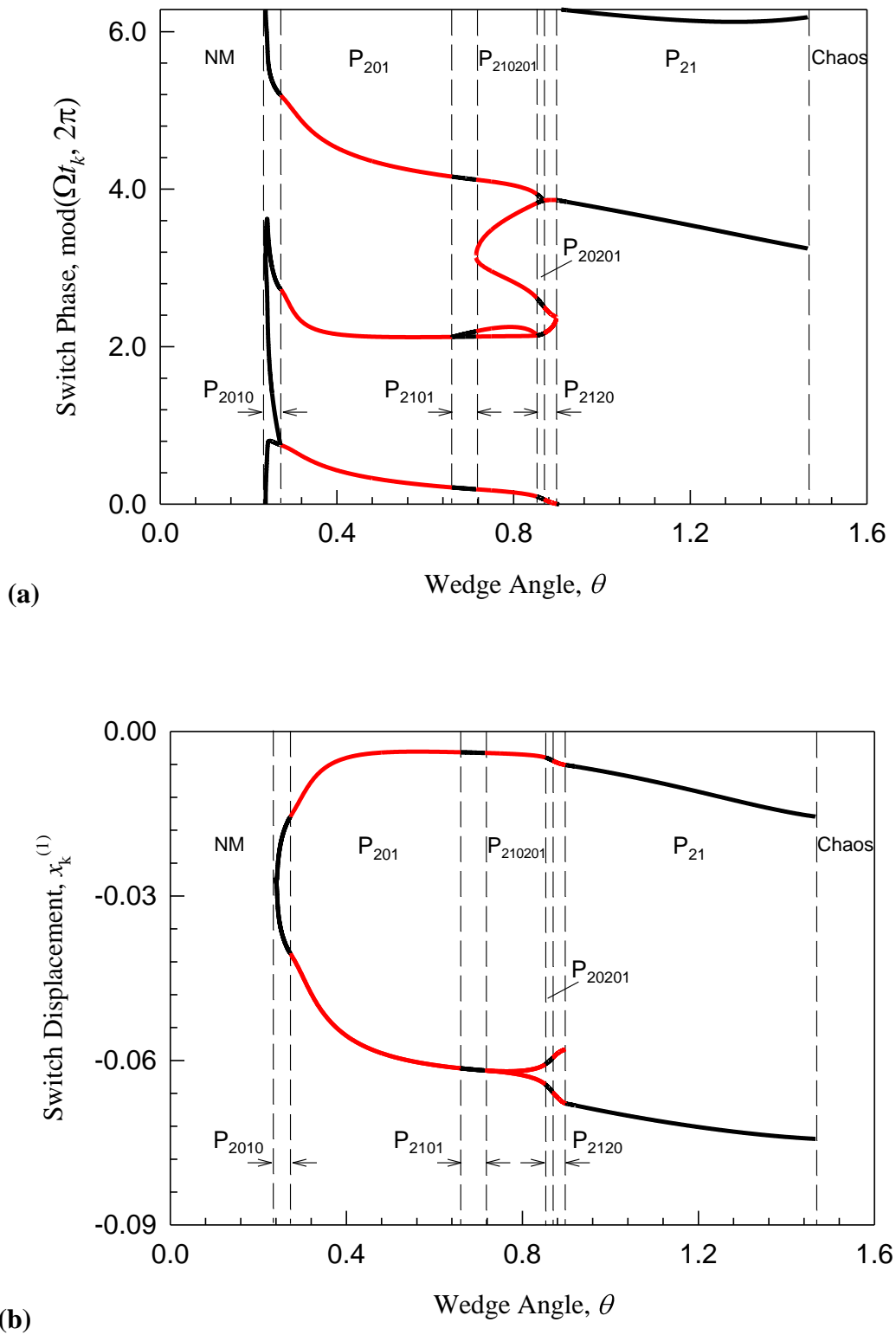
Figure 6.3. Analytical prediction of switching phase and displacement.

(a)

(b)
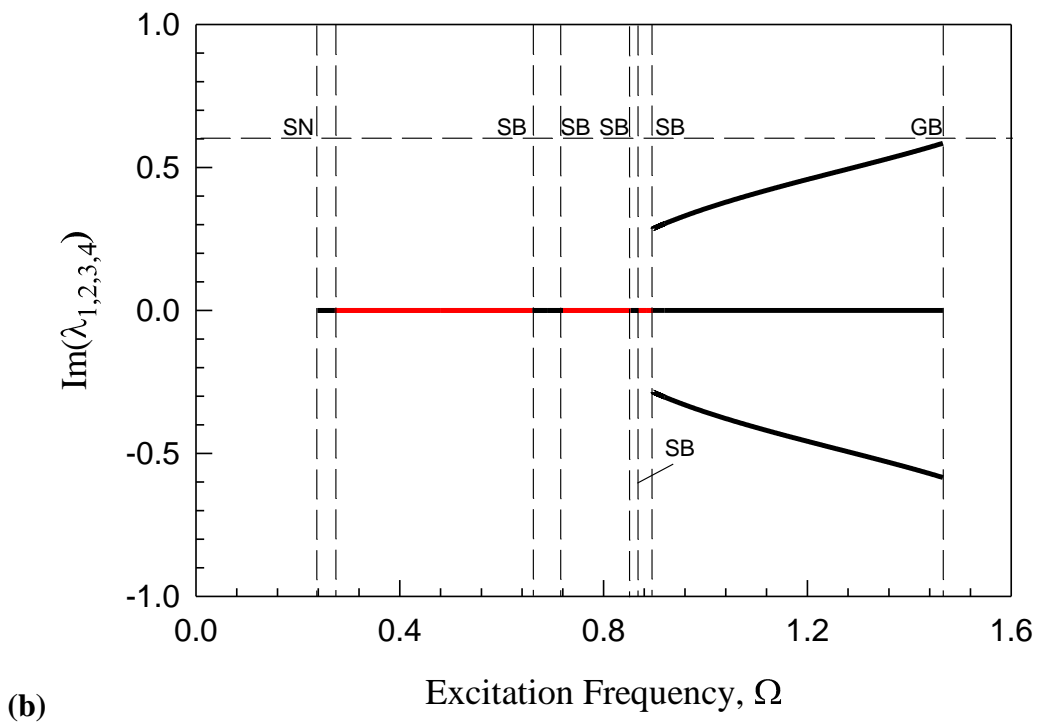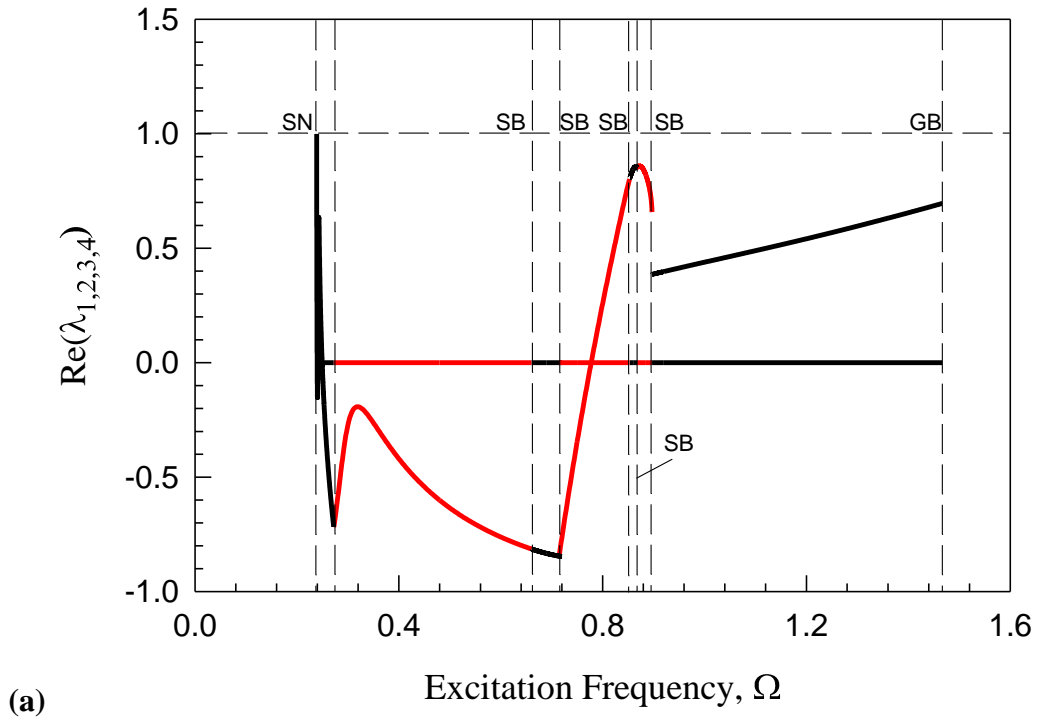
Figure 6.4. Analytical eigenvalues (a) $\mathrm{Re}(\lambda_{1,2,3,4})$ **and (b)** $\mathrm{Im}(\lambda_{1,2,3,4})$**.**

Table 6.1. Summary of excitation frequency for impacting chatter with stick.

Mapping Structure		Wedge Angle, θ
	chaos	$(1.46607, \pi/2)$
P_{21}	P(T)	$(0.89708, 1.46606)$
P_{2010}	P(T)	$(0.86757, 0.89708), (0.23843, 0.272)$
P_{20201}	P(T)	$(0.85375, 0.86756)$
P_{210201}	P(T)	$(0.71472, 0.85374)$
P_{2101}	P(T)	$(0.66042, 0.71471)$
P_{210}	P(T)	$(0.27201, 0.66041)$
	NM	$(0.2720, 0)$

wedge are identical while the switching velocity is necessarily zero since stick motion is always satisfied.

The corresponding eigenvalues to the analytical prediction described in Figure 6.3, are presented in Figure 6.4. Note, for the given set of analytical prediction, all solution are stable, (i.e., the magnitude of all eigenvalues lie in the unit circle). In Figure 6.4(a), the $\text{Re}(\lambda_{1,2,3,4})$ show a saddle node "SN" bifurcation at $\theta \approx 0.23843$ for P_{2010}. The P_{2010} mapping structure ends, and for $\theta < 0.23843$ the wedge and bolster become permanently stuck. This region is labeled "NM" for no motion. Also, "SB" stands for stuck bifurcation. Recall the stuck mapping P_0 means that the wedge and bolster are locked against the side-frame for a given amount of time, (i.e., $x_k^{(i)} = x_{k+1}^{(i)} = C$, $y_k^{(i)} = y_{k+1}^{(i)} = 0$ for $i = 1, 2$). This means that the Jacobean matrix for stability will have rank 1 and three of the four eigenvalues will necessarily equal zero. On the other hand, for the P_{21} mapping $\theta \in (0.89708, 1.46606)$, only $y_k^{(i)} = y_{k+1}^{(i)} = 0$ is true, so two of the

eigenvalues will equal zero. Table 6.1 describes the mapping structures and their respective

wedge angle ranges.

6.3 Numerical Simulation

From the analytical prediction discussed in the previous section, the following numerical

simulations will help illustrate the importance of the wedge angle. For the parameter set

($m_1 = 50000$, $m_1 = 100$, $r_1 = r_2 = 0.1$, $k_1 = k_2 = 367747.3$, $A_0 = 50000$, $B_0 = -100000$, $\Omega = 3.14$,

$\mu_k = 0.2$, and $e = 0.6$), the initial conditions are selected from the predicted periodic solutions

for motion involving stick and stuck motion.. For $\theta = 0.654 rad$, the initial condition is selected

from the switching point $t_0 \approx 0.6763449$, $x_0^{(1)} = x_0^{(2)} \approx$ -0.0613692, and $y_0^{(1)} = y_0^{(2)} = 0.0$ to

achieve P_{210}. From such an initial condition, the bolster and wedge remain in stick motion always

and endure a periodic stuck motion. In Figure 6.5, the displacement and velocity trajectories are

presented. Since the bolster and wedge are always sticking together, the shaded area labeled

"WS" signifies stuck motion, and the letters "SSP" and "SEP" represent the stuck motion starting

and ending point, respectively. The acceleration response and phase plane trajectory are

presented in Figure 6.6. The magnitude of acceleration can help to quantify the effectiveness of

the wedge damping. In Figure 6.7, the wedge normal force is presented through time-history and

wedge displacement. Notice, the jump in normal force corresponds well with the jump seen in

field data test presented in Figure 6. Also, the jump in normal force occurs when the velocity

crosses the switching boundary. For the wall stuck motion, observe that $F_2^{(1)} < 0$ and $F_3^{(1)} > 0$ in

Figure 6.8(a) until for vanishing stuck $F_2^{(1)} = 0$ and $F_3^{(1)} > 0$. At the same time, in Figure 6.8(b),

$G_1^{(2,1)} > 0$. This means that for $t > t_k + \varepsilon$, $F_2^{(1)} > 0$ and $F_3^{(1)} > 0$ and the stuck vanishing
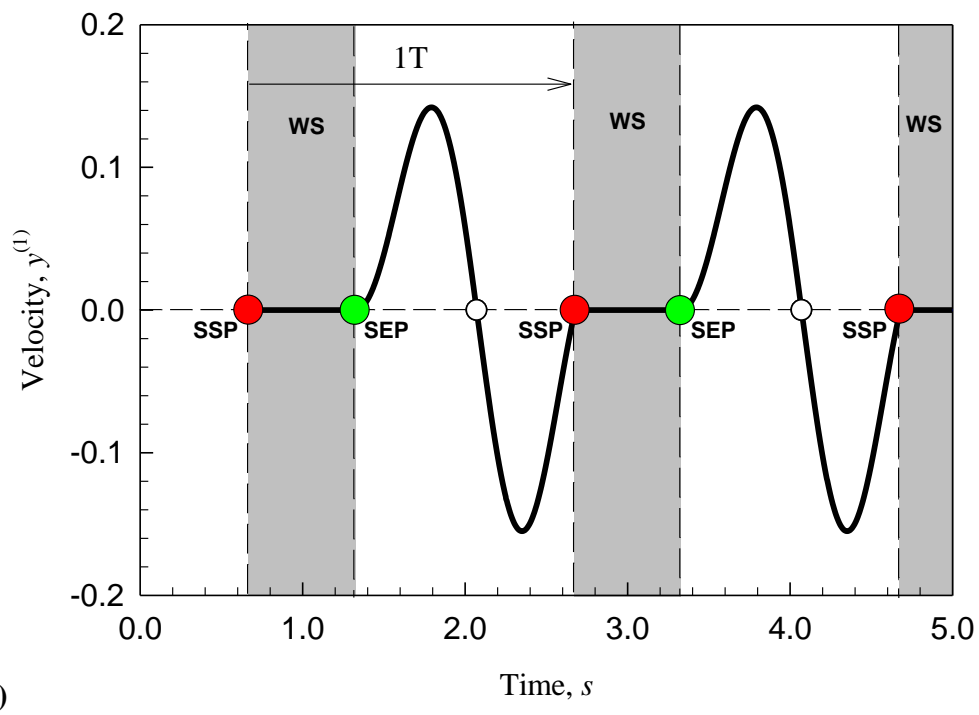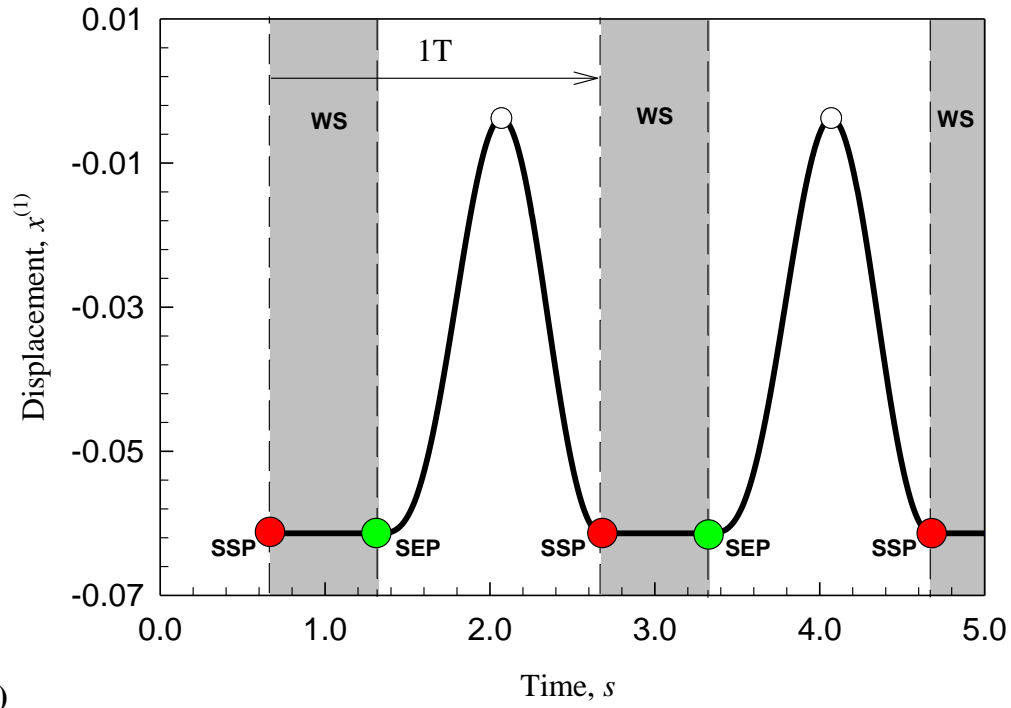
Figure 6.5. Displacement and velocity response for P_{210} **.**

(a)

(b)
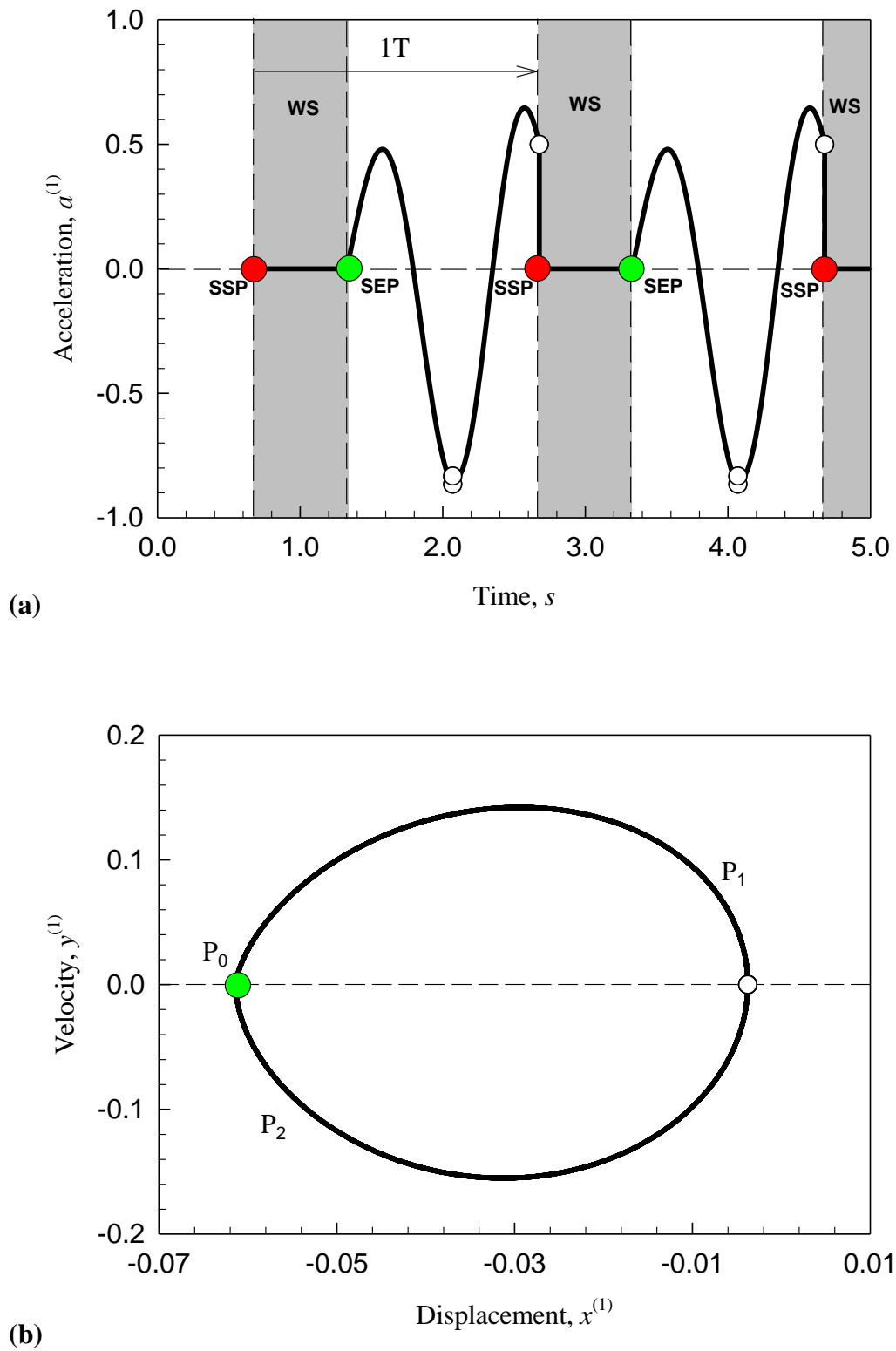
Figure 6.6. Acceleration response and phase plane trajectory for P_{210}.

(a)

(b)
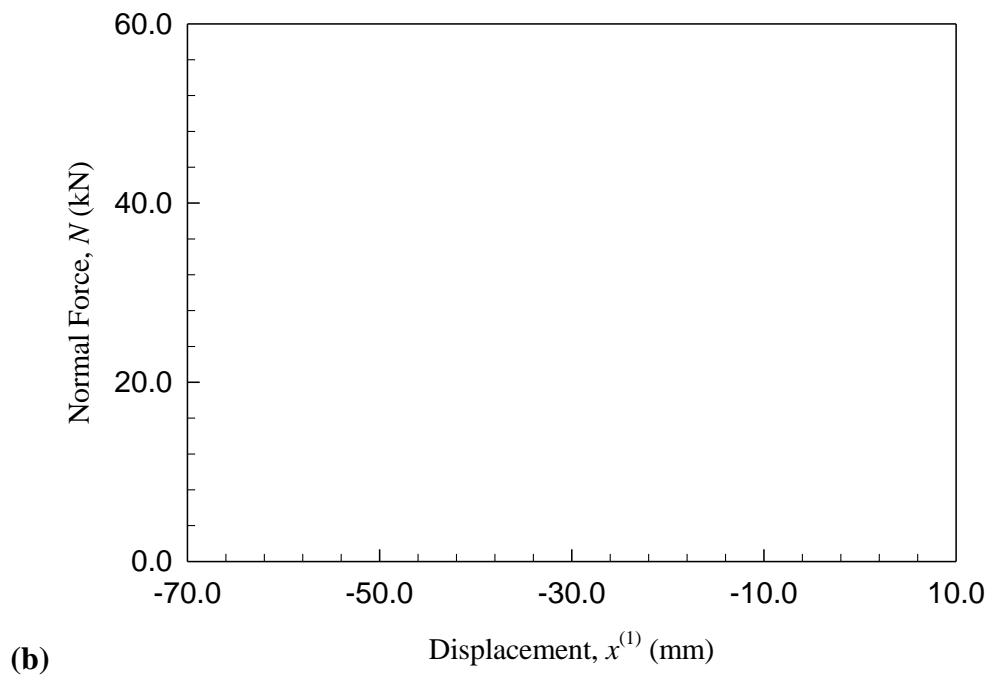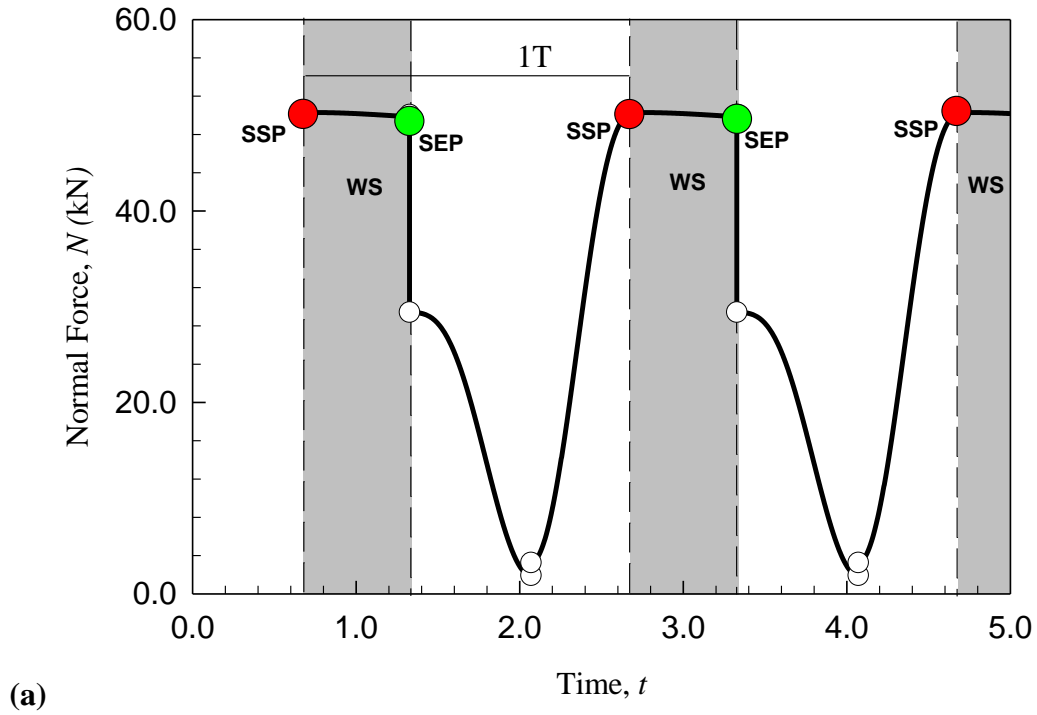
Figure 6.7. Wedge normal force time-history and wedge normal force versus displacement

for P_{210}.

(a)

(b)
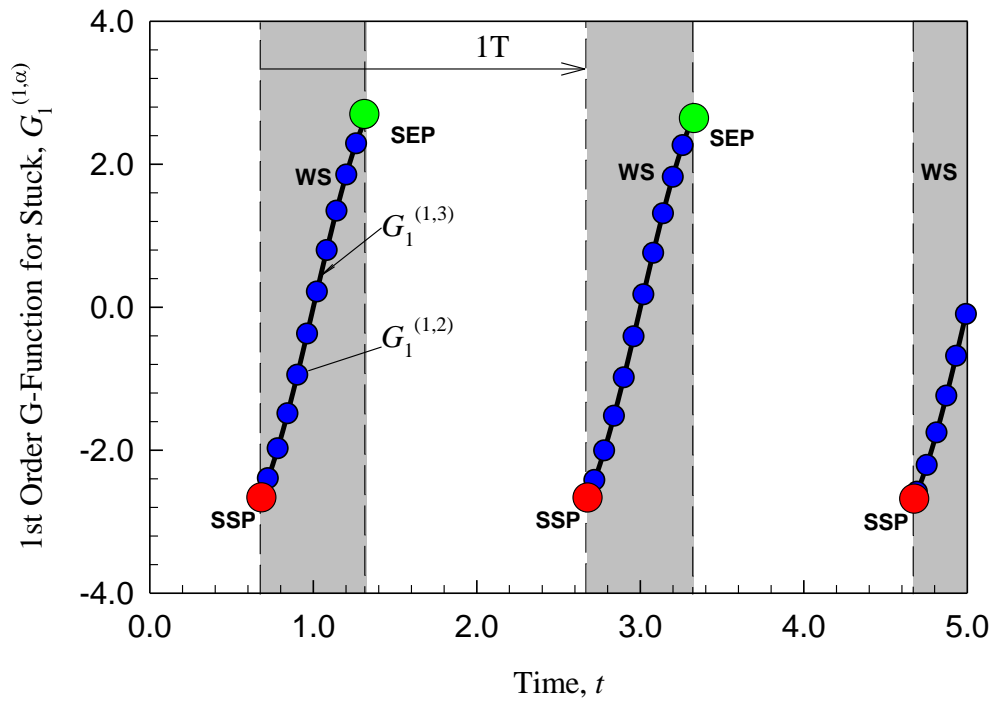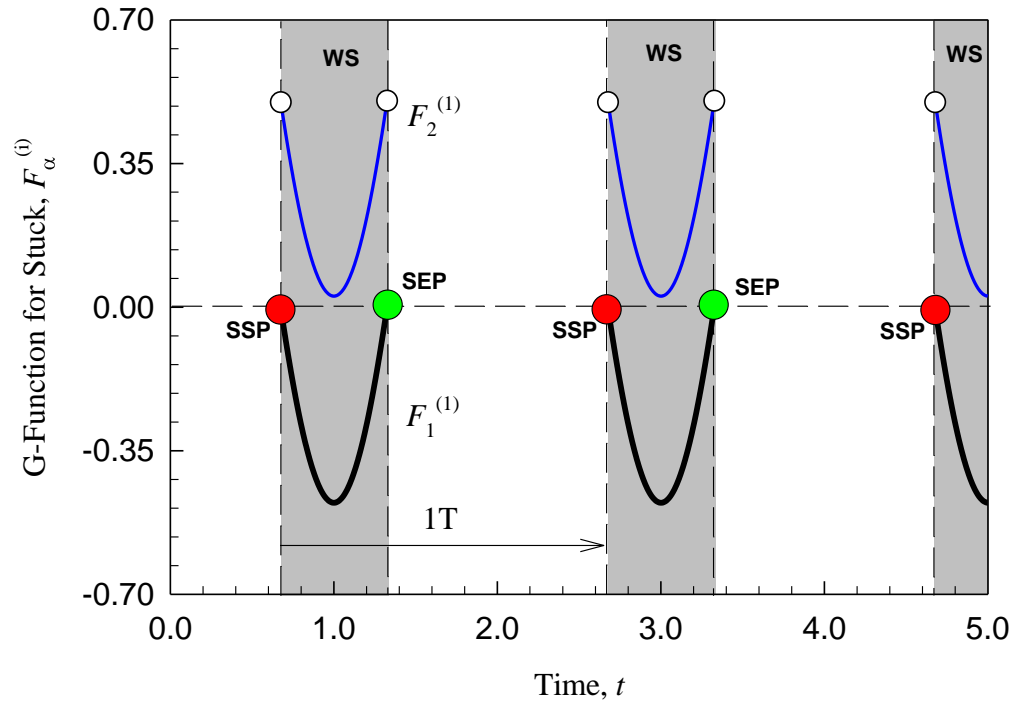
Figure 6.8. First and second order stuck condition function for P_{210}.

conditions are satisfied. Furthermore, stuck motion for the freight train suspension system may

be catastrophic because there will be no system damping.

6.4 Work Dissipation by Friction

From the analytical prediction of periodic solutions for the entire possible range of wedge

angles, clearly the wedge angle plays a critical role in determining the train suspension response.

From the mapping structure, smaller wedge angles presented the addition of one or more stuck

mappings. Since a smaller wedge angle will transfers more of the normal force between the

wedge and bolster into the side-frame, there is an increasing likelihood of stuck motion. While

the goal of the wedge is to act as a friction damper, there is a trade-off between increasing the

friction damping and causing more stuck motion. Furthermore, stuck motion for the train

suspension system means a temporary loss of suspension. Without an active suspension system, a

train may lose control and derail. On the other hand, a larger wedge angle transfers less normal

force and thus is less likely to endure stuck motion. In fact, with larger wedge angles, the stuck

motion disappears. The trade-off now becomes less or no stuck motion versus reduced damping

capacity. To help quantify the differences in wedge angle performance, the displacement,

acceleration, and work done by friction will be considered for various wedge angles.

From Physics, the work done by a force is given by

$$W = \int F(s)ds \tag{121}$$

where $F(s)$ is the force acting over a known distance. For the force of friction acting on the

wedge and bolster, the work done can be determined by

$$W = \int_{x_1}^{x_2} F_k(x)dx \tag{122}$$
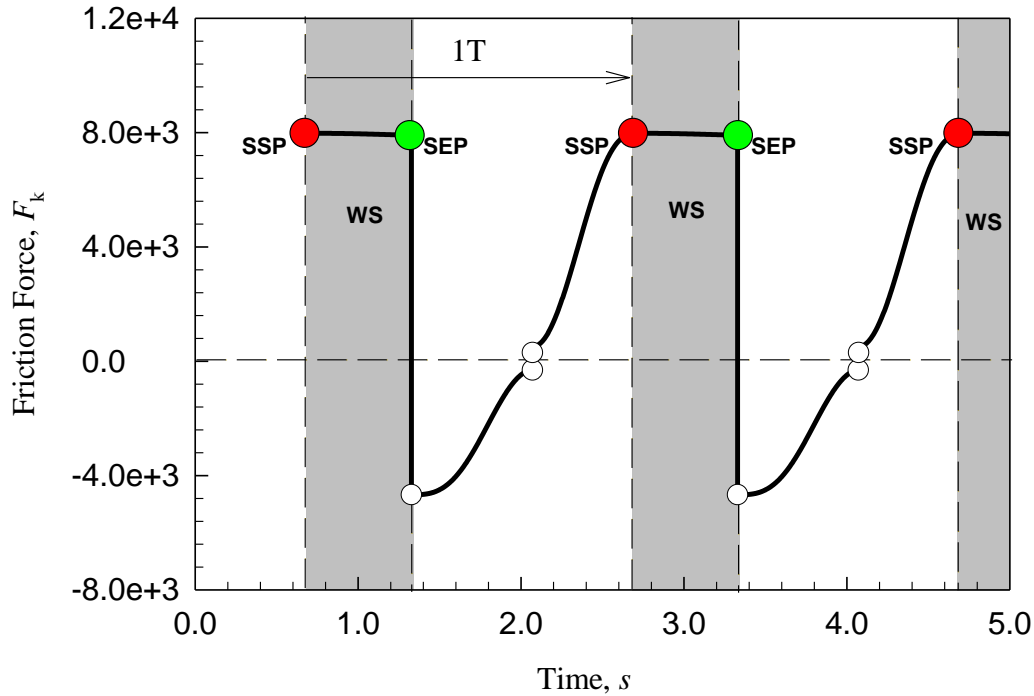
Figure 6.9. Friction force response for P_{210}.

From Figure 6.7(a), the normal force was shown to both vary with time and be different in

magnitude based on the direction of movement. This means that for one period of motion, the

net work done by Friction will not be zero. With Eqs.(5) and (6) from Chapter 2, the force of

friction can be given in terms of the normal force and kinetic friction by

$$F_k = \mu_k N \cos \theta .$$ (123)

From the analytical prediction and numerical simulation of $\theta = 0.654$ and parameter set

$m_1 = 50000,\ m_1 = 100,\ r_1 = r_2 = 0.1,\ k_1 = k_2 = 367747.3,\ A_0 = 50000,\ B_0 = -100000,\ \Omega = 3.14$,

$\mu_k = 0.2,$ and $e = 0.6$, the kinetic friction force time-history is plotted in Figure 6.9. As

mentioned previously, the shaded region labeled "WS" is for the stuck motion. Since the wedge

and bolster are stationary, the friction force does zero work during stuck motion. To calculate the

work during one period, the friction force versus displacement must be considered. In Figure

6.10, the friction force is plotted for negative and positive velocity, respectively. The area under the curve denotes the amount of work done by Friction.

Based on the simulation results, the curves in Figures 6.10(a) and (b) were numerically integrated to give -142.64J and -242.94J for the friction during negative and positive velocity, respectively. Note, since friction acts in the opposite direction to movement the work will necessary be negative. Based on the amount of work done, the friction damping is significantly more effective when the wedge and bolster are moving downward as opposed to upward. This "wedge effect" is also confirmed by the field testing data provided by *Amsted Rail*. From Figure 6.2, the normal force is significantly larger with negative velocity, which means that the friction damping would also be much larger.

To further discuss the wedge angle relationship to suspension performance, additional wedge angles must be considered. From the analytical prediction, several wedge angle solutions were simulated to quantify displacement, acceleration and work. In Table 6.2, the results are tabulated for the sake of brevity and clarity. As the wedge angle is increased, the displacement range increases slightly while the work done by friction decreases. Notice, for $\theta = 0.38$ and $\theta = 0.92$ the maximum displacement is -0.0542 and -0.0682, respectively. If friction is doing less work in damping, the displacement of the bolster and wedge will likely increase. On the other hand, the acceleration is also an important response. With smaller angles the acceleration is larger, (i.e., -0.7288 and -0.894 for $\theta = 0.38$ and $\theta = 0.92$, respectively). Slowing the bolster down over a smaller distance will certainly require higher acceleration and vice versa. The current wedge angle used by industry is $37.5°$ or $\theta = 0.654 rad$, also described in Table 6.2. As compared to the larger wedge angle $\theta = 0.92$, the displacement, acceleration, and work done by
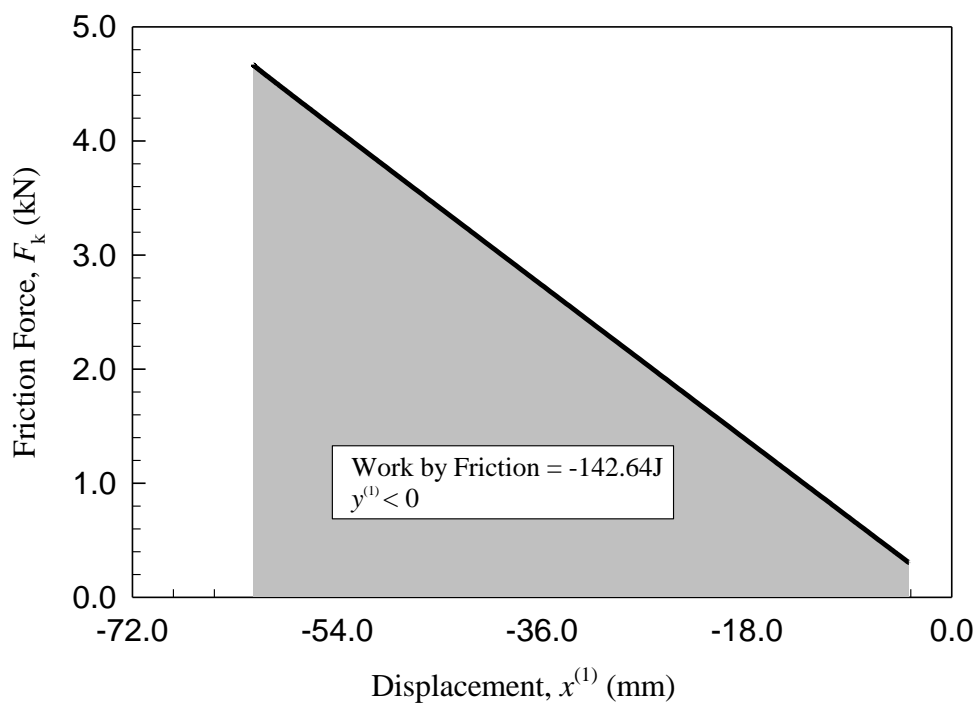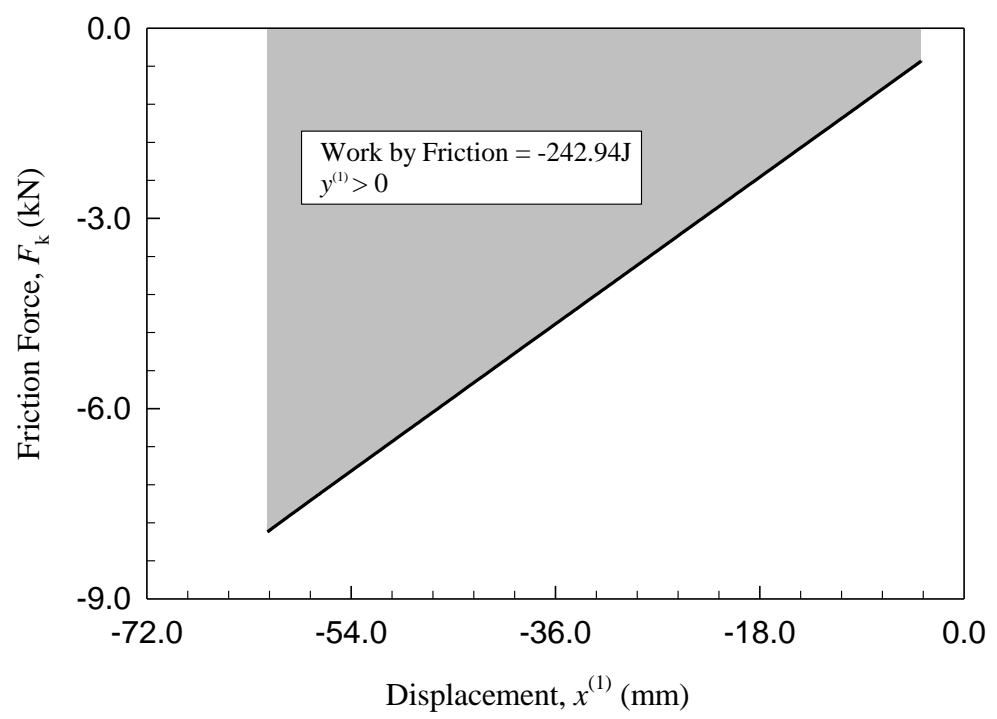
Figure 6.10. Friction force versus displacement for (a) negative velocity and (b) positive velocity, $\theta = 0.654 \, rad$ **.**

friction are quite similar. The major and most important difference is the mapping structure. By

increasing the wedge angle from 0.654 to 0.92, the wedge and bolster no longer endure stuck

motion at the cost of slightly less friction damping.

Table 6.2. Tabulated values of displacement acceleration and work.

Wedge, θ (rad)	Displacement Range (m)	Acceleration Range (m/s^2)	Work by Friction, (J)
0.38, P_{210}	(-0.0542, -0.00535)	(-0.8941, 0.6169)	-152.43, -456.88
0.50, P_{210}	(-0.0592, -0.00375)	(-0.8953, 0.5846)	-155.28, -333.07
0.654, P_{210}	(-0.0614, -0.0542)	(-0.8656, -0.0542)	-142.64, -242.94
0.92, P_{21}	(-0.0682, -0.00637)	(-0.7288, 0.4212)	-146.67, -199.06

CHAPTER VII

SUMMARY

In this Dissertation, a mechanical model for a freight train suspension system was developed to include all possible types of motion such as free-flight, stick, and stuck motion. The dynamic mechanism of the impacting chatter with stick was investigated from the local singularity theory of discontinuous dynamical systems. The analytical conditions for the onset and vanishing of stick motions were presented, and the condition for maintaining stick motion was achieved as well. Due to the possibility of stuck motion, additional analytical conditions were developed to determine the onset and vanishing conditions for stuck motion. Analytical prediction of periodic motions relative to impacting chatter with stick and stuck in train suspension was completed through the mapping structure. The corresponding local stability and bifurcation analyses were carried out, and the grazing and stick conditions were used for the existence of periodic motions. Numerical simulations were performed to illustrate the periodic motions of stick and stuck motion. Finally, based on field testing data, an investigation into the effects of wedge angle was conducted to find a more desirable suspension response.

In Chapter 1, the mechanical model of a typical freight train suspension system was presented. The corresponding literature survey about the previous and more current status of train suspension systems was completed. In Chapter 2, because of the discontinuity between the wedge and bolster with friction, the domain partition in phase plane was discussed. The corresponding dynamical system on such sub-domains was presented in the absolute and relative frames. Further, the mathematical description of the train suspension system was given. In Chapter 3, the analytical conditions for grazing and stick phenomena, as well as stuck motion,

were developed, which included the necessary and sufficient conditions. In Chapter 4, the basic mappings and switching sets were introduced in the absolute and relative frame. The generalized mapping structure for periodic motion was presented. In addition, consider generic parameters, the bifurcation scenario versus excitation frequency was presented. In Chapter 5, the methodology for analytical prediction of periodic motion was given, and the local stability and bifurcation conditions were presented. The impacting chatter with stick and stuck were analytically predicted, and the local stability and bifurcation was given through the eigenvalue analysis. To help one better understand such mathematical conditions, numerical illustrations of period motion from the predicted solutions demonstrated the physical interpretation of the stick and stuck conditions. In Chapter 6, field testing data was considered to obtain a more realistic parameter set. Based on analytical predictions of periodic motion, the entire range of possible wedge angles was investigated. Considering the displacement, acceleration, and work done by friction in damping the system, a comparison study described the benefits of having a larger wedge angle.

Through this investigation, the motion mechanism of the ubiquitous freight train suspension system can be further understood, which may provide some clues to reduce the possibility of poor suspension performance and further derailment. According to industry, a leading cause for derailment at high speeds is suspension performance. Current investigations are interested in what industry calls the "slip-stick" phenomena. Here "slip-stick" refers to the wedge and bolster sticking to the side-wall, otherwise known as "stuck" motion herein. Through further parameter studies, the mechanical model presented herein can be utilized to recommend better performing suspension characteristics such as wedge angle, spring stiffness, friction coefficients, etc.

REFERENCES

Chandiramani, N.K., Srinivasan, K. Nagendra, J. (2006). "Experimental study of stick-slip dynamics in a friction wedge damper", *Journal of Sound and Vibration*, **291**, pp. 1-18.

Comparin, R.J. and Singh, R. (1989). "Nonlinear frequency response characteristics of an impact pair," *Journal of Sound and Vibration*, **134**, pp.259-290.

Feeny, B.F. (1992). "A nonsmooth Coulomb friction oscillator", *Physics D,* **59**, pp. 25–38.

Gardner, J.F. and Cusumano, J. P. (1997). "Dynamic models of friction wedge dampers", *Proceedings of the 1997 IEEE/ASME Joint Railroad Conference, Boston, MA,* pp. 65-69.

Gottzein, E. and Lange, B. (1975). "Magnetic suspension control systems for the MBB high speed train", *Automatica*, **11**, pp.271-284.

Ju, S.-H. and Lin, H.-T. (2008). "Experimentally investigating finite element accuracy for ground vibrations induced by high-speed trains", *Engineering Structures*, **30**, pp. 733-746.

Kaiser A. B., Cusumano J. P., and Gardner J. F. (2002). "Modeling and dynamics of friction wedge dampers in railroad freight trucks", *Vehicle System Dynamics*, **38**, pp.55-82.

Pfeiffer, F. (1984). "Mechanische Systems mit unstetigen Ubergangen," *Ingeniuer- Archiv*, **54**, pp.232-240.

Hinrichs, N., Oestreich, M., and Popp. K. (1997). "Dynamics of oscillators with impact and friction", *Chaos, Solitons, and Fractals,* **8** (4), pp. 535–558.

Hundal, M.S. (1979). "Response of a base excited system with Coulomb and viscous friction", *Journal of Sound and Vibration*, **64**, pp. 371–378.

Karagiannis, K. and Pfeiffer, F. (1991). "Theoretical and experimental investigations of gear box", *Nonlinear Dynamics,* **2**, pp.367-387.

Karlström, A. B. (2006). "An analytical model for train-induced ground vibrations from railways", *Journal of Sound and Vibration*, **292**, pp. 221-241.

Luo, A.C.J. (2005). "A theory for non-smooth dynamic systems on the connectable Domains," *Communications in Nonlinear Science and Numerical Simulation*, **10**, pp.1-55.

Luo, A.C.J., and Chen, L.D. (2005). "Periodic motion and grazing in a harmonically forced, piecewise linear, oscillator with impacts," *Chaos, Solitons and Fractals*, **24,** pp.567-578.

Luo, A.C.J. and Gegg, B.C. (2006). "Stick and non-stick periodic motions in periodically forced oscillators with dry friction", *Journal of Sound and Vibration*, **291**, pp.132-168.

Luo, A.C.J. and O'Connor, D.M. (2009). "Mechanism of impacting chatter with stick in a gear transmission system", *International Journal of Bifurcation and Chaos*, **19**, pp.2093-2105.

Luo, A.C.J. and O'Connor, D.M. (2009). "Periodic motions and Chaos with Impacting Chatter and stick in a Gear Transmission System", *International Journal of Bifurcation and Chaos,* **19**, pp.1975-1994.

Sayyaadi, H. and Shokouhi, N. (2009). "A new model in rail–vehicles dynamics considering nonlinear suspension components behavior", *International Journal of Mechanical Sciences*, **51**, pp. 222-232.

Shieh, N.-C., Lin, C.-L., Lin, Y.-C. Liang, K.-Z. (2005). "Optimal design for passive suspension of a light rail vehicle using constrained multiobjective evolutionary search" *Journal of Sound and Vibration*, **285**, pp. 407-424.

Shaw, S.W. (1986). "On the dynamic response of a system with dry-friction", *Journal of Sound and Vibration,* **108**, pp. 305–325.

Shaw, S. W. and Holmes, P.J. (1983). "A Periodically Forced Piecewise Linear Oscillator," *Journal of Sound and Vibration*, **90**(1), pp.129-155.

Theodossiades, S. and Natsiavas, S. (2000). "Non-linear dynamics of gear-pair systems with periodic stiffness and backlash," *Journal of Sound and Vibration*, 229(2), pp 287-310.

Wu, Y.-S., and Yang, Y.-B. (2003). "Steady-state response and riding comfort of trains moving over a series of simply supported bridges", *Engineering Structures*, **25**, pp. 251-265.

APPENDICES

APPENDIX A

GENERAL SOLUTIONS

With an initial condition $(t, x^{(i)}, \dot{x}^{(i)}) = (t_k, x_k^{(i)}, y_k^{(i)})$, the general solutions for wedge and bolster for three regions are given as follows:

Case I $(d_\alpha^{(i)})^2 - c_\alpha^{(i)} > 0$

$$x_\alpha^{(i)} = e^{-d_\alpha^{(i)}(t-t_k)}(C_1^{(\alpha,i)}e^{\omega_d^{(i)}(t-t_k)} + C_2^{(\alpha,i)}e^{-\omega_d^{(\alpha,i)}(t-t_k)}) + D_1^{(\alpha,i)}\cos\Omega t + D_2^{(\alpha,i)}\sin\Omega t + D_0^{(\alpha,i)}, \quad \textbf{(A1)}$$

$$\begin{aligned}\dot{x}_\alpha^{(i)} = e^{-d_\alpha^{(i)}(t-t_k)}&[(\omega_d^{(\alpha,i)} - d_\alpha^{(i)})C_1^{(\alpha,i)}e^{\omega_d^{(\alpha,i)}(t-t_k)} - (\omega_d^{(\alpha,i)} + d_\alpha^{(i)})C_2^{(\alpha,i)}e^{-\omega_d^{(\alpha,i)}(t-t_k)}] \\ &- D_1^{(\alpha,i)}\Omega\sin\Omega t + D_2^{(\alpha,i)}\Omega\cos\Omega t;\end{aligned} \quad \textbf{(A2)}$$

$$\left.\begin{aligned}C_1^{(\alpha,i)} = \frac{1}{2\omega_d^{(\alpha,i)}}&\{-\dot{x}_k + (x_k - D_0^{(\alpha,i)})(-d_\alpha^{(i)} + \omega_d^{(\alpha,i)}) - [D_1^{(\alpha,i)}\Omega + D_2^{(j)}(-d_\alpha^{(i)} + \omega_d^{(\alpha,i)})]\sin\Omega t_k \\ &- [D_1^{(\alpha,i)}(-d_\alpha^{(i)} + \omega_d^{(\alpha,i)}) - D_2^{(\alpha,i)}\Omega]\cos\Omega t_k\}, \\ C_1^{(\alpha,i)} = \frac{1}{2\omega_d^{(j)}}&\{\dot{x}_k + (x_k - D_0^{(\alpha,i)})(d_\alpha^{(i)} + \omega_d^{(\alpha,i)}) - [D_1^{(\alpha,i)}(d_\alpha^{(i)} + \omega_d^{(\alpha,i)}) + D_1^{(\alpha,i)}\Omega]\cos\Omega t_k \\ &+ [D_1^{(\alpha,i)}\Omega - D_2^{(\alpha,i)}(d_\alpha^{(i)} + \omega_d^{(\alpha,i)})]\sin\Omega t_k\}.\end{aligned}\right\} \quad \textbf{(A3)}$$

$$D_0^{(\alpha,i)} = -\frac{b_\alpha^{(i)}}{c_\alpha^{(i)}}, \ D_1^{(\alpha,i)} = \frac{Q_0^{(i)}(c_\alpha^{(i)} - \Omega^2)}{(c_\alpha^{(i)} - \Omega^2)^2 + (2d_\alpha^{(i)}\Omega)^2}, \ D_2^{(\alpha,i)} = \frac{Q_0^{(i)}(2d_\alpha^{(i)}\Omega)}{(c_\alpha^{(i)} - \Omega^2)^2 + (2d_\alpha^{(i)}\Omega)^2}, \ \omega_d^{(\alpha,i)} = \sqrt{(d_\alpha^{(i)})^2 - c_\alpha^{(i)}} \quad \textbf{(A4)}$$

Case II. $(d_\alpha^{(i)})^2 - c_\alpha^{(i)} < 0$

$$\begin{aligned}x^{(i)} = e^{-d_\alpha^{(i)}(t-t_i)}&[C_1^{(\alpha,i)}\cos\omega_d^{(j)}(t-t_k) + C_2^{(\alpha,i)}\sin\omega_d^{(j)}(t-t_k)] + D_1^{(\alpha,i)}\cos\Omega t \\ &+ D_2^{(\alpha,i)}\sin\Omega t + D_0^{(\alpha,i)},\end{aligned} \quad \textbf{(A5)}$$

$$\begin{aligned}\dot{x}^{(i)} = e^{-d_\alpha^{(i)}(t-t_i)}&[(C_2^{(\alpha,i)}\omega_d^{(\alpha,i)} - d_\alpha^{(i)}C_1^{(\alpha,i)})\cos\omega_d^{(\alpha,i)}(t-t_k) - (C_1^{(\alpha,i)}\omega_d^{(\alpha,i)} + d_\alpha^{(i)}C_2^{(\alpha,i)})\sin\omega_d^{(\alpha,i)}(t-t_k)] \\ &- D_1^{(\alpha,i)}\Omega\sin\Omega t + D_2^{(\alpha,i)}\Omega\cos\Omega t;\end{aligned} \quad \textbf{(A6)}$$

$$C_1^{(\alpha,i)} = x_k - D_1^{(\alpha,i)} \cos \Omega t_k - D_2^{(\alpha,i)} \sin \Omega t_k - D_0^{(\alpha,i)},$$

$$C_2^{(\alpha,i)} = \frac{1}{\omega_d^{(j)}} [d_\alpha^{(i)} (x_k - D_1^{(\alpha,i)} \cos \Omega t_k - D_2^{(\alpha,i)} \sin \Omega t_k - D_0^{(\alpha,i)}) + \dot{x}_k + D_1^{(\alpha,i)} \Omega \sin \Omega t_k$$

$$- D_2^{(\alpha,i)} \Omega \cos \Omega t_k)],$$

$$\omega_d^{(\alpha,i)} = \sqrt{c_\alpha^{(i)} - (d_\alpha^{(i)})^2}.$$

(A7)

Case III: $(d_\alpha^{(i)})^2 - c_\alpha^{(i)} = 0$

$$x^{(i)} = e^{-d_\alpha^{(i)}(t-t_i)} [C_1^{(\alpha,i)}(t-t_i) + C_2^{(\alpha,i)}] + D_1^{(\alpha,i)} \cos \Omega t + D_2^{(\alpha,i)} \sin \Omega t + D_0^{(\alpha,i)}$$

(A8)

$$\dot{x}^{(i)} = e^{-d_\alpha^{(i)}(t-t_i)} [C_1^{(\alpha,i)} - C_1^{(\alpha,i)} d_\alpha^{(i)}(t-t_i) - d_\alpha^{(i)} C_2^{(\alpha,i)}] - D_1^{(\alpha,i)} \Omega \sin \Omega t + D_2^{(\alpha,i)} \Omega \cos \Omega t;$$

(A9)

$$C_2^{(\alpha,i)} = x_k - D_1^{(\alpha,i)} \cos \Omega t_k - D_2^{(\alpha,i)} \sin \Omega t_k - D_0^{(\alpha,i)},$$

$$C_2^{(\alpha,i)} = x_k + (D_2^{(\alpha,i)} \Omega - d_\alpha^{(i)} D_1^{(\alpha,i)}) \cos \Omega t_k - (D_1^{(\alpha,i)} \Omega + d_\alpha^{(i)} D_2^{(\alpha,i)}) \sin \Omega t_k - d_\alpha^{(i)} D_1^{(\alpha,i)}.$$

(A10)

CASE IV: $d_\alpha^{(i)} \neq 0, c_\alpha^{(i)} = 0$

$$x^{(i)} = C_1^{(\alpha,i)} e^{-2d_\alpha^{(i)}(t-t_k)} + D_1^{(\alpha,i)} \cos \Omega t + D_2^{(\alpha,i)} \sin \Omega t + D_0^{(\alpha,i)} t + C_2^{(\alpha,i)},$$

(A11)

$$\dot{x}^{(i)} = -2d_\alpha^{(i)} C_1^{(\alpha,i)} e^{-2d_\alpha^{(i)}(t-t_k)} - D_1^{(\alpha,i)} \Omega \sin \Omega t + D_2^{(\alpha,i)} \Omega \cos \Omega t + D_0^{(\alpha,i)};$$

(A12)

$$C_1^{(\alpha,i)} = -\frac{1}{2d_\alpha^{(i)}} (\dot{x}_k + D_1^{(\alpha,i)} \Omega \sin \Omega t_k - D_2^{(\alpha,i)} \Omega \cos \Omega t_k - D_0^{(\alpha,i)}),$$

$$C_2^{(\alpha,i)} = \frac{1}{2d_\alpha^{(i)}} [2d_\alpha^{(i)} x_k + \dot{x}_k + (D_1^{(\alpha,i)} \Omega - 2d_\alpha^{(i)} D_2^{(\alpha,i)}) \sin \Omega t_k$$

$$- (2d_\alpha^{(i)} D_1^{(\alpha,i)} + D_2^{(\alpha,i)} \Omega) \cos \Omega t_k - 2d_\alpha^{(i)} D_0^{(\alpha,i)} t_k - D_0^{(\alpha,i)}].$$

(A14)

CASE V: $d_\alpha^{(i)} = 0, c_\alpha^{(i)} = 0$

$$x^{(i)} = -\frac{Q_0^{(i)}}{\Omega^2} \cos \Omega t - \frac{1}{2} b_\alpha^{(i)} t^2 + C_1^{(\alpha,i)} t + C_2^{(\alpha,i)},$$

(A15)

$$\dot{x}^{(i)} = \frac{Q_0^{(i)}}{\Omega} \sin \Omega t - b_\alpha^{(i)} t + C_1^{(\alpha,i)};$$

(A16)

$$
\left.
\begin{aligned}
C_1^{(\alpha,i)} &= \dot{x}_k - \frac{Q_0^{(i)}}{\Omega} \sin \Omega t_k + b_\alpha^{(i)} t_k, \\
C_2^{(\alpha,i)} &= x_k - \dot{x} t_k + \frac{Q_0^{(i)}}{\Omega^2} \cos \Omega t_k + \frac{Q_0^{(i)}}{\Omega} t_k \sin \Omega t_k - \frac{1}{2} b_\alpha^{(i)} t_k^{\,2}.
\end{aligned}
\right\}
$$

(A17)

APPENDIX B

NUMERICAL SIMULATION ALGORITHM

The numerical simulation algorithm used in this thesis is for plotting the displacement and velocity response of each oscillator in the mechanical model in Fig.2. For the equations of motion in Eqs.(1) and (7), the closed form solutions and their corresponding homogeneous coefficients (i.e., displacement and velocity equations) can be found in Appendix A. These equations are programmed in C++. Additionally, the impact relationship in Eq.(4) as well as the analytical conditions for stick onset and vanishing are programmed. Assuming that the oscillators are described by Eq.(1) with initial conditions $(t_k, x_k^{(i)}, \dot{x}_k^{(i)}, \dot{x}_k^{(\bar{i})})$ and by incrementing time by a small amount Δt_k, the new displacement and velocity of each mass can be computed for the new time. After each increment, the conditions for impact are checked. Once impact occurs at the boundary, the initial conditions $(t_k, x_k^{(i)}, \dot{x}_k^{(i)}, \dot{x}_k^{(\bar{i})})$ are updated. If the stick conditions are satisfied, then the two oscillators are described by Eq.(7). While in stick motion, the wedge and bolster may become stuck when crossing the velocity boundary. If the analytical conditions for stuck are satisfied, the oscillators will become fixed to the side frame. This process of incrementing time, computing displacements and velocities, checking impact and stick conditions, and updating the initial conditions to be those at the domain boundaries is repeated until the motion can be considered either periodic or chaotic. By keeping track of the switching boundaries, the mapping structure can be defined and a bifurcation scenario presented as shown in Chapter 4. Furthermore, by recording all the computations at each time step, the motion can be numerically simulated as shown in Chapter 5.

APPENDIX C

JACOBEAN MATRIX

From the analytical prediction in Chapter 5, the stability analysis of periodic solutions is achieved through the eigenvalues of the Jacobean matrix. Herein, the Jacobean matrix is derived for a P_2 mapping. From Eq.(95), consider the following vector

$$\mathbf{f}^{(2)}\left(\mathbf{y}_{k+1},\mathbf{y}_k\right)=0. \tag{B1}$$

Equation (B1) can be rewritten as

$$\mathbf{y}_{k+1}=\mathbf{g}^{(2)}\left(\mathbf{y}_k\right), \tag{B2}$$

where $\mathbf{g}^{(2)}\left(\mathbf{y}_k\right)$ is the vector of solutions to Eq.(2) that relate the initial and final switching sets.

For the predicted switching sets $\mathbf{y}_{k+1}^*$ and $\mathbf{y}_k^*$, Equation (B2) becomes

$$\mathbf{y}_{k+1}^*=\mathbf{g}^{(2)}\left(\mathbf{y}_k^*\right). \tag{B3}$$

The predicted solutions are perturbed by a small amount $\Delta(\cdot)$ in

$$\mathbf{y}_{k+1}^*+\Delta\mathbf{y}_{k+1}=\mathbf{g}^{(2)}\left(\mathbf{y}_k^*+\Delta\mathbf{y}_k\right). \tag{B4}$$

From the first order Taylor Series expansion

$$\mathbf{g}^{(2)}\left(\mathbf{y}_k^*+\Delta\mathbf{y}_k\right)=\mathbf{g}^{(2)}\left(\mathbf{y}_k^*\right)+D\mathbf{g}^{(2)}\Big|_{\mathbf{y}_k^*}\Delta\mathbf{y}_k. \tag{B5}$$

Substitution of Eq.(B5) into Eq.(B4) gives

$$\mathbf{y}_{k+1}^*+\Delta\mathbf{y}_{k+1}=\mathbf{g}^{(2)}\left(\mathbf{y}_k^*\right)+D\mathbf{g}^{(2)}\Big|_{\mathbf{y}_k^*}\Delta\mathbf{y}_k. \tag{B6}$$

Further simplification gives the variational equation for $\mathbf{y}_{k+1}^*$ and $\mathbf{y}_k^*$ as

$$\Delta\mathbf{y}_{k+1}=DP(\mathbf{y}_k^*)\Delta\mathbf{y}_k, \tag{B7}$$

where the Jacobean Matrix $D\mathbf{g}^{(2)}\big|_{\mathbf{y}_k^*}$ is represented by $DP(\mathbf{y}_k^*)$. The total derivatives of the

displacement and velocity functions represented in Eq.(B1) provide the components of DP.

$$
\left\{
\begin{aligned}
&\frac{\partial f_1^{(2)}}{\partial t_k} + \frac{\partial f_1^{(2)}}{\partial t_{k+1}}\frac{\partial t_{k+1}}{\partial t_k} + \frac{\partial f_1^{(2)}}{\partial x_{k+1}^{(1)}}\frac{\partial x_{k+1}^{(1)}}{\partial t_k} + \frac{\partial f_1^{(2)}}{\partial y_{k+1}^{(1)}}\frac{\partial y_{k+1}^{(1)}}{\partial t_k} + \frac{\partial f_1^{(2)}}{\partial y_{k+1}^{(2)}}\frac{\partial y_{k+1}^{(2)}}{\partial t_k} = 0 \\[2mm]
&\frac{\partial f_1^{(2)}}{\partial x_k^{(1)}} + \frac{\partial f_1^{(2)}}{\partial t_{k+1}}\frac{\partial t_{k+1}}{\partial x_k^{(1)}} + \frac{\partial f_1^{(2)}}{\partial x_{k+1}^{(1)}}\frac{\partial x_{k+1}^{(1)}}{\partial x_k^{(1)}} + \frac{\partial f_1^{(2)}}{\partial y_{k+1}^{(1)}}\frac{\partial y_{k+1}^{(1)}}{\partial x_k^{(1)}} + \frac{\partial f_1^{(2)}}{\partial y_{k+1}^{(2)}}\frac{\partial y_{k+1}^{(2)}}{\partial x_k^{(1)}} = 0 \\[2mm]
&\frac{\partial f_1^{(2)}}{\partial y_k^{(1)}} + \frac{\partial f_1^{(2)}}{\partial t_{k+1}}\frac{\partial t_{k+1}}{\partial y_k^{(1)}} + \frac{\partial f_1^{(2)}}{\partial x_{k+1}^{(1)}}\frac{\partial x_{k+1}^{(1)}}{\partial y_k^{(1)}} + \frac{\partial f_1^{(2)}}{\partial y_{k+1}^{(1)}}\frac{\partial y_{i+1}^{(1)}}{\partial y_k^{(1)}} + \frac{\partial f_1^{(2)}}{\partial y_{k+1}^{(2)}}\frac{\partial \dot{x}_{k+1}^{(2)}}{\partial y_k^{(1)}} = 0 \\[2mm]
&\frac{\partial f_1^{(2)}}{\partial y_k^2} + \frac{\partial f_1^{(2)}}{\partial t_{k+1}}\frac{\partial t_{k+1}}{\partial y_k^{(2)}} + \frac{\partial f_1^{(2)}}{\partial x_{k+1}^{(1)}}\frac{\partial x_{k+1}^{(1)}}{\partial y_k^{(2)}} + \frac{\partial f_1^{(2)}}{\partial y_{k+1}^{(1)}}\frac{\partial y_{k+1}^{(1)}}{\partial y_k^{(2)}} + \frac{\partial f_1^{(2)}}{\partial y_{k+1}^{(2)}}\frac{\partial y_{k+1}^{(2)}}{\partial y_k^{(2)}} = 0
\end{aligned}
\right. , \tag{B8}
$$

$$
\left\{
\begin{aligned}
&\frac{\partial f_2^{(2)}}{\partial t_k} + \frac{\partial f_2^{(2)}}{\partial t_{k+1}}\frac{\partial t_{k+1}}{\partial t_k} + \frac{\partial f_2^{(2)}}{\partial x_{k+1}^{(1)}}\frac{\partial x_{k+1}^{(1)}}{\partial t_k} + \frac{\partial f_2^{(2)}}{\partial y_{k+1}^{(1)}}\frac{\partial y_{k+1}^{(1)}}{\partial t_k} + \frac{\partial f_2^{(2)}}{\partial y_{k+1}^{(2)}}\frac{\partial y_{k+1}^{(2)}}{\partial t_k} = 0 \\[2mm]
&\frac{\partial f_2^{(2)}}{\partial x_k^{(1)}} + \frac{\partial f_2^{(2)}}{\partial t_{k+1}}\frac{\partial t_{k+1}}{\partial x_k^{(1)}} + \frac{\partial f_2^{(2)}}{\partial x_{k+1}^{(1)}}\frac{\partial x_{k+1}^{(1)}}{\partial x_k^{(1)}} + \frac{\partial f_2^{(2)}}{\partial y_{k+1}^{(1)}}\frac{\partial y_{k+1}^{(1)}}{\partial x_k^{(1)}} + \frac{\partial f_2^{(2)}}{\partial y_{k+1}^{(2)}}\frac{\partial y_{k+1}^{(2)}}{\partial x_k^{(1)}} = 0 \\[2mm]
&\frac{\partial f_2^{(2)}}{\partial y_k^{(1)}} + \frac{\partial f_2^{(2)}}{\partial t_{k+1}}\frac{\partial t_{k+1}}{\partial y_k^{(1)}} + \frac{\partial f_2^{(2)}}{\partial x_{k+1}^{(1)}}\frac{\partial x_{k+1}^{(1)}}{\partial y_k^{(1)}} + \frac{\partial f_2^{(2)}}{\partial y_{k+1}^{(1)}}\frac{\partial y_{i+1}^{(1)}}{\partial y_k^{(1)}} + \frac{\partial f_2^{(2)}}{\partial y_{k+1}^{(2)}}\frac{\partial \dot{x}_{k+1}^{(2)}}{\partial y_k^{(1)}} = 0 \\[2mm]
&\frac{\partial f_2^{(2)}}{\partial y_k^2} + \frac{\partial f_2^{(2)}}{\partial t_{k+1}}\frac{\partial t_{k+1}}{\partial y_k^{(2)}} + \frac{\partial f_2^{(2)}}{\partial x_{k+1}^{(1)}}\frac{\partial x_{k+1}^{(1)}}{\partial y_k^{(2)}} + \frac{\partial f_2^{(2)}}{\partial y_{k+1}^{(1)}}\frac{\partial y_{k+1}^{(1)}}{\partial y_k^{(2)}} + \frac{\partial f_2^{(2)}}{\partial y_{k+1}^{(2)}}\frac{\partial y_{k+1}^{(2)}}{\partial y_k^{(2)}} = 0
\end{aligned}
\right. , \tag{B9}
$$

$$
\left\{
\begin{aligned}
&\frac{\partial f_3^{(2)}}{\partial t_k} + \frac{\partial f_3^{(2)}}{\partial t_{k+1}}\frac{\partial t_{k+1}}{\partial t_k} + \frac{\partial f_3^{(2)}}{\partial x_{k+1}^{(1)}}\frac{\partial x_{k+1}^{(1)}}{\partial t_k} + \frac{\partial f_3^{(2)}}{\partial y_{k+1}^{(1)}}\frac{\partial y_{k+1}^{(1)}}{\partial t_k} + \frac{\partial f_3^{(2)}}{\partial y_{k+1}^{(2)}}\frac{\partial y_{k+1}^{(2)}}{\partial t_k} = 0 \\[2mm]
&\frac{\partial f_3^{(2)}}{\partial x_k^{(1)}} + \frac{\partial f_3^{(2)}}{\partial t_{k+1}}\frac{\partial t_{k+1}}{\partial x_k^{(1)}} + \frac{\partial f_3^{(2)}}{\partial x_{k+1}^{(1)}}\frac{\partial x_{k+1}^{(1)}}{\partial x_k^{(1)}} + \frac{\partial f_3^{(2)}}{\partial y_{k+1}^{(1)}}\frac{\partial y_{k+1}^{(1)}}{\partial x_k^{(1)}} + \frac{\partial f_3^{(2)}}{\partial y_{k+1}^{(2)}}\frac{\partial y_{k+1}^{(2)}}{\partial x_k^{(1)}} = 0 \\[2mm]
&\frac{\partial f_3^{(2)}}{\partial y_k^{(1)}} + \frac{\partial f_3^{(2)}}{\partial t_{k+1}}\frac{\partial t_{k+1}}{\partial y_k^{(1)}} + \frac{\partial f_3^{(2)}}{\partial x_{k+1}^{(1)}}\frac{\partial x_{k+1}^{(1)}}{\partial y_k^{(1)}} + \frac{\partial f_3^{(2)}}{\partial y_{k+1}^{(1)}}\frac{\partial y_{i+1}^{(1)}}{\partial y_k^{(1)}} + \frac{\partial f_3^{(2)}}{\partial y_{k+1}^{(2)}}\frac{\partial \dot{x}_{k+1}^{(2)}}{\partial y_k^{(1)}} = 0 \\[2mm]
&\frac{\partial f_3^{(2)}}{\partial y_k^2} + \frac{\partial f_3^{(2)}}{\partial t_{k+1}}\frac{\partial t_{k+1}}{\partial y_k^{(2)}} + \frac{\partial f_3^{(2)}}{\partial x_{k+1}^{(1)}}\frac{\partial x_{k+1}^{(1)}}{\partial y_k^{(2)}} + \frac{\partial f_3^{(2)}}{\partial y_{k+1}^{(1)}}\frac{\partial y_{k+1}^{(1)}}{\partial y_k^{(2)}} + \frac{\partial f_3^{(2)}}{\partial y_{k+1}^{(2)}}\frac{\partial y_{k+1}^{(2)}}{\partial y_k^{(2)}} = 0
\end{aligned}
\right. , \tag{B10}
$$

$$\begin{cases} \dfrac{\partial f_4^{(2)}}{\partial t_k} + \dfrac{\partial f_4^{(2)}}{\partial t_{k+1}}\dfrac{\partial t_{k+1}}{\partial t_k} + \dfrac{\partial f_4^{(2)}}{\partial x_{k+1}^{(1)}}\dfrac{\partial x_{k+1}^{(1)}}{\partial t_k} + \dfrac{\partial f_4^{(2)}}{\partial y_{k+1}^{(1)}}\dfrac{\partial y_{k+1}^{(1)}}{\partial t_k} + \dfrac{\partial f_4^{(2)}}{\partial y_{k+1}^{(2)}}\dfrac{\partial y_{k+1}^{(2)}}{\partial t_k} = 0 \\[3mm]
\dfrac{\partial f_4^{(2)}}{\partial x_k^{(1)}} + \dfrac{\partial f_4^{(2)}}{\partial t_{k+1}}\dfrac{\partial t_{k+1}}{\partial x_k^{(1)}} + \dfrac{\partial f_4^{(2)}}{\partial x_{k+1}^{(1)}}\dfrac{\partial x_{k+1}^{(1)}}{\partial x_k^{(1)}} + \dfrac{\partial f_4^{(2)}}{\partial y_{k+1}^{(1)}}\dfrac{\partial y_{k+1}^{(1)}}{\partial x_k^{(1)}} + \dfrac{\partial f_4^{(2)}}{\partial y_{k+1}^{(2)}}\dfrac{\partial y_{k+1}^{(2)}}{\partial x_k^{(1)}} = 0 \\[3mm]
\dfrac{\partial f_4^{(2)}}{\partial y_k^{(1)}} + \dfrac{\partial f_4^{(2)}}{\partial t_{k+1}}\dfrac{\partial t_{k+1}}{\partial y_k^{(1)}} + \dfrac{\partial f_4^{(2)}}{\partial x_{k+1}^{(1)}}\dfrac{\partial x_{k+1}^{(1)}}{\partial y_k^{(1)}} + \dfrac{\partial f_4^{(2)}}{\partial y_{k+1}^{(1)}}\dfrac{\partial y_{i+1}^{(1)}}{\partial y_k^{(1)}} + \dfrac{\partial f_4^{(2)}}{\partial y_{k+1}^{(2)}}\dfrac{\partial \dot{x}_{k+1}^{(2)}}{\partial y_k^{(1)}} = 0 \\[3mm]
\dfrac{\partial f_4^{(2)}}{\partial y_k^{2}} + \dfrac{\partial f_4^{(2)}}{\partial t_{k+1}}\dfrac{\partial t_{k+1}}{\partial y_k^{(2)}} + \dfrac{\partial f_4^{(2)}}{\partial x_{k+1}^{(1)}}\dfrac{\partial x_{k+1}^{(1)}}{\partial y_k^{(2)}} + \dfrac{\partial f_4^{(2)}}{\partial y_{k+1}^{(1)}}\dfrac{\partial y_{k+1}^{(1)}}{\partial y_k^{(2)}} + \dfrac{\partial f_4^{(2)}}{\partial y_{k+1}^{(2)}}\dfrac{\partial y_{k+1}^{(2)}}{\partial y_k^{(2)}} = 0 \end{cases} . \qquad (B11)$$

The partial derivatives of the final time, position, and velocities in Eqs.(B8)-(B11) are the necessary derivatives for Jacobean matrix DP in Eq.(108). These derivatives can be found by arranging the functions in matrix form (i.e., solve four systems of four equations each with four unknowns).

$$\begin{bmatrix} \dfrac{\partial t_{k+1}}{\partial t_k} \\[3mm] \dfrac{\partial x_{k+1}^{(1)}}{\partial t_i} \\[3mm] \dfrac{\partial y_{k+1}^{(1)}}{\partial t_k} \\[3mm] \dfrac{\partial y_{k+1}^{(2)}}{\partial t_k} \end{bmatrix} = [\Lambda]^{-1} \begin{bmatrix} -\dfrac{\partial f_1^{(2)}}{\partial t_k} \\[3mm] -\dfrac{\partial f_2^{(2)}}{\partial t_k} \\[3mm] -\dfrac{\partial f_3^{(2)}}{\partial t_k} \\[3mm] -\dfrac{\partial f_4^{(2)}}{\partial t_k} \end{bmatrix}, \quad \begin{bmatrix} \dfrac{\partial t_{k+1}}{\partial x_k^{(1)}} \\[3mm] \dfrac{\partial x_{k+1}^{(1)}}{\partial x_k^{(1)}} \\[3mm] \dfrac{\partial y_{k+1}^{(1)}}{\partial x_k^{(1)}} \\[3mm] \dfrac{\partial y_{k+1}^{(2)}}{\partial x_k^{(1)}} \end{bmatrix} = [\Lambda]^{-1} \begin{bmatrix} -\dfrac{\partial f_1^{(2)}}{\partial x_k^{(1)}} \\[3mm] -\dfrac{\partial f_2^{(2)}}{\partial x_k^{(1)}} \\[3mm] -\dfrac{\partial f_3^{(2)}}{\partial x_k^{(1)}} \\[3mm] -\dfrac{\partial f_4^{(2)}}{\partial x_k^{(1)}} \end{bmatrix}, \qquad (B12)$$

$$\begin{bmatrix} \dfrac{\partial t_{k+1}}{\partial y_k^{(1)}} \\[3mm] \dfrac{\partial x_{k+1}^{(1)}}{\partial y_k^{(1)}} \\[3mm] \dfrac{\partial y_{k+1}^{(1)}}{\partial y_k^{(1)}} \\[3mm] \dfrac{\partial y_{k+1}^{(2)}}{\partial y_k^{(1)}} \end{bmatrix} = [\Lambda]^{-1} \begin{bmatrix} -\dfrac{\partial f_1^{(2)}}{\partial y_k^{(1)}} \\[3mm] -\dfrac{\partial f_2^{(2)}}{\partial y_k^{(1)}} \\[3mm] -\dfrac{\partial f_3^{(2)}}{\partial y_k^{(1)}} \\[3mm] -\dfrac{\partial f_4^{(2)}}{\partial y_k^{(1)}} \end{bmatrix}, \quad \begin{bmatrix} \dfrac{\partial t_{k+1}}{\partial y_k^{(2)}} \\[3mm] \dfrac{\partial x_{k+1}^{(1)}}{\partial y_k^{(2)}} \\[3mm] \dfrac{\partial y_{k+1}^{(1)}}{\partial y_k^{(2)}} \\[3mm] \dfrac{\partial y_{k+1}^{(2)}}{\partial y_k^{(2)}} \end{bmatrix} = [\Lambda]^{-1} \begin{bmatrix} -\dfrac{\partial f_1^{(2)}}{\partial y_k^{(2)}} \\[3mm] -\dfrac{\partial f_2^{(2)}}{\partial y_k^{(2)}} \\[3mm] -\dfrac{\partial f_3^{(2)}}{\partial y_k^{(2)}} \\[3mm] -\dfrac{\partial f_4^{(2)}}{\partial y_k^{(2)}} \end{bmatrix} . \qquad (B13)$$

The Lambda matrix is defined by

$$
\Lambda = \begin{bmatrix}
\dfrac{\partial f_1^{(2)}}{\partial t_{k+1}} & \dfrac{\partial f_1^{(2)}}{\partial x_{k+1}^{(1)}} & \dfrac{\partial f_1^{(2)}}{\partial y_{k+1}^{(1)}} & \dfrac{\partial f_1^{(2)}}{\partial y_{i+1}^{(2)}} \\[2ex]
\dfrac{\partial f_2^{(2)}}{\partial t_{k+1}} & \dfrac{\partial f_2^{(2)}}{\partial x_{k+1}^{(1)}} & \dfrac{\partial f_2^{(2)}}{\partial y_{k+1}^{(1)}} & \dfrac{\partial f_2^{(2)}}{\partial y_{k+1}^{(2)}} \\[2ex]
\dfrac{\partial f_3^{(2)}}{\partial t_{k+1}} & \dfrac{\partial f_3^{(2)}}{\partial x_{k+1}^{(1)}} & \dfrac{\partial f_3^{(2)}}{\partial y_{k+1}^{(1)}} & \dfrac{\partial f_3^{(2)}}{\partial y_{k+1}^{(2)}} \\[2ex]
\dfrac{\partial f_4^{(2)}}{\partial t_{k+1}} & \dfrac{\partial f_4^{(2)}}{\partial x_{k+1}^{(1)}} & \dfrac{\partial f_4^{(2)}}{\partial y_{k+1}^{(1)}} & \dfrac{\partial f_4^{(2)}}{\partial y_{k+1}^{(2)}}
\end{bmatrix}. \tag{B14}
$$

After solving each system of equations in Eqs.(B12) and (B13), the derivatives for the Jacobean

matrix are known and the first DP_2 matrix of Eq.(107) can be given. The above process is

repeated for each subsequent mapping.

VITA

Graduate School
Southern Illinois University

Dennis O'Connor

doconno@siue.edu

Southern Illinois University Edwardsville
Bachelor of Science, Mechanical Engineering, May 2004

Southern Illinois University Edwardsville
Master of Science, Mechanical Engineering, May 2007

Dissertation Title:

ON MOTION MECHANISMS IN FREIGHT TRAIN SUSPENSION SYSTEMS

Major Professor: Albert C.J. Luo

Publications:

Journal Articles

1. Luo, Albert C.J. and Dennis O'Connor (2014), "On periodic motions in a parametric hardening Duffing oscillator", *International Journal of Bifurcation and Chaos*, **24**, 1430004.
2. Luo, Albert C.J. and Dennis O'Connor (2009), "Periodic Motions with Impacting Chatter and Stick in a Gear Transmission System", ASME *Journal of Vibration and Acoustics*, **131**, 041013
3. Luo, Albert C.J. and Dennis O'Connor (2009), "Impact Chatter in a gear transmission system with two oscillators", *IMeChe Part K: Journal of Multi-body Dynamics*, **223**, 159-188.
4. Luo, Albert C.J. and Dennis O'Connor (2009), "Mechanism of impacting chatter with stick in a gear transmission system", *International Journal of Bifurcation and Chaos*, **19**, 1975-1994
5. Luo, Albert C.J. and Dennis O'Connor (2009), "Periodic motions and chaos with impacting chatter with stick in a gear transmission system", *International Journal of Bifurcation and Chaos*, **19**, 2093-2105.

Conference Papers
1. Luo, Albert C. J. and Dennis O'Connor, "Analytical Solutions for periodic motions in a Hard-ening Mathieu-Duffing oscillator", in 2013 ASME San Diego, California, USA
2. Luo, Albert C. J. and Dennis O'Connor, "Coexisting Asymmetric and Symmetric Periodic Mo-tions in the Mathieu-Duffing Oscillator", in 2012 ASME International Mechanical Engineering Congress and Exposition, Houston, Texas, November 9-15, 2012. IMECE2012-86849.

3. Luo, A.C.J. and Dennis O'Connor, "Stable and Unstable Periodic Solutions to Mathiu-Duffing Oscillator", Proceedings of IEEE 4th Conference on Nonlinear Science and Complexity, Bu-dapest, Hungary, August 6-11, 2012. pp.201-204.

4. Luo, Albert C. J. and Dennis O'Connor, "Analytical Dynamics of Complex Motions in a Train Suspension System", in 2011 ASME International Mechanical Engineering Congress and Ex-position, Denver, Colorado, November 11-17, 2011. IMECE2011-62944.

5. Luo, Albert C. J. and Dennis O'Connor, "Dynamic mechanism of a train suspension system", in 2010 ASME International Mechanical Engineering Congress and Exposition, Vancouver, British Columbia, November 12-18, 2010. IMECE2010-39202.

6. Luo, Albert C.J. and Dennis O'Connor, "Periodic and chaotic motions in a gear-pair transmis-sion systems with impacts", The second International Conference on Nonlinear Science and Complexity, Porto, Portugal, July 26-31, 2008.

7. Luo, Albert C.J. and Dennis O'Connor, "Nonlinear dynamics of a gear transmission system: Part I: Mechanism of impact chatters with stick", 2007 ASME International Design Engineer-ing Technical Conference